Physiological Chemistry and Physics and Medical NMR Volume 35, Number 2, 2003

Addresses of Chief Editor and Editorial College

George M. Mrevlishvili
Department of Physics
Tbilisi State University
380028 Tbilisi
Republic of Georgia

Toshihiko Ubuka
Department of Clinical Nutrition
Kawasaki University of Medical Welfare
Kurashiki, Okayama, 701-0193, Japan

Vasile Vasilescu
Department of Biophysics
Faculty of Medicine
Bucharest 76241, Romania

Denys Wheatley
Department of Pathology
University of Aberdeen
Aberdeen AB9 2ZD, Scotland

EDITORIAL AND BUSINESS OFFICE

Physiological Chemistry and Physics
and Medical NMR
P.O. Box 1452
Melville, New York 11747

Editor In Chief, Dr. Gilbert N. Ling
Managing Editor, Margaret M. Ochsenfeld

SCOPE: PCP provides a forum for the review and publication of reports of original research in a broad range of subjects in biophysics, biochemistry and cellular physiology. Reports of direct applications of basic knowledge to human studies are invited; examples would include the measurements of relaxation times as part of NMR imaging. Single experiments, conclusions based on inadequate statistics, purely speculative papers, and clinical case reports are not accepted.

POLICY: The pages of PCP are accessible to competing viewpoints, interpretations, theories and opinions. Debate is invited via Editorial Comments and Letters to the Editor. Criteria for evaluating submissions include soundness of the study and clarity of presentation, and papers are not rejected on the basis of interpretation or theory, however controversial. PCP believes that scientific issues should be settled by investigation and open debate, not by an appeal to anonymous authority.

PCP attempts to achieve a balance between freedom of expression and constructive peer review. All papers are refereed by reviewers who may remain anonymous, but the Chief Editors make all final decisions, and will handle appeals from authors who feel their papers are unfairly reviewed.

The Editors endeavor to make decisions regarding acceptance or rejection of manuscripts quickly, and have set self-imposed deadlines for doing so. Referees also are given deadlines.

TYPES OF PAPERS: *Regular papers* may be experimental or theoretical. *Short notes, Priority notes* and *Letters* in response to published papers are invited. *Reviews* are desired, but authors are urged to contact an Editor before sending a finished review manuscript. *Symposia* may be published as regular or supplemental issues.

SUBSCRIPTIONS: Price is US$80.00 per volume in the United States and US$87.00 outside the United States. *Physiological Chemistry and Physics and Medical NMR* is published biannually, 2 issues per year, the volume numbered yearly. New subscriptions will start with the first issue of the volume in progress, unless the subscriber directs otherwise. Most back issues are available

Instructions to Authors

SUBMISSIONS: An original and two copies of all material are requested. The original must be typewritten on one side only, but the copies may be double-sided to reduce cost of mailing. Papers should be sent to Dr. Gilbert N. Ling, Editor, P.O. Box 1452, Melville, New York 11747 U.S.A. Authors, especially those outside of North America, may send their papers to a member of the Editorial College in the same or a nearby country; the member of the college may elect to review the manuscript and/or obtain a second review before forwarding it to the Chief Editors. Manuscripts should be submitted only to this journal and not have been published in part or whole in another publication, except as short preliminary notes, abstracts, or as unpublished work in reviews or symposia. Be sure to keep a copy of your manuscript.

NOTE: Referees will be instructed to destroy their copies of the manuscript after reviewing them. We will return only the original manuscript to you for revision or if rejected.

MANUSCRIPTS: All material should be typed double-spaced with margins at least one inch wide and pages numbered beginning with the title page. In addition to a paper copy, you may send an IBM-compatible file on a floppy disk in Word, Wordperfect, ASCII or text. *Title Page* should include title (of at most 100 characters and spaces), full names of authors as you wish them to be published, names and cities of institutional affiliation(s) of authors and of institution(s) where the studies were performed, and name, full address and telephone number of the person to whom correspondence, proofs, and reprint requests are to be sent. Three or four *key words* should be listed on the title page.

Abstract should be concise and no longer than 225 words. *Body* may or may not be divided into Introduction, Materials and Methods, Results and Discussion, depending on the length and nature of the paper. Introductory remarks should indicate clearly the significance of the work presented. *References* may be indicated in the text and listed in the reference list in whatever style the author prefers, but we prefer that titles of articles be omitted.

TABLES: Tables should be typewritten on separate sheets and identified by roman numerals (eg. Table 111) and titles. Table notes should be keyed by superscript italic lower-case letters (eg. ^{a}Control). The approximate locations of *tables* and *figures* should be indicated in the margins of the manuscript.

EQUATIONS should be broken in a manner estimated to fit into a column 5 inches wide when published. Solidus fraction (a/c) should be used instead of built-up ones ($\frac{a}{c}$) wherever possible.

ILLUSTRATIONS: Original artwork or glossy photostatic prints, together with two photocopies (like Xerox copies) should be provided. Each illustration should be numbered on the back in pencil, along with the authors' names. It is preferred that line drawings be made on paper that is not larger than $8^1/_2$ by 13 inches, and that the drawing be its intended size in the printed paper. Most figures will occupy $^1/_2$ to full column, that is 5 inches wide. Lines and lettering should be thick enough to allow reduction. A drawing of overall dimension of 8 by 10 inches that will be reduced to $^1/_4$ of its original size should be lettered with 18-point (capitals 6 mm high, lower-case 4 mm high) or larger lettering. Graphs and line drawings must be drawn and labeled in black India ink. Glossy photostatic prints are acceptable, and should be attached firmly to a sheet of paper the same size as the manuscript.

PHOTOGRAPHS: High-quality black and white glossy prints should be provided in triplicate, and may be provided as one print plus two photocopies if the photocopies are sufficiently clear to portray the original to referees. Photographs should be attached firmly to a sheet of paper the same size as the manuscript.

REFEREES: Two anonymous referees will be sought for each paper. Authors are encouraged to suggest names and addresses of suitable referees. Referees will be given deadlines for mailing manuscripts back or phoning reviews in, and will be invited to provide editorial statements or Letters that deal with issues raised by submitted papers.

REPRINTS: An order form is enclosed with proofs sent to authors.

PAGE CHARGES: Page charge is $20.00 per published page. It may be waived in the case of severe international exchange difficulties. An additional charge of $10.00 will be levied for photographs that require screening (eg., E.M's, chromatograms, scans).

Physiol. Chem. Phys. & Med. NMR (2003) *35*: 91–130

A New Theoretical Foundation for the Polarized-Oriented Multilayer Theory of Cell Water and for Inanimate Systems Demonstrating Long-range Dynamic Structuring of Water Molecules

Gilbert N. Ling

Damadian Foundation for Basic and Cancer Research
Tim & Kim Ling Foundation for Basic and Cancer Research
c/o Fonar Corporation, 110 Marcus Drive, Melville, NY 11747
E-mail: gilbertling@dobar.org

Abstract: Over the centuries, a vast amount of evidence has been gathering that layers of water sometimes measuring tens of thousands of water molecules thick exhibit altered properties in consequence of exposure to some solid surfaces. Yet, a clear cut theory based on the laws of physics that would predict this kind of long range dynamic ordering of water molecules has been long missing.

It is thus with great joy that I announce that a new theory has been developed, which offers theoretical confirmation of the phenomena of long-range dynamic structuring of water by appropriate solid surfaces and which gives clear cut quantitative answers to some key questions about the phenomenon. Thus, for example, under an ideal condition, an idealized checkerboard of alternatingly positively-, and negatively-charged sites of the correct size and distribution could polarize and orient deep layers of water molecules *ad infinitum*. Based on the quantitative data thus obtained and a relevant simple statistical mechanical law, the new theory predicts that a thin layer of water held between two juxtaposed ideal or near-ideal NP surfaces will not freeze at any (attainable) temperature.

On the other hand, water polarized and oriented by an ideal or near-ideal NP-NP system may also not evaporate at temperature hundreds of degrees higher than the normal boiling temperature of water.

Both predictions have been confirmed (retroactively) by experimental observations made in the past, accidentally or by design. In a following paper, I will demonstrate that the conclusion reached from the study of the two-dimensional NP surface can be smoothly passed on to the living cells. In the living cell, only one-dimensional linear chains of fully extended protein chains exist. Nonetheless, by proper orientation and distribution, they can achieve similar though less intense water polarization-orientation—as experimentally demonstrated worldwide during the 40 years past.

TEN YEARS after an early embryonic version was presented at a Symposium on Phosphorus Metabolism in Baltimore (Ling 1952), a theory of cell and subcellular physiology

made its debut (Ling 1962.) It bears the title: "A Physical Theory of the Living State: the Association-Induction (AI) Hypothesis." Three years later in 1965 the Polarized Multilayer Theory of Cell Water (now renamed Polarized-Oriented Multilayer Theory, though still represented by the same short name, PM Thoery) was added (Ling 1965, 1969, 1972, 1972a, 1993, Ling *et al* 1993.) The association-induction hypothesis then became in essence complete and, as such, unifying.

Part of an original figure from the 1965 paper is reproduced as Figure 1 here to show very succinctly how the PM theory began. Further developments of the AI Hypothesis (before and after its completion) and results of its world-wide testing from before-1952 to early 2001 have been reviewed in three monographs published respectively in 1984 (Ling 1984), 1992 (Ling 1992) and 2001 (Ling 2001.) The present communication describes results of a recent effort further to strengthen the theoretical foundation of the PM theory. Under normal condition, this is perhaps all I need to say in an introduction. Unfortunately, the time is not normal. And, accordingly, more needs to be included in the introduction.

The time is not normal because a man-made information embargo has blinded the world of biomedical science to most, if not all, the propitious new developments as well as to the disproof of the century-old membrane theory (Wu and Yang 1931, Kaplanskii and Boldyreva 1934, Nasonov and Aizenberg 1937, Kamnev 1938, Cohn and Cohn 1939, Heppel 1939, Steinbach 1940) as well as its later modified version called the membrane pump theory (Ling 1962, Chapter 8; for a later review, Ling 1997.)

Withholding vital knowledge from other researchers, teachers and generations after generations of students worldwide is a very grave offense with foreboding implications for the long term well-being and even survival of our species. And it would take the concerted efforts of many good people over a long period of time to set it right again. But before the eventual lifting of the global information embargo, and in order that the reader of

Symbols and Abbreviations: a, amount of water (or other gas) adsorbed per unit weight of adsorbent; α, polarizability; d, distance between nearest-neighboring N and P site of an NP surface; δ, distance between a flat and a curved glass surface; E, (negative) adsorption energy or (negative) interaction energy of water molecules; $E^{(i)(j)(k)}$, (negative) adsorption energy of water molecule located at the ith row, jth and kth column; E^n, (negative) adsorption or interaction energy of water molecule polarized by, but far from an idealized NP surface; ε_i, the ith quantum-mechanically allowed energy level; k, Botzmann constant; μ, the permanent dipole moment; $\boldsymbol{\mu}$, total dipole moment equal to the sum of permanent and induced dipole moment; N, a negatively charged site; P, a positively charged site; O, a vacant site; NP surface, a checker board of alternatingly P and N sites; idealized NP surface, see Figure 6; NO surface, a checkerboard of alternatingly N and O sites; PO surface, a checker board of alternatingly P and O sites; NP-NP system, a system of juxtaposed NP surfaces; NO-NO system, a system of juxtaposed NO systems; PO-PO system, a system of juxtaposed PO system; NP-NP-NP system, a system of a matrix of parallel arrays of fully extended linear chains carrying properly spaced N and P sites; p, vapor ressure; p_o, vapor pressure at full saturation; p/p_o, relative vapor pressure; P_o, (molecular) orientation polarization; P_d (molecular) distortion polarization; (p.f.), partition function, equal to $1 + \exp(-\varepsilon_1/kT) + \exp(-\varepsilon_2/kT) + \ldots \exp(-\varepsilon_r/kT)$; $(p.f.)_v$, partition function of water vapor; $(p.f.)_l$, partition function of liquid water; $(p.f.)_s$, partition function of solid ice I; r, distance between nearest neighboring water molecules; T, absolute temperature; T_m, melting temperature (of water); T_b, boiling temperature (of water); T_{mp}, melting temperature of polarized-oriented water; T_{bp}, boiling temperature of polarized-oriented water; u_f, enthalpy of fusion; u_v, enthalpy of vaporization; u_{fp}, enthalpy of fusion of polarized-oriented water; u_{vp}, enthalpy of vaporization of polarized-oriented water.

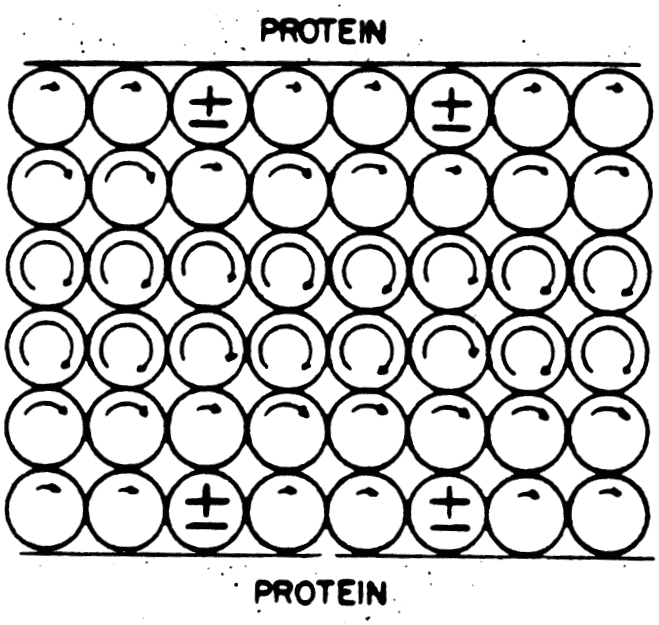

FIGURE 1. A section of the original graph that launched in 1965 the polarized multilayer theory — now modified to read polarized-oriented multilayer theory of cell water. In this theory, all cell water is dynamically structured. The decreasing length of the curved arrows in each water molecule indicates diminishing degree of motional freedom as one moves away from the protein surface — a concept that is contradicted by more recent evidence indicating a more even degree of polarization and orientation (See Discussion.) The figure also hinted at dipolar sites of proteins as the seat of polarization and orientation of cell water. This concept was more fully developed later (Ling 1970, 1972.) In this later view, backbone (dipolar) NH and CO groups offer the most important seats of water molecule polarization and orientation (modified after Ling 1965, by permission of New York Academy of Sciences,USA.)

this paper would be able to evaluate progress described below, it would be necessary to add something specific to this introduction. That something specific comes under two headings: (i) a summary of the PM theory and (ii) a short history of the investigation of multilayer adsorption of water vapor and other gases.

A summary of the PM theory and results of its 40 some years of world-wide testing

As extensive evidence reviewed in the three monographs mentioned above indicates (Ling 1984, 1992, 2001), the bulk-phase cell water does not exist in the form of normal liquid water — as widely believed and taught as truth even to this day. Instead, the weight of existing evidence suggests that the bulk of water in a typical living cell assumes the dynamic structure of polarized and oriented multilayers.

According to the AI Hypothesis, this dynamic structure and its propensity to undergo reversible changes enable cell water to play key roles in physiological activities at the most basic cell and below-cell level (Ling 2001, Chapters 14–15.) Many distinctive attributes of the living cells, — which in the conventional view of the living cell have been delegated to a host of often disconnected causes (e.g., the sodium pump, Dean 1941; tetracy-

cline pump, Hutchings 1969; arrow-poison pump, Ehrenpreis 1967, etc.) — may simply reflect various aspects of the polarized-oriented cell water and other adsorptions on cell proteins (Ling 1993, 1997; Ling *et al* 1993.)

According to the PM theory, the assumption of the distinctive dynamic structure by the cell water results from its interaction with some intracellular proteins. More specifically, the dynamic structure of cell water results from its direct or indirect interaction of cell water with the positively-charged NH groups (P sites) and negatively-charged CO groups (N sites) on the "backbones" of a pervasive matrix of fully-extended proteins. These P- and N-site-bearing proteins and the water molecules with which they interact constitute what is called a NP-NP-NP system. To explain what "NP-NP-NP system" stands for, I shall begin with its prototype or classic NP system and NP-NP system.

Electrical polarization and directional orientation of multiple layers of water molecules may occur under the influence of one or two (juxtaposed) checkerboard(s) of alternately positive and negative sites. See Figure 3 below for earlier publication of the same idea. Figure 2d shows two juxtaposed polarizing-orienting surfaces in what I call a NP-NP system.

Thc NP-NP-NP system mentioned above is a variant of the classic NP-NP system (Ling 1980-1981.) As such, a NP-NP-NP system exists in the form of properly spaced, orderly sequence of (free) N and P sites carried on a parallel array of fully-extended protein(s) or other linear water-polarizing-orienting polymer chains (See below and another new publication, Ling 2004a.) Parenthetically, water molecules may also be polarized and oriented in multilayers by a NO system or a PO system, in which electrically-neutral O sites replace properly-spaced electrically-charged P or N sites of a classic NP system respectively (Figure 2e, 2f.)

The aggregate physical impacts of the NP sites on the bulk-phase water may be somewhat arbitrarily divided into three components: to enhance the average water-to-water interaction of (all) the water molecules in the system (Component 1); to reduce the translational as well as rotational motional freedom of the water molecules (Component 2); and to prolong the stay or *residence time* of each water molecule at a specific preferred location (Component 3.) In statistical-thermodynamic terms, each of these three components refers respectively to a rise of the (negative) energy (or more precisely, enthalpy) of the system, a fall of its thermal entropy and a decrease of its configurational entropy.

In testing a theory on a subject as complex as life, cell physiologists do not have the luxury of following the footsteps of physicists, who have the freedom to choose the simplest system to study. Instead, cell physiologists must develop their own strategy best suited to cope with very complex systems. One of these involves a well-orchestrated study of suitable inanimate models side by side with their living counterparts. Vastly simpler in its makeup and usually more tolerant of harsh treatments, the inanimate models more readily reveal what are more important, and what are less important in producing the attribute, which the most cogent model and its living counterpart share. A cogent inanimate model which behaves like its living counterpart is called a *positive model*. A *negative model*, though sharing some attributes of the positive model, either does not, or does weakly what the living cell and its positive model does strongly — because in its makeup, a negative model does not possess one or more key qualifying attribute(s) demanded by the theory.

And if a theoretically predicted attribute is confirmed in both the living cell-protoplasm and a positive model but not or significantly less in the corresponding negative model, we

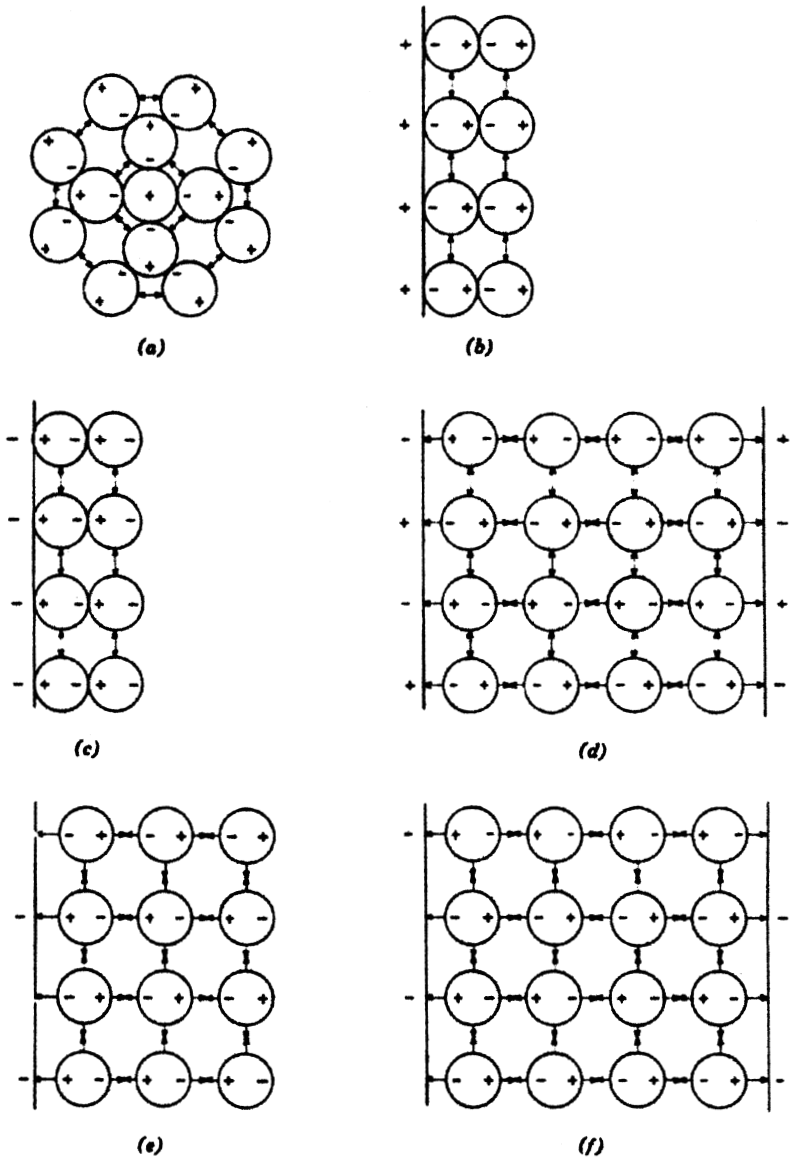

FIGURE 2. Diagrammatic illustration of the way that individual ions (a) and checkerboards of evenly distributed positively charged P sites alone (b) or negatively charged N sites alone (c) polarize and orient water molecules in immediate contact and farther away. Emphasis was, however, on uniformly distanced bipolar surfaces containing alternatingly positive (P) and negative (N) sites called an NP surface. When two juxtaposed NP surfaces face one another, the system is called an NP-NP system (d). If one type of charged sites is replaced with vacant sites, the system would be referred to as PO or NO surface (e). Juxtaposed NO or PO surfaces constitutes respectively an PO-PO system or NO-NO system (f). Not shown here is the NP-NP-NP system comprising parallel arrays of linear chains carrying properly distanced alternating N and P sites. Note how directions of paired small arrows indicate attraction or repulsion (modified after Ling 1972; reprinted by permission of John Wiley & Sons Inc.)

would call the combination a *triple confirmation*. A triple confirmation offers the reassurance that the investigator has probably been on the right track.

However, a failed model study (followed by a prompt and judicious response) may prove equally important in the long run. For it tells the investigator that it is time to consider seriously other alternative explanations. A scientific revolution with its usual sequel of rapid progress may then follow.

For testing the PM theory specifically, we have elected two kinds of inanimate models, referred to respectively as (positive) *extroverts* and (negative) *introverts* (Ling 1992 p. 107.) Extroverts include isolated proteins that by nature or for other reason exist substantially in the *fully extended conformation* (Ling 2004a.). This may result from an unusual amino-acid-residue composition (for details of the introduction of this interpretation, see Ling 1978; Ling *et al*, 1980; Ling 1992 p. 81) (e.g., gelatin, containing an abundance of non-helix-forming amino-acid residues proline, hydroxyproline and reluctant helix-forming glycine — see Eastoe and Leach 1958). Or it may occur on exposure to NH- and CO-group-exposing denaturants (e.g., urea, Ling 1992 Figures 5-6 and 5-7). *Extrovert* models also include other linear polymers carrying properly spaced atoms with available *lone pair* electrons (e.g., oxygen atoms in poly(ethylene oxide) or PEO for short.) A (concentrated) aqueous solution of PEO constitutes a NO-NO-NO system.

In contrast, *introvert* models, which include most globular proteins like native hemoglobin, act differently. With most of their polypeptide chains NH and CO groups neutralized and shielded in forming intra-molecular H bonds, they do not alter the property of bulk-phase water or do so only weakly (Ling 1992, pp.107–110; Ling and Hu 1988.)

As shown in the following, the PM theory of cell water has witnessed world-wide triple confirmation on all eight major physiological traits investigated in depth thus far.

(1) (Lengthening of) NMR rotational correlation time (τ_c) (Cope 1969; Hazlewood *et al* 1969, Damadian 1971, Ling and Murphy 1983); (2) (lengthening of) Debye reorientation time (τ_D) (Clegg *et al* 1984; Kaatze *et al* 1978); (3) (reduction of rotational diffusion coefficient from) Quasi-elastic neutron scattering (Trantham *et al* 1984; Heidorn *et al* 1986; Rorschach 1984); (4) vapor sorption at near saturation vapor pressure (Ling and Negendank 1970; Ling and Hu 1987); (5) freezing point depression (Chamber and Hale 1932; Miller and Ling 1970; Ling and Zhang 1983); (6) swelling and shrinkage (Ling 1987; Ling and Ochsenfeld 1987); (7) osmotic activity (Ling 1992 p. 101; Ling and Walton 1976); but above all (8) solute distribution, which could and did yield unequivocal, quantitative data on the amount and the mutual interaction energy of altered water in a sample (see below; also Ling 1965, 1970 and 1972; Ling and Hu 1988; Ling and Ochsenfeld 1989; Ling 1993 and Ling *et al* 1993.)

As mentioned above, I have divided the impact of a NP system/NP-NP system or their variants on the bulk-phase water into three components. Based on this system, one may say that studies (1), (2) and (3) listed above have confirmed the predicted motional restriction of water molecule (Component 2.) Study (4) has confirmed the increased localized residence time (both Component 1 and Component 3.) Studies (5) and (7) have confirmed the predicted enhanced water-to-water interaction energy (Component 1 and Component 3.) Studies (6) and (8) have confirmed both Components 1 and 2.

The combination of these eight sets of mutually supportive triple confirmations, offers strong confirmation of the PM theory in specific and the AI Hypothesis in general. However, there are other challenges that so far have not been fully met by investigators pri-

marily interested in cell water. As will be made clear below, recent progress to be described below has changed all that.

Beyond the introvert and extrovert models, there are other inanimate systems discovered or created by workers in a different field, and yet exhibit behaviors and properties, which often in grossly exaggerated manner resemble those of *bona fide* positive models of the PM theory. It is conceivable that further attention to these *inadvertent positive models* may offer insight, which in its milder form seen in the more familiar extrovert models, might be masked and therefore undetectable.

Thus, many such inadvertent models for the PM theory can be found among widely scattered older reports, which describe layers of water hundreds, thousands and even tens of thousands molecules deep that are profoundly altered in their properties by contact with a foreign surface like glass (for a rich collection of these highly provocative findings reported before 1949, see "The Depth of the Surface Zone of a Liquid", a fine critical review by J.C. Henniker of the Stanford Research Institute published in the *Review of Modern Physics*, 1949. See also Drost-Hansen 1971; Israelachvili and Adams 1976; Peschel and Belouscheck 1979; Deryaguin 1933, 1987; Deryaguin and Landau 1941.) Anticipating a more detailed discussion below, I mention very briefly just one striking example published 7 years after the Henniker review.

Prof. Takeo Hori of the Institute of Low Temperature Science of the Hokkaido University, Japan showed that water films, thousands of molecules thick, would not freeze and turn into ice at a temperature as low as –90° C, if that water is held between two polished glass surfaces (Hori 1956; Ling 1970, 1972.)

The relevance of this reported "nonfreezing water" to our study of water in living cells would become self-evident from two well-established facts: (1) Human embryos, like all other living beings, are largely made of water. (2) Human embryos can be kept for a long time at liquid nitrogen temperature, (which could be as low as –195.8° C) and then promptly resume normal development into healthy human beings by merely thawing and warming to normal body temperature (Polge *et al* 1949, Rall 1987, Wennerholm *et al.* 1998.)

With both facts in mind, one sees that *being alive* is cogently modeled not only by inanimate systems existing at an ambient or body temperature, it can also be cogently modeled by inanimate systems existing at a severely cold temperature.

Hori's non-freezing water between polished glass surfaces has yet something else to offer. That is, other than serving as an appropriate model for cell water in the cold, it is also in fact a highly instructive inanimate model of even broader significance. For unlike the living cell itself and the extrovert models we studied extensively thus far, all of which represent the derivative NP-NP-NP systems, non-freezing water film held between polished glass surfaces represents a *bona fide classic NP-NP system*.

A short historical background of the PM theory of cell water and model systems

The physical phenomenon *adsorption* is, according to the AI Hypothesis, central to all basic physiological phenomena. The word and concept of, adsorption, was first introduced by Gehler (1825) but soon forgotten. It was reintroduced by H. Kayser 46 years later at the suggestion of Emile Du Bois-Reymond, one of the four great physiologists of the mid-19th Century nicknamed the *Reductionist Four* (McBain 1932 p. 7.) As if they were one, Du Bois-Reymond and his friends vigorously fought for their belief that the laws governing the behaviors of the dead world, also govern the living (Rothschuh 1973.).

In its modern definition, adsorption signifies the *association* of molecules and ions with solid surfaces, macromolecules or other fully or partly immobilized systems. For this reason, the title, association-induction hypothesis begins with the word, *association*. The second word, *induction* or electric polarization, is also portrayed in the polarization (and orientation) of cell water. But that is not all it signifies. For in the AI Hypothesis, induction is a part of the general molecular mechanism of information and energy transfer over distance in living cells (Ling 1962, Chapters 5, 6; Ling 1984, Chapter 7; Ling 1992 Chapters 6, 7 and Ling 2001, Chapters 14, 15.)

A shirt may smell of tobacco after a party. That is an example of adsorption of odorous gaseous products of burning tobacco on the cellulose of a cotton shirt. But historically, it is burned cellulose of wood, or charcoal that has been the favorite material for studying this phenomenon of adsorption. Thus students once attending classes in the 19th century, and even later years might have witnessed a dramatic laboratory demonstration introduced by Abbé Fontana of Italy in the 18th century. A piece of glowing charcoal was plunged into a pool of mercury. Thus cooled, the charcoal was allowed to float up into an inverted gas-filled glass tube. The subsequent rapidly rising level of mercury in the glass tube eloquently demonstrates the strong affinity of charcoal for gases of all kinds previously introduced into the glass tube (McBain 1932 p.1.)

To explain gas adsorption by charcoal, two kinds of theories were introduced known respectively as the *condensed thick film theory* of the old physicists and the *capillary condensation theory* of a later crowd.

In the condensed film theory, long-range attractive forces emanating directly from the solid surface hold deep layers of gas molecules captive on or near the solid surface (Saussure 1814; Polányi 1914.) This view, according to McBain, was eventually abandoned because no such long-range force could be found. Direct forces between molecules and even ions are short in reach, rarely going beyond one or two molecule diameters. However, in more recent years Israelachvili and his coworkers (Israelachvili 1985, 1987; Israelachvili and Adams 1976) appeared to have introduced their version of direct long-range force on distant water molecules that seem to resemble in appearance at least the old condensed thick film theory (Compare Figure 7 of Israelachvili's 1987 paper with Figure 136 in McBain's 1932 book.) (See Discussion.)

For a long time, the most popular view on the adsorption of deep layers of water vapor and other gases was the *capillary condensation theory* (Zsigmondy 1911.) As well known then, when a glass capillary is dipped into water, the water level inside the capillary rises to much higher than that outside the capillary. Since charcoal is highly porous and presumably contains many fine interstices behaving like the enclosed narrow spaces in glass capillaries, it was postulated that water and other gases would condense inside these internal capillaries just as water does in regular stand-alone capillaries. Eventually, this model too was abandoned. The interstices in charcoal were found to be only molecular in dimension and thus far too narrow to act like glass capillaries in sucking up columns of water (Coolidge 1926.)

Then Irving Langmuir dramatically revolutionized the basic concept of adsorption by his theory of *localized monomolecular adsorption* (Langmuir 1918, 1921.) That is, each adsorbed gas molecule does not just freely roam around in the vicinity of the solid surface but occupies a specific location or *adsorption site* on the surface for a finite lifetime (until it leaves). Langmuir introduced a mathematical expression of his concept later known as the *Langmuir adsorption isotherm* or simply *Langmuir equation*.

The Langmuir equation predicts that the uptake of a gas is strong at lower vapor pressure, becoming weaker and weaker as the vapor pressure increases until it becomes flat altogether. Thus, as a whole, the adsorption curve looks like a lying-down inverted letter, J. The sorption of CO_2 in charcoal follows this pattern (Zeise 1928.) The adsorption curve of water vapor in charcoal, on the other hand, looks more like a flattened letter S (Coolidge 1927; McBain 1932 Figure 52.). That is, weak uptake occurs at low vapor pressure followed by abruptly stronger uptake at higher vapor pressure.

While the condensed thick film theory and the capillary condensation theory were holding sway, other scientists offered what were at the time less popular ideas. One is called the *laminated or enchained multimolecular film theory*. In this, a series of monomolecular layers of gas molecules collect on the solid surface such that each layer is adsorbed on the layer immediately beneath it except the last one, which adsorbs directly on the solid surface. Among the earliest advocates of this theory was the same H. Kayser of Germany (1881), who as mentioned earlier, reintroduced the concept of adsorption. Another 38 years later, de Boer and Zwikker further pursued this line of thinking.

What de Boer and Zwikker did was to offer for the first time an analytically-derived isotherm for the S-shaped adsorption of neutral gas molecules on solid surfaces. They gave their theory the title, *Polarization Theory* (de Boer and Zwikker 1929.) Furthermore, they pointed out how a checkerboard of alternatingly positive and negative sites on the surface of a salt crystal might enhance multilayer adsorption of gas molecules. To give due credit for this then-original concept, I have reproduced two of their original figures (their Figure 3 and 4) as Figure 3A and 3B respectively in the present paper. Shortly after de Boer and Zwikker published their paper, Bradley derived two similar adsorption isotherms one for gas molecules *without* a permanent dipole moment, the other one for gas molecules *with* a permanent dipole moment (Bradley 1936a, 1936b.). These three isotherms, (one) by de Boer and Zwikker and (two) by Bradley, can all be written in the form:

$$\log_{10}(p_o / p) = K_1 K_3^{a} + K_4, \tag{1}$$

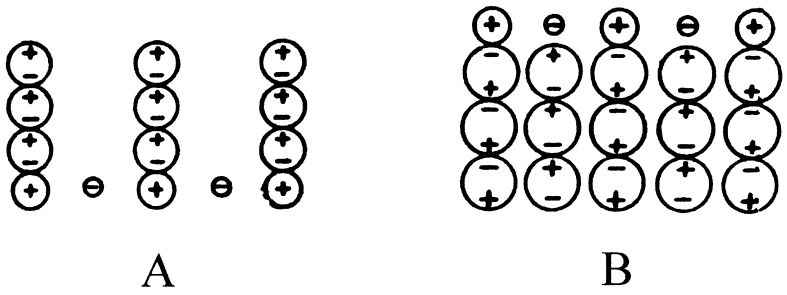

FIGURE 3. Reproduction of figures presented in the paper by de Boer and Zwikker in 1929, showing their vision of a checkerboard of alternating negatively-charged and positively-charged sites and two different ways as to how gas molecules might adsorb on them as polarized multilayers. These checkerboard of alternating positively-charged and negatively charged sites are what later I call the NP surface, a concept of considerable importance in the subsequent developments of the PM theory. The reproduction of their figures reminds us of the contribution de Boer and Zwikker made in 1929. A and B are respectively what they labeled as Figure 3 and 4 respectively in their original paper.

where a is the amount of gas taken up by a unit weight of the absorbent, p is the existing gas pressure and p_o the pressure of the gas at full saturation. Thus p_o/p is the reciprocal of the relative vapor pressure, p/p_o. The respective meanings of K_1, K_3 and K_4 are different in each of the isotherms. In all, they are constants at a fixed temperature. Equation 1 can also be written in the double log form:

$$\log_{10} [\log_{10} (p_o/p) - K_4] = a \log_{10} K_3 + \log_{10} K_1. \quad (2)$$

If a set of numerical values can be found respectively for K_1, K_3 and K_4 such that the experimentally measured amounts of water sorbed (a) at different relative vapor pressure (p/p_o) can be shown to be rectilinearly related to the reciprocal of the modified relative vapor pressure (i.e., that represented by the entire left-hand-side of Equation 2), one then regards the data as fitting the theoretical isotherm shown as Equation 1 (or 2.)

As mentioned, de Boer and Zwikker envisaged in 1929 a surface of salt crystals as a checkerboard of alternating positively- and negatively-charged sites (Figure 2c and Figures 3A and 3B.) These fixed electric charges then induce electric dipole moments in a layer of gas molecules in immediate contact with the charged sites of the salt crystal surface. The induced dipole moments thus generated in the first layer of adsorbed gas molecules in turn induce dipole moments in the second layer of gas molecules and this process repeats itself many times until a deep layer of adsorbed gas molecules is achieved. To repeat, in the de Boer-Zwikker polarization theory, the force holding layers of gas molecules away from the solid surface is entirely attributed to the *induced dipoles* and to nothing else beyond the induced dipoles.

de Boer and Zwikker knew, of course, that many gas molecules like (vapor) water possess *permanent dipole moments*, which arise from the asymmetrical distribution of the positive charges (carried on the hydrogen atoms) and the negative charge (carried on the oxygen atom) in a water molecule. But they decided to ignore these permanent dipole moments, arguing that thermal agitation makes their orientation near the salt crystal surface constantly changing. In Part I of his 1936 paper, Bradley also ignored the permanent dipole moment but for a less controvertible reason — he was addressing in that paper specifically *only* gas molecules without a permanent dipole moment (e.g., argon.) But in presenting a **general theory** for gases of all kinds in Part II of his paper, Bradley did take into account the permanent dipole moments.

Brunauer, Emmett and Teller (the Teller of the H bomb fame) (1938) took issue with de Boer and Zwikker's Polarization Theory as well as Bradley's theory on sorption of non-polar gases on salt crystal surfaces. Brunauer *et al*'s main criticism centers on the dimensionless term α/r^2 — where α is the *polarizability* of the gas molecule and r the distance between the nearest neighboring adsorbed gas molecules. They showed that even in gas molecules with a very large polarizability like argon, its α/r^2 is still too low to allow a propagation of electric polarization to beyond the first layer. However, they did add this. "...if the adsorbed gas has a large permanent dipole it is possible that many layers may be successfully polarized by the mechanism of de Boer and Zwikker. This case has been treated by Bradley" (Brunauer *et al* 1938, p. 311.)

That, however, was all Braunaer *et al* said on the subject of adsorption of gas molecules with permanent dipole moment. Nor to my knowledge have de Boer and Zwikker nor Bradley responded to Brunauer *et al*'s criticism.

Meanwhile, Brunauer, Emmett and Teller (1938) had introduced a theory on multilayer gas adsorption of their own. In time this theory has become broadly known as the BET theory after the first letters of the three authors's respective names. Cassie (1945) and later Hill (1946) made improvements on the BET formulation of multilayer adsorption of gas molecules.

Now, in Bradley's multilayer adsorption theory for polar gas molecules, the gas molecules adsorbed at low as well as high vapor pressure are polarized respectively by the solid surface charges and by neighboring water molecules. In the BET theory, on the other hand, only the small number of gas molecules in direct contact with the adsorption sites is adsorbed, the remaining great majority of gas molecules is simply normal liquid water and as such not additionally polarized on account of their (non-immediate) propinquity to the solid surface.

Thus, although the authors did not make this point clear, the BET theory in fact represents a return to the capillary condensation theory (minus pores and interstices) as envisaged by Coolidge (1926, 1927, see also McBain 1932, p. 147.) In this connection, a new question arises, Have Brunauer and coworkers by at once endorsing Bradley's theory, (in which all adsorbed molecules are polarized) and advocating their own BET theory, (in which only gas molecules immediately in contact with the solid surface are polarized) contradicted themselves? As far as I know, they have not publicly provided an answer to this question.

Actually, this conflict does exist. But it might be readily resolved by making an additional assumption. That is, gases without a permanent dipole moment like argon follow the BET theory. (For reservation on account of some additional theoretical problem with the BET theory, see Cassie 1945, p. 450.). Gases with a large permanent dipole moment like (vapor) water follow the Bradley isotherm. In fact, experimental support for this dual assignment already exists in the literature.

In 1965 I analyzed Bull's data on the adsorption of water vapor on two proteins, collagen and sheep's wool (Bull 1944). At low vapor pressures, the data can be described well by the BET theory. At vapor pressure higher than 50%, however, theory and data diverge sharply (Ling 1965.) In contrast, at low as well as high vapor pressures, water sorption on both collagen and sheep's wool fit the Bradley isotherm.

Similarly, if one views together the incisive findings of Benson, Ellis and Zwanzig (1950) on one hand and Hoover, Mellon and their coworkers (1950) on the other, one also finds support for this duality.

Thus, Benson and Ellis showed that the adsorption of non-polar gases like nitrogen on frozen-dried (lyophilized) proteins follow the BET theory (Benson and Ellis 1948.) Furthermore, the amount of gas taken up depends entirely upon the state of division of the frozen-dried (or lyophilized) proteins, the finer the division, the higher the uptakes.

In contrast, the adsorption of water molecules (with its large permanent dipole moment) on the same lyophilized proteins is, firstly, several orders of magnitude higher than the uptake of non-polar gases (Benson *et al* 1950.) Secondly, the uptake of water vapor is totally independent of the state of division of the proteins — in diametric contrast to the uptake of non-polar gases. Instead, the uptake of water vapor is entirely dependent upon the chemical structure of the protein. What is that structure favoring water adsorption as polarized multilayers? To that question, Hoover and Mellon have also provided a clear answer.

Hoover and Mellon (1950) studied the sorption of water by polyglycine and silk on one hand and by wool and ovalbumin on the other. At vapor pressure from 0.05 to 0.95, all

four sets of data fit a simplified version of the Bradley adsorption isotherm. Now, as potential water-adsorbing sites, polyglycine has (virtually) only the positively-charged NH groups and negatively-charged CO groups on its backbone. Yet the maximum uptake of water vapor by polyglycine matches that of sheep's wool, which carries as potential water-adsorbing sites both backbone CO and NH groups and polar side chains including β- and γ-carboxyl groups, ϵ-amino groups and hydroxyl groups, for example.

Such a comparison led Hoover and Mellon to conclude that the major seat of water adsorption on proteins is the positively charged NH and negatively charged CO groups of the protein backbone. Their conclusion is in harmony with a similar but earlier view of Lloyd herself (1933) and of Lloyd and Phillips (1933) and with a later view of Ling in his PM theory, according to which the NH and CO groups of the backbones of a parallel array of fully-extended protein chains polarize and orient the bulk of cell water (Ling 1970, 1972.)

In summary, the two sets of experimental data described briefly above also verify the idea that the BET theory is applicable only to the adsorption of non-polar gases. For polar molecules like water, the BET theory is not applicable while the Bradley theory is.

In further testing the PM theory of cell water, Ling and Negendank (1970) demonstrated that the equilibrium water contents of surviving frog muscle cells at different relative vapor pressure ranging from near-zero (4.3%) to near saturation (99.6%) fall into two fractions. A small fraction (5%) of the cell water begins and completes its strong adsorption at very low vapor pressure (apparently all on polar side chains, see Leeder and Watt 1974.) This fraction can be described by a Langmuir monolayer adsorption isotherm. The remaining 95% of cell water follows the Bradley adsorption isotherm all the way up from 4.3% to 99.6% relative vapor pressure (Figure 4.)

This work of Ling and Negendank represents the first of its kind on the water vapor sorption of surviving (frog muscle) cells from near zero to 99.6% saturation. Furthermore, the data (Figure 4) shows that fully 3/4 of the water uptake of these cells occurs at above the relative vapor pressure of 95%, which is the upper limit of the great majority of earlier publications on water sorption *in vitro* on proteins and polymers.

Moreover, the water vapor uptake of frog muscle cells matches quantitatively McLaren and Rowen's data on the water sorption of poly(glycine-D,L-alanine), which like polyglycine mentioned above carries its water adsorbing sites almost exclusively in the form of backbone NH and CO groups (McLaren and Rowen 1951.) This quantitative matching between the water uptake of polyglycine-D,L-alanine and that of surviving frog muscle shown in Figure 5 was one of the earliest evidence I cited in support of the PM theory that the bulk of cell water is adsorbed on the backbone NH and CO groups of a matrix of *fully-extended* intracellular proteins chains (Ling 1972, p. 697.)

Further confirmation of the dipolar backbone NH and CO groups as the primary seat of water sorption — but especially the carbonyl oxygen atoms with its lone pair electrons — came from Ling and Hu (1987.) They demonstrated that at physiological relative vapor pressure (0.996), the uptake of water vapor by frog muscle also matches that by poly(ethylene oxide) (and other oxygen-carrying linear polymers,) on which the only hydrophilic groups are the oxygen atom with its lone-pair electrons.

Seen side by side with other data like those of Hoover and Mellon discussed above, Ling and Negendank's finding represented a step forward in verifying the PM theory. Indeed, on various occasions of the past, the Bradley isotherm (with the explicit endorsement of Brunauer, Emmett and Teller) has been cited as the theoretical-physical foundation of the PM theory.

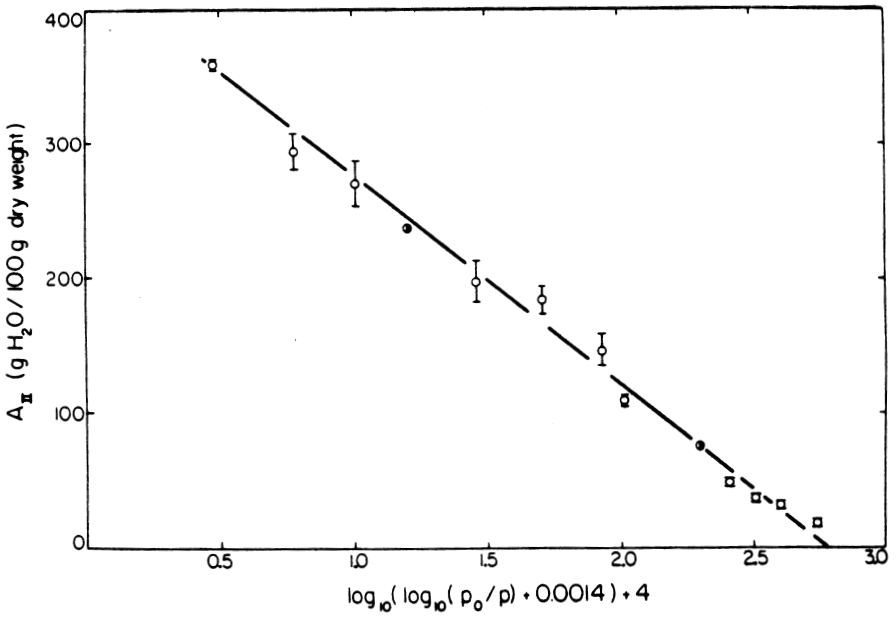

FIGURE 4. Water sorption isotherm of isolated surviving frog muscles. Data on 95% of the muscle water. The remaining 5% of muscle water is completed at very low relative water vapor pressure (p/p_o); it is described by a Langmuir adsorption isotherm and has been subtracted from the total water uptake to yield the data points plotted in the graph. Straight line plot indicates obedience to the Bradley isotherm. Half filled circles were from time course studies. (From Ling and Negendank, 1970.)

However, as the mounting experimental evidence has all but established the general validity of the PM theory of cell water, the Bradley theory, in comparison, has slowly fallen behind as a sort of a limping ally that is helpful but also hard to defend with conviction. And unless strengthened by new development, this weak theory might actually become a handicap for future progress. But before entering into a detailed analysis of my reasons for this concern, I would like to cite what another scientist did and did not do that might shed some light on the issue.

That scientist is the reviewer, J.C. Henniker mentioned earlier. In his 1949 review, he stated on page 323 of Volume 21 of the *Review on Modern Physics* that the "theoretical basis for adsorption in multilayers is firm. The isotherm of Brunauer, Emmett and Teller is based on more than one layer and is experimentally justified." But in my view, this is, strictly speaking, not entirely correct. The bulk of the deep layers of water found near (appropriate) solid surfaces, with which Henniker's review dealt, exhibits properties exquisitely different from those of normal liquid water. In contrast, (and as made clear above,) in the BET theory the bulk of water collecting on solid surfaces is simply normal liquid water. But more relevant to the question here on the strength and weakness of the Bradley isotherm, is its total omission. That is, Henniker made no reference to Bradley's theory of multilayer adsorption at all — even though it was up to now the only published theory of multilayer adsorption of gas molecules with large permanent dipole moment, and even though it was explicitly endorsed by Brunauer, Emmett and Teller in the same paper in

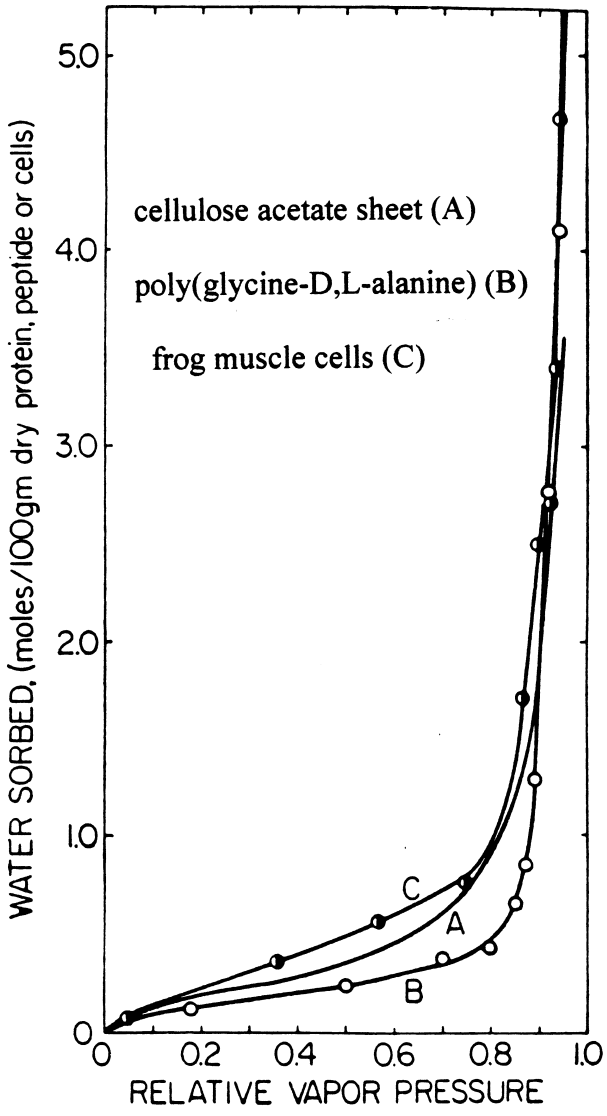

FIGURE 5. The strikingly similar steep uptake of water molecules at relative vapor pressure close to saturation of surviving frog muscle cells (marked C) and of the synthetic polypeptide, poly(glycine-D,L-alanine) (marked B, data of McLaren and Rowen, 1951), one finds evidence that the backbone NH and CO groups (which are virtually all the functional groups that can interact with water molecules in this synthetic polypeptide) are the major seats of (multilayer) water adsorption in living cells as suggested in the polarized-oriented multilayer theory of cell water. The third curve from unpublished work of Palmer and Ling shows that water taken up by commercial cellulose acetate sheets are similarly adsorbed on dipolar sites — a matter of great significance because later work of Ling (1973) shows that the permeability of this membrane strikingly resembles the permeability of a live membrane (inverted frog skin.) (Figure reproduced from Ling 1972; reprinted by permisssion of John Wiley & Sons Inc.)

which Brunauer, Emmett and Teller presented their own BET theory, which Henniker gave admiring recognition.

One possible explanation for this omission is that it was deliberate despite Brunauer, Emmett and Teller's endorsement. Thus, Henneker himself might have discovered that the Bradley isotherm has problems that Brunauer, Emmett and Teller had overlooked.

Now that we have reason to believe that the BET theory is only applicable to non-polar gases, the theoretical foundation for the adsorption of multilayers of polar gases like water is thus less firm than Henniker's statement cited above appeared to indicate. Perhaps this unstated uncertainty is also what prompted Henniker to say early in his review that "A basic theoretical treatment has not been attempted in this paper,…" Subsequent history, however, shows that neither Henniker nor anyone else has to my knowledge written such a basic theoretical treatment, nor even a follow-up of Henniker's masterful review — notwithstanding new observations of deep layers of altered water on solid surfaces like those described by Hori continued to accumulate.

Whatever the true reasons might be for the less than enthusiastic subscription to Bradley's isotherm, the net result is that the study of long-range water adsorption on solid surface has become more and more shunted to the side line. That one of the chief advocates of the concept of long-range water interaction, the talented and capable B.V. Deryaguin, has suffered a setbback — for making the (honest) mistake of believing in the existence of (non-existing) "polywater" — might have added another confusing and false reason for skepticism toward long-range water adsorption. But in my view, things may change and change soon. It is too exciting to stay suppressed for long.

The difficulty that had thwarted de Boer & Zwikker as well as Bradley

The weakness and even downright failure of the de Boer-Zwikker and Bradley theories do not reflect on the authors's knowledge and skill. Rather, in my view it is an almost inescapable consequence when a capable physicist attempts to achieve the same level of sophisticated mathematical formulation they have been accustomed to in dealing with simpler subjects, in dealing with a problem that is, by nature, unalterably complex.

And in order to make things manageable mathematically, de Boer and Zwikker decided to throw the permanent dipole moment out of the window — with disastrous result. Of course, Bradley did not throw the permanent dipole moment out of the window. He threw out something else. Namely, the fixed negatively charged N sites on the surface of salt crystals.

His explanation for this omission was that the anionic N site are too large, a lame explanation at best, not to mention that his announced intention was to write a *general theory* for gas adsorption on various salt crystals some with large and others with small anions. This omission of the N sites does not end up with what I call a PO system, which would be still relevant. Rather, it became what I would call a PP system, in which all surface sites are positively charged P sites with lateral repulsion between nearest neighboring adsorbed gas molecules. All in all, this elimination alone has created a model no longer compatible with adsorption on most salt crystal surfaces as Bradley intended to do or with the classic NP and NP-NP systems of the PM theory.

As Bradley pointed out himself, numerical fitting of experimental data to his isotherm (Equation 1 or 2) does not prove that the data follow the theory. Nor does fitting the Bradley isotherm provide answers to various important questions. Thus, fitting the isotherm does

not tell us why the permanent dipole moment is so vital that its elimination has invalidated both the de Boer-Zwikker and Bradley's own isotherm for non-polar gas adsorption. Nor does fitting the Bradley isotherm offer even a hint if this theory can explain the polarization and orientation of all of the cell water — let alone the truly long-range impact of polished glass surface on water molecules thousands of molecules thick as reported by Prof. Hori. In general, fitting the Bradley isotherm does not provide quantitative data on the adsorption at all.

Now, to seek new ways to find answers to these important questions, we must first determine what specific obstacle has prevented de Boer and Zwikker as well as Bradley from producing a more powerful theory. And why did Brunauer, Emmett and Teller not take notice of the weakness of the Bradley isotherm for polar gases and give their unqualified blessing? And why did Brunauer, Emmett and Teller not derive a theory better than the BET theory they introduced, which cannot explain multilayer adsorption of water molecules and other polar gases?

A careful reading of the papers from de Boer and Zwikker and from Bradley shows quite clearly that they were plagued by the effect of thermal bombardment on the orientation of the permanent dipole moments of the gas molecules. It is the *uncertainty* thus created by heat on the orientation of the permananent dipole moments that has undermined the theory of de Boer and Zwikker as well as of Bradley.

A shortcut to a simple but more rewarding new theory

I now suggest that there is a short cut to get around the difficulty that had so far hampered all workers on multilayers adsorption of polar molecules on salt crystal surface. That short cut is *via* lowering the temperature of the model to one or two degrees above absolute zero.

For at this low temperature, the kinetic energy of the water molecules kT approaches zero and the thermal bombardments, to all intent and purposes, come to a stop. And in that quiet setting, electrostatics in all its simplicity and certainty takes over. If I am not wrong, quantitative knowledge on the polarization and orientation of water and other polar molecules on solid surfaces that have eluded de Boer-Zwikker and Bradley might be within reach. However, for this near absolute zero strategy to work, water must not freeze as the temperature is brought down lower and lower. For the moment, one must take it on faith. Rigorous proof will come later (p. 117.)

Theory

As well known, as yet no widely-accepted theory of the structure of liquid water exists. There is no shortage of theories. But at the current state of their developments, these models are too complex, As such, they do not lend themselves readily to helping me solve the very simple specific problems of the PM theory

As mentioned above, I chose a much simpler approach. The tetrahedral structure of water molecules, the H-bonds formed among them and many other related advanced knowledge on liquid water and protein structure will be shelved for now. In their place, each water molecule is treated as a simple dipole possessing a permanent dipole moment of 1.86 Debye (1.86×10^{-18} e.s.u., Moelwyn-Hughes, 1964; see also Sänger and Steiger 1928; McClellan 1963; Eisenberg and Kauzmann 1969, p.12) and a polarizability of

1.444 x 10^{-24} cm^3 (Conway 1952). This approach is nothing new to the reader. For example, it is that underlying the development of the de Boer-Zwikker as well as of the Bradley multilayer adsorption isotherm.

I began by considering an infinitely broad but thin solid sheet. The upper surface of this solid sheet is perfectly smooth and fully covered with a checker board of alternatingly positively-charged and negatively-charged sites, called an *idealized NP surface* as illustrated in Figure 6 and more fully described in the paragraph following the next one.

The other surface of the thin solid sheet is in intimate and full contact with a metallic conductor which is cooled by a powerful but carefully-controlled refrigeration system. The surface of the sheet carrying the N and P sites faces an open space filled with a flowing stream of *pure* water vapor at a pressure and temperature just below the triple point (Figure 7.) As the solid sheet and its N and P sites are being cooled by conduction (only), water molecules that have condensed on the NP surface are rapidly cooled to a lower and lower temperature. The perfectly orchestrated condensation and cooling of water molecules continue until an infinitely deep layer of condensed water chilled to the temperature close to absolute zero is obtained.

Each of these N sites on the *idealized NP surface* is separated from its nearest neighboring P sites by a distance, d. For an idealized NP surface, d is or close to 3.10 Å. We chose this d value because it is equal to what we can figure out to be the average distance

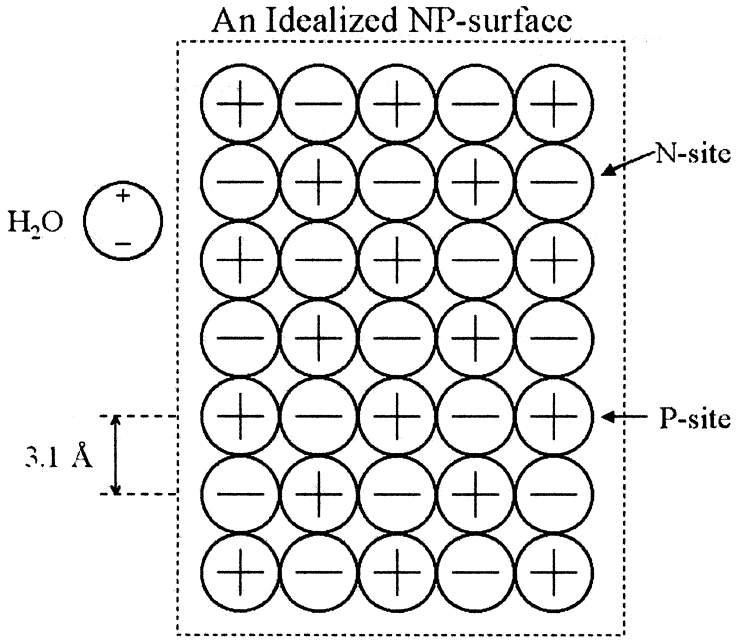

FIGURE 6. An idealized NP surface. The distance between a pair of the nearest-neighboring N and P site in the idealized NP surface is represented by the letter d and it is equal to r, the average distance between two nearest-neighboring water molecules in normal liquid water and is estimated at 3.1 Å .

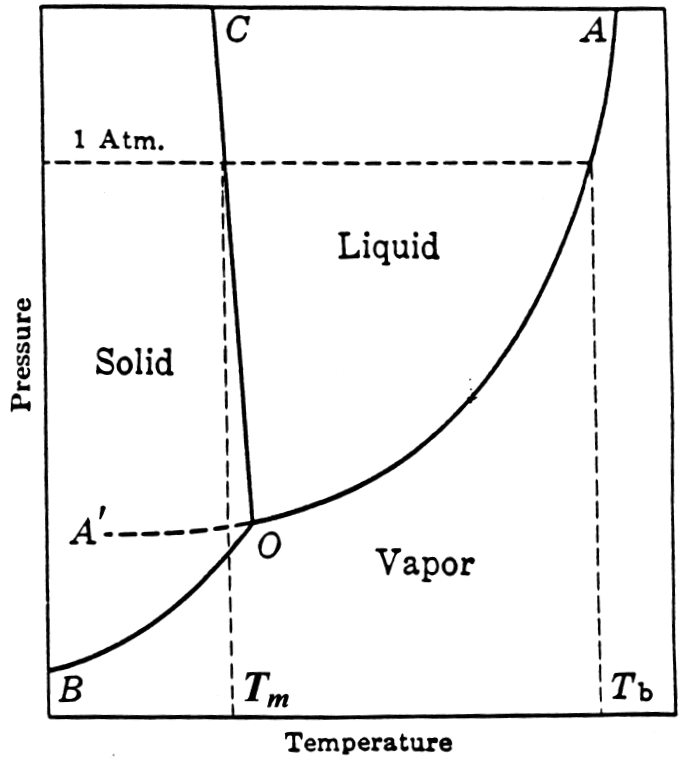

FIGURE 7. A phase diagram, showing solid-liquid-vapor equilibria. T_m and T_b are respectively the melting temperature and the boiling temperature. O represents the triple point. The sharpness of the transitions demonstrate intensely (auto)cooperative nature of the transitions (Modified after Glasstone, 1946; Ling 1980.)

between one liquid water molecule to its immediately neighboring water molecule and called r. The distance r is obtained by taking the cube root of the "unit cell volume" of each liquid water molecule, which in turn is obtained by dividing the molar volume of water equal to 18.016 cm^3 by the Avogadro number, 6.023 x 10^{23}.

Next, I assume that each of the fixed N or P site carries one-half of a negative or positive electronic charge (1/2 x 4.804 x 10^{-10} e.s.u. = 2.402 x 10^{-10} e.s.u.) and that these electronic charges are each located d/2 or 3.104/2 = 1.552 Å from the center of the nearest water molecule. Furthermore, in my entire treatment, only electrostatic interactions between the nearest neighboring molecules or sites are considered. The justification for these choices will come later.

Let us first consider the successive layers of water in immediate contact with our idealized NP surface as the ith layers with i = 1, 2 and n. Next we focus our attention on a specific reference N site in the middle of the checkerboard of N and P sites and call the columns of individual water molecules going left-right from the reference N site as the jth and the columns of individual water molecules back and front from the reference N sites as the kth.

The immediately neighboring columns to the left and to the right of the N site are then referred to as the j−1 and j+1 column respectively. The immediately neighboring column to the front (toward the reader) and back of the reference N site as k+1 and k−1 respectively. The single column of water molecules going through the reference N site is then seen at once as j=0 and k=0. A water molecule designated 3(+2)(−4) is located in the 3rd row, the second column to the right and 4th column away (from the reader) from the reference N site. On the other hand, 2(0)(0) is the water molecule in the second row in the column j=0 and k=0.

In most cases, each water molecule is surrounded on all four sides by four other water molecules with their permanent dipoles oriented in the opposite direction to its own. And, with the exception of the water molecules in the first row, each water molecule is also in contact with two neighboring water molecules with their permanent dipole moment oriented in the same direction as its own, one in front of, or closer to the NP surface and another one behind it. As mentioned, there is an exception to this rule of four surrounding oppositely-oriented neighbors and two similarly oriented ones in front and behind. The exception is the water molecules in the first row. In this case, each water molecule faces either an N or P site on one side and oppositely oriented water dipoles on all four sides in the same row and only one water molecule oriented in the same direction in the row behind.

Now the electric field due to a point charge, ε, is ϵ/r^2, where r is the distance between the point charge and the point of measurement. The (negative) interaction energy of the negative electric charge on the N site with the permanent dipole, μ of an adjacent water molecule 1(0)(0) at a distance d/2 away — without taking into account the favorable induced dipole the point charge produces and interacts with — is $\varepsilon\mu/(d/2)^2$. And accordingly, it equals

$$(2.402 \times 10^{-10} \times 1.834 \times 10^{-18})/ (1.552\times10^{-8}/2)^2 = 2.838\times10^{-12} \text{ ergs/molecule},$$

equivalent to 40.82 kcal./mole. This is more than four times stronger than the (negative) water-to-water interaction energy in liquid water at its boiling point (9.7171 kcal/mole, Rossini *et al*, 1952.) Here we see how a fixed N (or P) site strongly adsorbs a water molecule and in so doing also orients the water molecule with the positive end of the water dipole facing the negatively-charged N site and the negative end of the water dipole pointing to the opposite direction.

This simple dipolar model offers other distinctive important insights. Thus, it shows without ambiguity not only the *attraction* among water molecules oriented the right way, it also provides a quantitative information on the *repulsion* a pair of nearest-neighboring water dipoles experiences for one another when they are oriented in the "wrong" way. Strong attraction for the right orientation coupled to strong repulsion for alternative wrong orientations ensures a specific, ordered and mutually enhancing or in *statistical mechanical* terms, (ferromagnetic or auto-) *cooperative* interaction among the assembly of water molecules (Ling 1980.)

(In contrast, if we had adopted a model in which each water molecule is linked to its neighbors by the formation of attractive hydrogen bonds, one would be hard-put to argue that the dissociation of such a bond and reorientation of the water molecules — which appears to be the only alternative action — can produce strong *repulsion*.)

Thus far, we have only dealt with the charge of an N-site interacting with a specific water molecule, 1(0)(0), in contact with the N site. Let us now go to the permanent

dipoles and the induced dipoles belonging to all the immediately neighboring water molecules and find out about their respective parts in producing an even stronger induced dipole in that 1(0)(0) water molecule.

The alternatingly positive and negative fixed sites described above, produce induced dipoles of equal absolute magnitude for all water molecules in the same row, though oriented in opposite directions in adjacent columns. I shall designate these induced dipoles as $p^{1(0)(0)}$, $p^{2(0)(0)}$, $p^{3(0)(0)}$, $p^{4(0)(0)}$ etc. for the first, second, third, fourth, etc. water molecules from the N site in the column designated as j=0 and k=0. Now, the electric field created by one dipole on another one oriented in the same direction in tandem ($\rightarrow \rightarrow$) is $2\mu/r^3$ and that due to two dipole arranged in parallel but opposite directions ($\leftrightarrows$) is μ/r^3, where r is the distance between a pair of nearest-neighboring water molecules and it is equal to d, the distance between the nearest neighboring N and P sites. Taking these relationships in mind, one finds that the induced dipole in water molecule 1(0)(0) is described by the equation:

$$p^{1(0)(0)} = \alpha\varepsilon / [2\,(d/2)^2] + \alpha/r^3\,(2\mu^{2(0)(0)} + \mu^{1(-1)(0)} + \mu^{1(+1)(0)} + \mu^{1(0)(-1)} + \mu^{1(0)(+1)} + 2p^{2(0)(0)} + p^{1(-1)(0)} + p^{1(+1)(0)} + p^{1(0)(-1)} + p^{1(0)(+1)}), \quad (3)$$

where the first term on the right-hand side is the induced dipole due to the charged site N at a distance of d/2, the next five terms are induced dipoles due to the five immediately-neighboring permanent dipoles and the last five terms are induced dipoles due to the five immediately-neighboring induced dipoles. But since the permanent dipole moments, $\mu^{2(0)}$, $\mu^{1(-1)}$, $\mu^{1(+1)}$, etc. are all equal, equation (3) reduces to

$$p^{1(0)(0)} = 2\alpha\varepsilon/d^2 + \alpha/r^3\,(6\mu + 2p^{2(0)(0)} + p^{1(-1)(0)} + p^{1(+1)(0)} + p^{1(0)(-1)} + p^{1(0)(+1)}). \quad (4)$$

And for a water molecule in the second (and succeeding) row, the charge-dipole interactions due to the N (or P) site is not between nearest-neighbors and — following the rule adopted — ignored. In consequence, all water molecules in the second (and succeeding) rows are each surrounded on all six sides by other water molecules. We then have

$$p^{2(0)(0)} = \alpha/r^3\,(2\mu^{1(0)(0)} + 2\mu^{3(0)(0)} + \mu^{2(-1)(0)} + \mu^{2(+1)(0)} + \mu^{2(0)(-1)} + \mu^{2(0)(+1)} + 2p^{1(0)(0)} + 2p^{3(0)(0)} + p^{2(-1)(0)} + p^{2(+1)(0)} + p^{2(0)(-1)} + p^{2(0)(+1)}). \quad (5)$$

Again, since all the μ's are equal, we have

$$p^{2(0)(0)} = \alpha/r^3\,(8\mu + 2p^{1(0)(0)} + 2p^{3(0)(0)} + p^{2(-1)(0)} + p^{2(+1)(0)} + p^{2(0)(-1)} + p^{2(0)(+1)}). \quad (6)$$

The induced dipoles of water molecules belonging to the different rows were calculated and shown in the second column of Table 1. A striking feature of the results shown here is that as one goes farther and farther away from the surface of N and P sites, the induced dipole in the water molecules does not taper off to zero. Instead, it asymptotically approaches and eventually assumes a constant value, p^n described by the expression

$$p^n = 8\alpha\mu/\,(r^3 - 8\alpha). \quad (7)$$

TABLE 1

row (i)	p (Debye)	$\boldsymbol{\mu}$ (Debye)	E (10^{-12}ergs/molecule)	E (kcal/mole)
1	2.842	4.702	6.984	100.4
2	1.378	3.238	1.542	22.18
3	1.206	3.066	1.272	18.29
4	1.177	3.037	1.236	17.78
5	1.173	3.033	1.231	17.70
6	1.173	3.033	1.230	17.69
7	1.172	3.032	1.229	17.68
8	1.170	3.030	1.228	17.66
n	1.170	3.030	1.228	17.66

The computed induced dipoles (p), total dipole moment ($\boldsymbol{\mu}$, which equals the induced dipole moment, p, plus the permanent dipole moment, μ) and the (negative) adsorption energy (E) of water molecules in successive layers of water molecules in direction away from the idealized NP surface maintained at a temperature very close to absolute zero. E given in two units, 10^{-12} ergs/molecule and kcal/mole.

As shown in Table 1, the induced dipole at a position very far away from the idealized N-P sites and designated as the nth is equal to 1.170 Debye — to be compared with 1.86 Debye of the permanent dipole moment of a water molecule.

Since the induced dipoles p's of all the water molecules are oriented in the same direction as their respective permanent dipoles, μ's, one may define a *total dipole moment* of water molecule to be represented by the bold-faced Greek letter mu, $\boldsymbol{\mu}$ as the sum of induced dipole moment, p and the permanent dipole moment, μ:

$$\boldsymbol{\mu} = \mu + p. \tag{8}$$

Column 3 of Table 1 presents the total dipole moments, $\boldsymbol{\mu}$'s of the successive layers of water molecules calculated. With these data on hand, our next task is to evaluate the (negative) adsorption energy of the successive layers of water molecules.

As mentioned above, the (negative) energy of interaction between an electric charge ε and a dipole moment μ at a distance r apart is $\varepsilon\mu/r^2$, that between two dipoles μ_1 and μ_2 arranged in the same direction and in tandem is $(2\,\mu_1\,\mu_2)/r^3$ and that between two dipoles arranged in opposite directions in parallel is $(\mu_1\,\mu_2)/r^3$.

With these in mind and remembering to divide each (negative) water-to-water interaction term by 2 to avoid redundancy, we have for the total (negative) energy of water molecules of the first row in this ideal array and it is represented by $E^{1(0)(0)}$, where:

$$E^{1(0)(0)} = \varepsilon\boldsymbol{\mu}^1/\{2\,(d/2)^2\} + \{\boldsymbol{\mu}^{1(0)(0)}/2r^3\}(2\boldsymbol{\mu}^{2(0)(0)} + \boldsymbol{\mu}^{1(-1)(0)} + \boldsymbol{\mu}^{1(+1)(0)} + \boldsymbol{\mu}^{1(0)(-1)} + \boldsymbol{\mu}^{1(0)(+1)}). \tag{9}$$

Since the last four total dipole moments on the same row are equal in absolute magnitude as well as orientation, the total (negative) energy $E^{1(0)(0)}$ from Equation 9 can be written as

$$E^{1(0)(0)} = 2\ \varepsilon\boldsymbol{\mu}^1/d^2 + \boldsymbol{\mu}^{1(0)(0)}\,(2\boldsymbol{\mu}^{2(0)(0)} + 4\boldsymbol{\mu}^{1(-1)(0)})\ /2r^3, \tag{10}$$

or

$$E^{1(0(0)} = 2\ \varepsilon\boldsymbol{\mu}^1/d^2 + \{\boldsymbol{\mu}^{1(0)(0)}/r^3\}(\boldsymbol{\mu}^{2(0)(0)} + 2\boldsymbol{\mu}^{1(-1)(0)}). \tag{11}$$

The total (negative) adsorption energy of a water molecule in the second (and higher) row, $E^{2(0)(0)}$, is then

$$E^{2(0)(0)} = \{\boldsymbol{\mu}^{2(0)(0)}/2r^3\}\ (2\boldsymbol{\mu}^{1(0)(0)} + 2\boldsymbol{\mu}^{3(0)(0)} + \boldsymbol{\mu}^{2(-1)(0)} + \boldsymbol{\mu}^{2(+1)(0)} + \boldsymbol{\mu}^{2(0)(-1)} + \boldsymbol{\mu}^{2(0)(+1)}). \tag{12}$$

Since the last four total dipole moments on the second row are identical, Equation 12 can be simplified into the following:

$$E^{2(0)(0)} = \{\boldsymbol{\mu}^{2(0)(0)}/r^3\}\ (\boldsymbol{\mu}^{1(0)(0)} + 2\boldsymbol{\mu}^{2(-1)(0)} + \boldsymbol{\mu}^{3(0)(0)}). \tag{13}$$

Like the induced dipoles moment, the total (negative) energy, E, also does not taper off to zero as one moves farther and farther away from the NP surface. Indeed as one moves farther and farther away from the polarizing N and P sites, the total (negative) adsorption energy of a water molecule, E^n, approaches and sustains a steady unchanging value, described by the following equation

$$E^n = \{4(\boldsymbol{\mu}^n)^2\}\ /\ r^3\ . \tag{14}$$

Substituting (7) and (8) into (14), we have

$$E^n = (4\mu^2r^3)/\ (r^3 - 8\alpha)^2. \tag{15}$$

The computed total (negative) energy of water molecules far away from the NP surface is listed in Column 4 of Table 1 in two units, respectively in 10^{-12} ergs/molecule and in kcal/mole. The data given in kcal/mole is also presented graphically and shown in Figure 8.

The implication of Equation 15 (and Table 1) is truly astonishing. It tells us that under an ideal condition described earlier, an idealized NP surface could strongly polarize and orient successive layers of water molecules *ad infinitum*.

Additional considerations and analyses of the theoretical model

In this new theory, the long-range impact on distant water molecules is not due to a propagated electrical polarization (induction) emanating from the electric charges at the N and P sites and proceeding through intervening water, molecule-by-molecule in the way first suggested by de Boer-Zwikker and also by Bradley. Nor can it be properly described

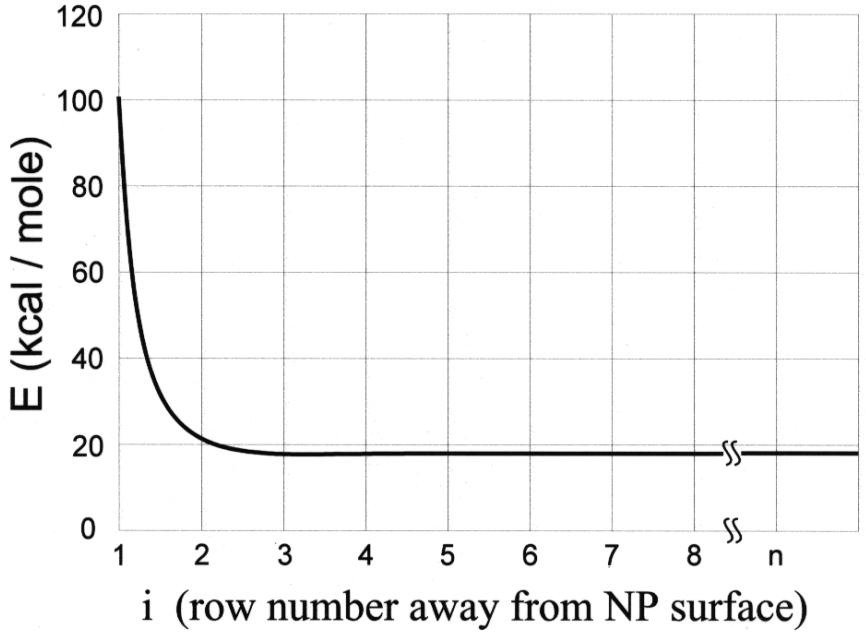

FIGURE 8. The theoretically computed (negative) adsorption energy of a water molecule, E, in one of successive layers of water molecules away from an idealized NP surface at a temperature very near absolute zero. Note that as the distance between the water molecule and idealized NP surface increases, the (negative) adsorption energy does not taper off to zero. Rather, it continues at a constant value described by Equation 15. For details on the makeup of an idealized NP surface, see Figure 7 and text.

as Brunauer *et al* did when they said that if a large permanent dipole moment is present in the gas molecules, then "many layers of the gas molecules will be successively polarized by the mechanism of de Boer and Zwikker."

Rather, a long-range multilayer dynamic structuring begins with a concerted orientation (of the permanent dipole moment of a nearby water molecule) and electrical polarization (creating in the neighboring water molecule an induced dipole oriented the same way the permanent dipole is oriented by the N or P site.) Each of these components corresponds respectively to what is called *orientation polarization* (P_o) — due to spatial orientation of the permanent dipole moment of the molecule — and *distortion polarization* (P_D) — as in the Debye's formula for the total polarization of a polar molecule in an electric field (Debye, in "Polar Molecules" 1924.)

The (properly) oriented permanent dipole and the newly created induced dipole of the immediately neighboring water molecules in turn orient and polarize *their* nearest-neighboring water molecules. And this process spreads farther and farther outward until all the water molecules in the assembly have acquired a similar oriented permanent dipole moment and induced dipole moment in a perfectly orderly array.

This polarization-orientation *ad infinitum* under an indelaized condtion is possible only because the gas molecules involved have a large permanent dipole moment. This was probably what motivated Brunauer, Emmett and Teller to endorse Bradley's theory on gas

molecules with large permanent dipole moments. It is more easily demonstrated here now that we have Equation 15. Set μ to zero; E^n, the (negative) adsorption energy of a water molecule far away from the ideal NP surface, becomes zero.

Note also that both the orientation component and the distortion component are of such a nature that they are highly *auto-cooperative* (Ling 1980.). That is, each time a water molecule is oriented and polarized in one direction, it will make all its six surrounding water molecules more likely to adopt the favorable low or high (negative) energy orientation. This three dimensional cooperativity provides the foundation for the stability of the dynamic structure formed. It is also the reason why multilayer water adsorption typically shows a pattern of *hysteresis*. Thus, the curve of *adsorption* of water is not identical to the curve of *desorption* but tends to occur at a higher relative vapor pressure as seen in many models studied (Anderson 1914 on silica gel; Urquhart and Williams 1924 on cellulose; Katchman & McLaren 1951 and Reyerson and Peterson 1953 on protein and virus.)

Next, I want to analyze and catalogue the assumed conditions in our specific model that have created in theory an endless polarization and orientation of water molecules. They fall into two categories.

The first five components listed below under Category A are essential and hence indispensable to produce in the idealized condition the *ad infinitum* polarization and orientation demonstrated theoretically above. The next two items listed under Category B, justified on the basis of the overall success of the effort built on these and the five other more essential conditions are less stringently required and can be changed (within limits) without serious adverse effects:

Category A

(1) a temperature very near absolute zero;

(2) a boundless, perfectly smooth surface carrying alternating P and N sites at the same distance, d, from all its nearest neighbors P or N sites;

(3) the distance, d is made equal to the average distance between nearest water molecules in liquid water r, obtained by taking the cube root of the average volume of each water molecule in liquid water, obtained by dividing the molar volume of water, 18.016 cm^3 by the Avogadro's number, 6.023 x 10^{23}, yielding a value of 3.10 Å. It is believed that this is the least arbitrary value of r one can find.

(Other values for comparison include twice the van der Waal radius of oxygen atom, 2 x 1.40 = 2.80 Å (Pauling 1960, p.260); the oxygen to oxygen distance in ice I, 2.76 Å (Eisenberg and Kauzmann 1969 p. 94); and a value of between 2.8 and 2.9 Å from the well-resolved peak of the X-ray radial distribution function of liquid water at 4°C. (Narton *et al*, 1967.)]

(4) an endless body of water in contact with the entire idealized NP surface;

(5) perfect insulation of the whole assembly from mechanical, acoustic, light, heat, gravitational and other perturbations from the outside.

Category B:

(1) Size and location of the negative and positive electric charge on the N and P sites are respectively set at one half electronic charge and d/2. No major difference is expected if the size is set at full electronic charge or much smaller than half electronic charge.

(2) Only the nearest neighbor interaction is considered. This is justified since $1/r^3$ decreases sharply as r increases. Due to the symmetry of the system, inclusion of the next-nearest neighboring interaction would only cause a uniform but small reduction of the energy terms, which for the quantitative accuracy we can expect to achieve is insignificant.

Two predictions from the present theory

If we designate each of the quantum-mechanically allowed energy states of water molecules as $\varepsilon_1, \varepsilon_2, \varepsilon_3 \ldots \varepsilon_r \ldots$, and divide each of these energy levels by kT, (the average kinetic energy of each water molecule, where k is the Boltzman constant and T the absolute temperature,) then the sum $1 + \exp(-\varepsilon_1/kT) + \exp(-\varepsilon_2/kT) + \ldots = \sum \exp(-\varepsilon_r/kT)$ is called the *partition function* (p.f.) of the water molecules in that specific state, which could be vapor, liquid or solid ice (Rushbrooke 1949.)

In a mixture of liquid water and solid ice, the trend is for all the water molecules to exist as liquid water or as solid ice. Which way it goes at a given pressure depends on the temperature and its relationship to that specific temperature we call the melting point as illustrated in the Phase Diagram shown in Figure 6. This can be put into a more quantitative form if we designate the partition function of normal liquid water as $(p.f.)_l$ and that of solid ice (I) as $(p.f.)_s$ and u_f as the *enthalpy of fusion* and equal to the energy (or more precisely, enthalpy) difference between the zero energy level of the liquid water state and that of the solid ice (I) state. The melting temperature, T_m, is then described by the following equation (Gurney 1949, p. 129.)

$$T_m = u_f / \{k \ln [(p.f.)_l / (p.f.)_s]\}. \tag{16}$$

Now, the melting point of normal liquid water is 273.15° K. u_f, the enthalpy of fusion of ice (I) is 1.4363 kcal mol^{-1} (Rossini *et al* 1952) or (divided by the Avogadro number) $1.4363 \times 10^3/(6.023 \times 10^{23}) = 2.39 \times 10^{-21}$ cal $molecule^{-1}$. The Boltzman constant, k, is equal to 0.330×10^{-23} cal $deg^{-1}molecule^{-1}$. Substituting the values of T_m, u_f and k into Equation 16, one finds that $\ln [(p.f.)_l/ (p.f.)_s]$ equals 2.647.

Similarly, we can write Equation 17 for the boiling point of water, T_b, and its relationship to u_v and $(p.f.)_v /(p.f.)_l$:

$$T_b = u_v / \{k \ln [(p.f.)_v /(p.f.)_l]\}, \tag{17}$$

where $(p.f.)_v$ is the partition function of water in the vapor state. T_b, the boiling point of water is 373.15° K. u_v, the enthalpy of vaporization is 9.7171 kcal mol^{-1} (Rossini *et al* 1952) or 1.6133×10^{-20} cal $molecules^{-1}$. Substituting T_b, u_v and k into Equation 17, one obtains $\ln [(p.f.)_v/ (p.f.)_l]$ equal to 13.11.

Now, we are ready to calculate the theoretically expected freezing point and boiling point of water molecules polarized and oriented by an idealized NP surface. Table 2 shows that the average water to water (negative) interaction energy, E^n, far from the NP surface for d (=r) equal to 3.10 Å is 17.76 kcal mol^{-1}. We now want to find out what is the boiling point and freezing point of this polarized-oriented water with the aid of Equation 16 and 17.

TABLE 2

d	E	
(Å)	(10^{-12} erg/molecule)	(kcal/mole)
2.5	12.83	184.6
2.6	6.633	95.40
2.7	4.088	58.80
2.8	3.221	46.32
2.9	2.791	40.15
3.0	2.038	29.31
3.1	1.235	17.76
3.2	1.009	14.51
3.3	0.834	12.00
3.4	0.710	10.13
3.5	0.604	8.68
3.6	0.523	7.52
3.7	0.458	6.59
3.8	0.404	5.81
3.9	0.359	5.16
4.0	0.322	4.63

The computed (negative) adsorption energy, E^n, of water molecules at a great distance away from the idealized NP surface at a temperature very close to absolute zero. E_n given respectively n units of 10^{-12} erg per molecules and kcal per mole in the second and third column.)

To do that, we must first determine the enthalpy of vaporization of the polarized-oriented water far from the idealized NP surface, designated as u_{vp} as well as its enthalpy of fusion, designated as u_{fp}. Assuming that the enthalpy of water vapor to be negligible, u_{vp} would be simply 17.76 – 0 = 17.76 kcal mol^{-1}. On the other hand, u_{fp} would be the enthalpy of sublimation of ice-I, 11.30 kcal mol^{-1} (Eisenberg and Kauzmann 1969, p.101) minus 17.76 kcal mol^{-1} equaling –6.46 kcal mol^{-1}. Substitute these values of u_{vp} and u_{bp} into Equations 16 and 17 respectively, one obtains the boiling point of polarized-oriented water far from the idealized NP surface at 724°K or 451°C and a freezing point of −1228° K.

Now, we examine more closely the values of ln $[(p.f.)_v / (p.f.)_l]$ and ln $[(p.f.)_l / (p.f.)_s]$ used in the calculations above. You recall that implicit in the use of these respective values of 13.11 and 2.647 is the assumption that the partition function of polarized-oriented water far from the idealized NP surface is the same as that of normal liquid water. That, or course, is not true. That polarized-oriented water suffers motional restriction especially in translational and rotational motions. As a result, the number of allowed energy levels are fewer than in normal liquid water and the partition function of polarized-oriented water or $(p.f.)_{lp}$ is significantly lower than that of normal liquid water, $(p.f.)_l$.

One way of solving the problem would be to estimate how much is the difference. But that is not what we intend to do here. A look at Equation 16 and 17 readily reveals that a reduction of the value of $(p.f.)_l$ would make the estimated boiling point of polarized-oriented water even higher than 451°C and the freezing point of polarized-oriented water even lower than −1228°K. And that is all we need to know here to arrive at our first prediction:

Prediction 1: *The boiling point of polarized-oriented water would be at least as high or higher than 451°C.*

Prediction 2: *Under ideal or near-ideal condition, the polarized-oriented water can never be frozen.*

But to know by exactly how much is the freezing point of polarized-oriented water still lower than −1228°K adds no valuable information here either. For a freezing point below absolute zero is not possible, because to reach such a temperature, the assembly must go through the temperature of absolute zero. Yet according to the Third Law of Thermodynamics: "It is impossible by any procedure, no matter how idealized, to reduce any assembly to the absolute zero in a finite number of operations." (Fowler and Guggenheim 1960, p. 224.) This then leads to our second prediction.

Right away, this theoretical discovery has accomplished one important purpose. It justifies the assumption we made above that we can in theory create the idealized polarized-oriented water at a near-absolute zero temperature. For if the water freezes on the way toward absolute zero, we would not be able to continue and achieve what we did without engaging ourselves in unproductive, distractive arguments.

We now go back to Table 2. This table shows that the (negative) adsorption energy E^n of far-away water molecules given in Equation 15 exceeds the sublimation energy of ice-I, at 11.30 kcal mol^{-1} only if d is equal to the water-to-water distance r, estimated at 3.1 Å or lower but not much higher than 3.1 Å. Thus, if d is, say, 3.4 Å or even higher, freezing may take place. So clearly, a decisive factor in freezing or not freezing is the value of d. To produce non-freezing water, it must equal or at least be close to the water-to-water distance, r. And it must be *uniformly* so. These criteria are, of course, what make our idealized NP system ideal.

Our next task is to verify experimentally the two predictions. To do that , we must first resolve a set of problems.

Number 1 condition under Category A is a temperature of near absolute zero. We have just shown, absolute zero as such is impossible to achieve. However, liquid helium can provide a temperature close to −272.2° C, which is a little less than one degree above absolute zero or −273.16° C. Failing liquid helium, the next best would be liquid nitrogen offering a temperature close to −195.8°C., which is 69.3° C above absolute zero.

Essential conditions described under (2) and (4) under Category A are impossible to achieve. There is no such thing as a boundless perfectly smooth NP surface, nor an infinite body of water, nor perfect isolation from the external real world. But a practical substitute is a thin layer of water held between two juxtaposed smooth near-ideal NP surfaces — in other words, a near-ideal NP-NP system (see Figure 2d.) The juxtaposed NP surfaces conserve the polarization-orientation indefinitely. Being very thin, it is not difficult to keep it insulated from external disturbances. The thinness of the water layer also minimizes edge effects.

Finally, perhaps the most challenging of all is to find a real world replica of the idealized NP surface, where a checkerboard of N and P sites separated from each nearest neighbor by a distance close to if not exactly equal to the distance between two nearest neighboring water molecules. The best example one can imagine is the smooth surface of salt crystals. This is not at all new. de Boer & Zwikker were among the first to introduce such an idea (Figure 3.) One recalls that Bradley also explicitly dealt with salt crystal surfaces. But neither de Boer-Zwikker nor Bradley mentioned any specific salt crystals. Harkins demonstrated multilayer adsorption of water molecules on diastase or titanium oxide crystal (Harkins 1945.) Another attractive model is the cubic NaCl crystals. Unfortunately, it is water-soluble.

However, there is another cubic salt crystal that has the same geometry as NaCl but hardly soluble in liquid water. That is silver chloride — especially large crystals artificially grown and used as lens for infrared spectroscopy, for example. In Figure 9, I reproduce (a modified version of) the silver chloride surface as given by Glaus and Cazzaferri (1999.) This may well be the best NP surface we know today. In his advanced textbook of inorganic chemistry, Moeller (1952, Table 18.5) gives the measured bond distance as 2.77 Å, the sum of ionic radius as 3.07 Å, which are close to the (r and) d value of 3.1 Å used in our computation.

Then there is Figure 10, which is a diagrammatic illustration of the surface structure of sodium silicate glass — a random network of silica oxide carrying negatively-charged

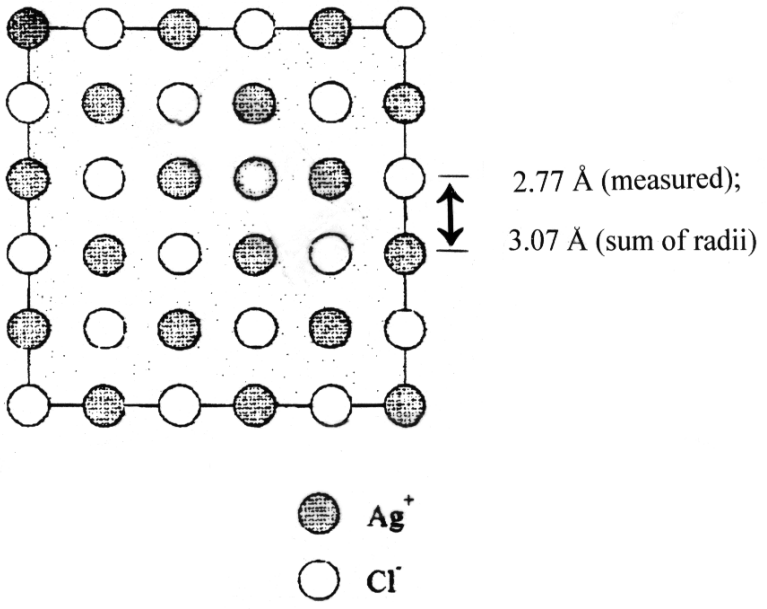

FIGURE 9. A diagrammatic illustration of the structure of the polished surface of silver chloride crystal and the distance between nearest neighboring Ag^+ and Cl^- ions from measurement of bond distance (2.77 Å) and from summation of atomic radii (3.07 Å.) (Modified after Glaus and Calzaferri 1999.) Reproduced with permission of J. Phys. Chem. ©1999 American Chemical Society.

free-hanging oxygen ions and positively-charged sodium ions (Pulker 1984.) All in all, the glass surface, though not nearly as ideal as the AgCl crystals, represents, nonetheless, an imperfect surface carrying alternatingly N and P sites. Since random network is only a postulation, and in Nature few things are truly random, the realistic surface of glass might be significantly closer to that of the AgCl crystal surface given in Figure 9.

In summary, we have with the aid of two sets of pictorial diagrams produced two specific model systems. They are the nearly ideal polished silver chloride crystal lenses with d close to 3.1Å. The more randomly oriented sodium silicate glass surface in contrast, may well have local areas with d-values at values both higher and lower than the ideal value.

Thus equipped, we return to where we started. Happily, here is where our good luck continues. For it turned out that the key experiments have already been done by scientists who had absolutely no idea that their findings were to play a key role in verifying a new theory of long-range polarization-orientation of water molecules by idealized NP surfaces. They only described their observations and their own reasons for making these observations.

Giguère and Harvey's accidental (retroactive) confirmation of the prediction that near-ideally polarized-oriented water between polished AgCl crystal lenses cannot freeze at subzero temperature all the way to the lowest temperature studied, i.e., –176°C.

That observation of singular value to the present work is that of Giguère and Harvey reported nearly half of a century ago in 1956. Its validity is enhanced by its chance discovery

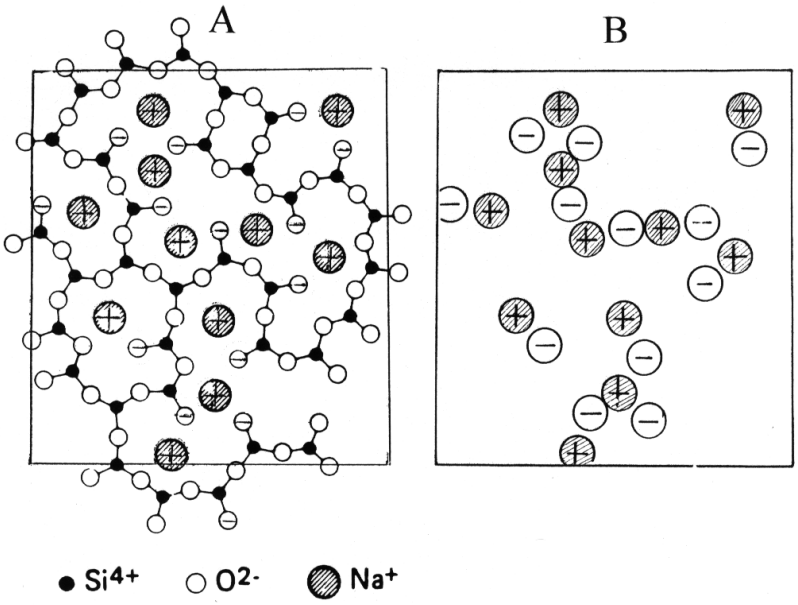

FIGURE 10. Visualization of the surface of sodium silicate glass based on the theory of random network of Zacchariasen (1932.) A. Picture from Pulker, 1984. B. Distribution of positive Na^+ and negative oxygen ion on polished glass surface. Locations of ions from A. (Partly modified after Pulker, 1984. Figures reprinted with permission from Elsevier.

not expected at all and by its later independent confirmation by another scientist (See below.)

Giguère and Harvey placed a thin layer of water between two polished (transparent) AgCl plates. To their surprise, they discovered that as shown in their Figure 1 reproduced here as Figure 11, "essentially the same spectrum was obtained for all temperature studied even down to that of liquid air, confirming that no crystallization of water has occurred." (p. 801.)

They also pointed out that this phenomenon could be repeated any number of times under the same conditions (p. 801) and "Our films of water pressed between silver chloride plates could be warmed and cooled over a wide temperature range without significant alteration in their spectra" (p. 805.)

Giguère and Harvey (who have since either deceased, retired or otherwise beyond reach) made no mention of the exact thickness of the water film they studied. Luckily, I reached their one-time associate, Dr. Rod Sovoie, who kindly wrote me that the water film between the AgCl plates investigated by Giguère and Harvey was 10 micrometer thick. Thus, a water layer well over thirty thousand (30,000)-water-molecule-thick cannot be frozen even at the temperature of −176° C, when held between two polished AgCl crystals.

It seems that Giguère and Harvey's incidental discovery has confirmed the essence of our Prediction 2.

Before going on to our next set of experimental testing and its result, I would like to point out that the ideally polarized-oriented water cannot be classified as vitreous water because vitreous state is a free-standing phenomenon. The ideally polarized-oriented state of water is a direct consequence of the NP-NP system and without the NP-NP system, it will return to the state of normal liquid water.

A second point I want to mention concerns the reproducibility of the results reported by Giguère and Harvey. The fact that it was a totally unexpected and it could be repeated

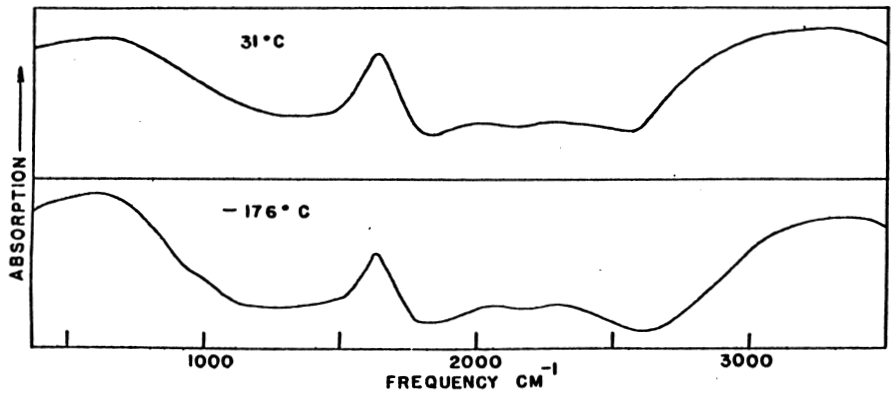

FIGURE 11. Infrared absorption spectrum of 10-micron-thick water film held between polished AgCl crystal plates. The two (indistinguishable) spectra were recorded respectively at ambient temperature (top, 31° C) and at liquid air temperature (bottom, −176°.) I am indebted to Dr. Rod Sovoie, the onetime associate of Drs. Giguère and Harvey, for the information on the thickness of the water films Drs. Giguère and Harvey earlier studied (from Giguère and Harvey 1956, by permission of *Canad. J. Chemistry*.)

any number of times the investigators chose speak volumes. However, in a 1982 review on "Supercooled Water", C.A. Angell mentioned on page 57 of his review that a scientist named "Glew" had in a private communication told Angell that he (Glew) had made a similar obsevation. However, Angell and his coworker, Barkatt, failed to supercool water between glass surfaces below −28° C (−31° C for quartz plates). Since even normal bulk phase liquid water can be cooled to −40° C (Dorsay 1940; Hallet 1965; see also Figure 12 of the present paper) Angell and Barkatt's difficulty in cooling water to −28° or −31° C could be from an inadvertent cause. If so, I suggest that this could be their inclusion of "a highly adsorbing dyestuff" into the water being cooled and that this dyestuff adsorbed onto the glass/quartz surface altered its water-polarizing-orienting attributes.

In harmony with this interpretation was Zocher and Coper's demonstration in 1928 that by simply rubbing vigorously with filter paper the surface property of glass was profoundly altered. Other evidence in harmony with this interpretation comes from industrial processes conferring new surface properties to glass surface by coating it with diverse strongly-adsorbed chemicals (see Pulker "Coating on Glass" 1984.)

Another point I would like to make is to use the word "supercooling" with caution. Supercooling as such creates a *metastable equilibrium state*. The nonfreezing water between AgCl surfaces, in my opinion based on the theoretical reasoning, suggests that it represents a *true equilibrium state*.

Finally, to add still more to the significance of this retroactive confirmation of nonfreezing water held between polished AgCl crystal surface with d close to 3.1 Å I cite the work of Fox and Martin (1940), who also tried to study the infra-red spectra of liquid water and ice I as Giguère & Harvey did, but had not encountered unusual difficulties as did Giguère & Harvey. (See Fox and Martin's Figure 3 on page 239 of their paper.) The main difference between Giguère & Harvey's study and Fox and Martin's lay in the nature of the absorption cells employed. The cells used by Giguère and Harvey comprised AgCl plates with cubic crystalline structure and near-perfect NP symmetry. In contrast, Fox and Martin used flurorite (CaF_2) plates, whose crystalline structure (see Pauling 1960, p. 534) is altogether different from that of the nearly ideal NP surface of silver chloride shown in Figure 9.

Hori's "non-freezing" and "non-boiling" water between polished glass and quartz surfaces

As mentioned earlier, Prof. Takeo Hori of the Low Temperature Science of Hokkaido University published in 1956 an article in Japanese entitled "On the Supercooling and Evaporation of Thin Water Films". It was translated into English for the US Army Snow Ice and Permafrost Research Establsihment in 1960 (Hori 1956.)

For the convenience of the reader, two key figures from Prof. Hori's paper are reproduced here respectively as Figures 12 and 13. Figure 12 shows that water held between two polished glass plates 1/100 mm (or 10 micrometer) or farther apart, could be supercooled to as low as −30° C but no further and is therefore just like ordinary liquid water (Dorsay 1940; Hallett 1965). However, when the water film held between glass plates is below 1/100 mm or 10 micrometer in thickness, it frequently reveals no traces of freezing at temperature lower than −90° C..." (Hori 1960, p. 3.) At a distance of 1/1000 mm or 1 micrometer apart, there is no evidence whatsoever of freezing at −90°C even though a 1-micrometer layer of water is well over three thousand (3000) water-molecules thick.

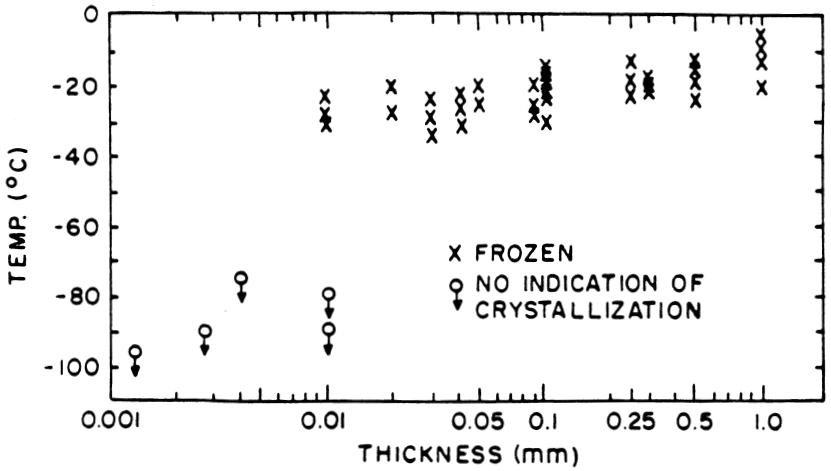

FIGURE 12. The influence of the thickness of water film (held between two flat polished glass or quartz plates) on the temperature at which freezing occurred or failed to occur. Prof. Hori pointed out that at a film thickness below 0.01 mm (or 100, 000 Å and thus more than 30,000-water molecules-thick), the water film frequently showed no trace of freezing at temperature as low as –90° C. Even in water films 0.1 mm thick, when freezing did take place, it took place only at isolated spots and not pervasively throughout. (from Hori, 1956, Institute of Low Temperature Science, (ALTS).)

Nonetheless, compared to the inability of a 10 micra thick water layer to freeze at –176° C, there is no question that a much more powerful and effective polarization-orientation of water molecules and over a much longer range was achieved by the more nearly perfect NP-NP system of AgCl plates than polished glass plates — further confirming the theory.

Let us now turn to the second figure reproduced from Prof. Hori (Figure 13). It shows the vapor pressure of water held between one flat polished glass plate (or quartz crystal plate) and a curved one on top of it — with a radius of curvature of 35 m. When water is introduced between the two surfaces, the distance of separation, called δ (not to be confused with d representing the distance between nearest neighboring water molecules in our study) varies from near zero at the center where the two plates meet to increasingly higher value toward the periphery of the water film. Viewed from the top, the water film shows a series of concentric light and dark bands or fringes which are known as Newtonian rings. From the location at a specific ring, the index of refraction of water or air between plates, the wave-length of the light, and its angle of incidence, the thickness of the film at that point, δ, could be determined with accuracy. To study the influence of film-thickness and of temperature on the vapor pressure of the water film, Hori placed the whole assembly in a vacuum chamber kept at different temperatures.

The water film at the periphery is relatively thick and the vapor pressure registered was not different from those of bulk-phase water at the same temperature. With time, this peripheral water evaporates away and the outer boundary of the water layer shrank toward the center of the water film. This continued until a final equilibrium position was reached,

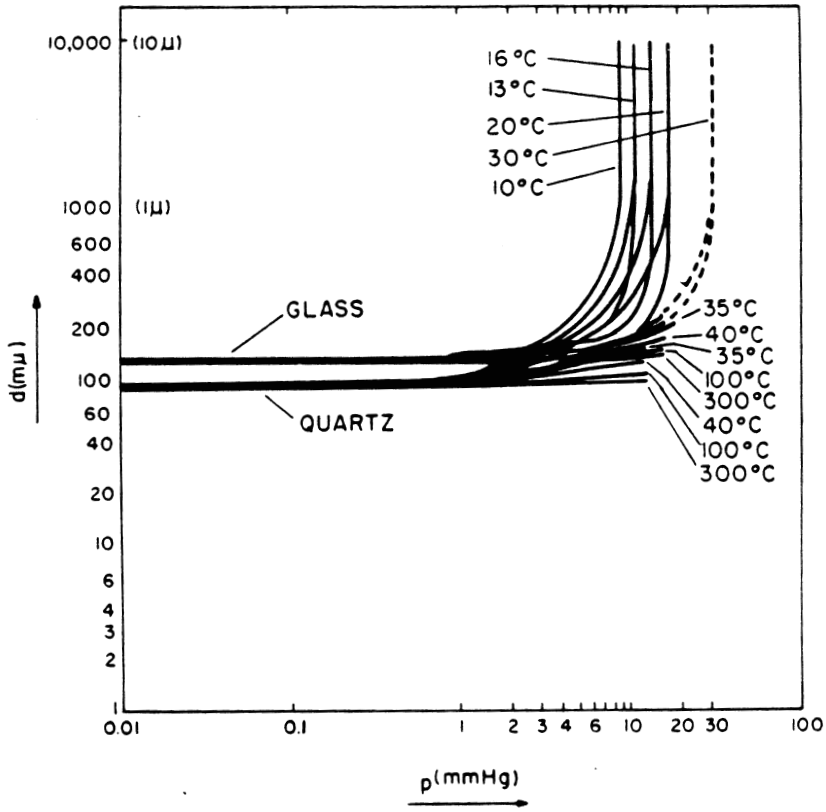

FIGURE 13. The vapor pressure (abscissa, in mm of Hg.) of water film at different thickness in units of mμ (or 10 Å) (ordinate). Water film of varying thickness was produced by placing water between one flat glass (or quartz) plate and another curved plate with radius of curvature of 35 m. The thickness mentioned above refers to the water film at the periphery of the doughnut-like ring of water. When the thickness was 1 μ or thicker, the vapor pressure was not different from normal liquid water. However, when the thickness fell to 90 mμ (900 Å or some 300 water molecules thick), the vapor pressure became zero even at temperature as high as 300° C. (From Ling 1972, redrawn after Hori 1956, Low Temperature Science.)

from then on net loss of water came to a halt. It is at this point that the vapor pressure dropped to zero.

Hori found that in the case of quartz crystal plates, when δ reached 90 (±20) millimicra (equivalent to about 300 water molecule thick), the measured vapor pressure became zero and there is "absolutely no evaporation even in a vacuum" at a temperature as high as 300° C (p. 5). But when the flat plate and curved lens are glass, the critical δ is 140 ±20 millimicra, (roughly equivalent to 500 water molecules thick), at which there is zero vapor pressure even at 300°C. Both sets of data affirm the first prediction that the ideally or nearly ideally polarized and oriented water would not boil at a temperature of 430° C or higher.

Discussion

A critical theoretical confirmation of the hypothesis of propagated short-range electrical polarization-orientation in the dynamic structuring of water in living cells and in a wide range of inanimate systems

The entire history of the study of the adsorption of multilayers of water molecules in living cells and in a wide variety of inanimate systems has been plagued by the absence of a physical theory that can unequivocally tell us how deep a layer of water molecules can be influenced by a solid surface under the best of conditions. If I am not mistaken, that problem has now been resolved. That is, under the favorable conditions defined, an idealized NP surface can enhance the water-to-water adsorption energy *ad infinitum*.

This new insight has not only further solidified the polarized-oriented multilayer (PM) theory of cell water and the association-induction hypothesis of which the PM theory is an integral part, it has also given new life to the many exciting discoveries of the past that have been banished to dusty shelves seemingly forever.

Do we need a revival of the classic condensed film theory to explain long-range dynamic water structuring?

As mentioned earlier, in as far back as the early 19th century, investigators of the highest caliber had subscribed to the idea that solid surfaces may strongly attract gaseous molecules over long distances. As an example, van der Waal had suggested it to J. R. Katz for his extensive data on the adsorpton of water on proteins, nucleic acids and other biomaterials (McBain 1932, p. 451; Katz 1912, 1912a.) However, when McBain wrote his monograph in 1932, the majority of the "old physicists" had already abandoned this theory. Nonetheless, a small minority hung on.

In more recent years, one notices that Israelachvili (1985, 1987) and his coworkers appeared to have returned to the condensed film theory with a twist. That is, they offered direct electrostatic force to achieve the long-range ordering of water molecules. However, I am inclined to disagree.

My reasons for disagreeing are twofold. The first is the Law of Macroscopic Neutrality (For a lucid discussion on the subject, see Guggenheim 1950, pp. 330–331.) That is, isolated electric charges in chemically measurable concentrations can only be found during thunderstorms and in high energy physics laboratories. They do not exist inside living cells. As a rule, where there are negative electric charges, there are an exactly equal number of positive charges. When isolated electric charges are found at exposed surfaces, their number is so small that they would have little impact on the sorption of water, which as a rule occurs at high concentrations.

My second reason can be understood with the help of Figures 2a, 2b and 2c. Water dipoles polarized and oriented by a surface carrying electric charges of the same kind are oriented in the same direction. As such, these similarly oriented water dipoles strongly repel one another. That is why ions (Figure 2a) and other surfaces with one kind of electric charges (Figure 2b, 2c) cannot polarize and orient water molecules much more than one or two layers.

Do the N and P sites on the surface of AgCl plates and polished glass represented in Figure 9 and Figure 10 truly represent respectively isolated negatively- and positively-charged sites?

Not exactly. I have chosen for the sake of simplicity to do something that is not entirely correct. However, the harm such a deviation from truth might cause is more than made up by the clarity on the main message that this simple approach brings. In reality, sitting behind each N (or P) site in the near-ideal NP surface in Figure 10 is (respectively) a P (or N) site. And sitting behind that P (or N) site is another N (or P) site and this goes on and on. Indeed, an even more precise way of doing it would be to represent what we now call an NP surface, a N(P)P(N) surface or even N(PNPN...)P(NPNP..) surface. But that would be too cumbersome to be worth the effort. For, after all, the AgCl salt crystal and the sodium silicate glass are not two dimensional sheets but three dimensional solid structures, in which each N or P site is surrounded by neighbors of the opposite polarity.

As far as the polarizing and orienting influence on the adjacent water molecules is concerned, if we had in fact replaced each of the N and P sites with a dipolar site with the appropriate negative end or positive end facing the water molecules, the overall impact on the water adsorption would be a reduction in the reach of the polarizing and orienting force locally with no significant consequences beyond that. The pervasive short range nature of the interaction in fact calls for limiting the computation of interaction to those between the nearest neighbors of the N and P sites and among the water molecules

Does the specific nature of the solid surface including the pattern of electric charge distribution affect the long range ordering of adjacent water molecules?

Prof. Walter Drost-Hansen expressed the view again and again that "proximity to most (or all) 'solid interfaces' regardless of the detailed specific chemical nature of the surfaces" would produce what he calls "vicinal water", which he defines as "water near interfaces." In my view, this is not a very good argument. It seems circuitous.

Referring to this alleged indifference to the nature of the solid surface as a "Paradoxical Effect", Drost-Hansen tentatively suggested in 1991 that it is "external geometrical constraints that produced such an effect" (Drost-Hansen and Singleton 1991, p. 14.)

Even though Drost-Hansen and I share a belief in the existence of long range ordering of water, we are on opposite sides on how such a long-range effect is produced. And it is my obligation to express why I do not share his view.

In my opinion, there are legions of evidence supporting my position but one example that seems most appropriate here is the profoundly different infrared absorption spectra of water held at, or below its normal freezing temperature when placed between AgCl plates as shown by Giguère & Harvey (Figure 11) or between CaF_2 or fluorite plates as shown by Fox & Martin (1940.) One could not be frozen at −176° C, while the other was frozen to ice I without any difficulty.

The steepness of the drop of adsorption energy of water molecules moving away from close to the NP surface. Or put differently, the question of the homogeneity of the adsorpton energy of water molecules in a deep layer of polarized-oriented water.

When I first introduced the PM theory, I believed that water molecules in immediate contact with the polarizing sites on the proteins are more strongly acted upon and suffer greater motional restriction than water molecules farther removed. This view is indicated

in Figure 1 by the decreasing size of the curved arrows in water molecules as one gets closer to the proteins. On the basis of this kind of reasoning, I believed then that this motional restriction, and hence reduction of entropy, was the main cause for the low steady level of sodium ion in cell water. As time went on, my ideas began to change. Thus, when I presented my quantitative theory for solute exclusion from living cells and model systems (Ling 1993), I solidified my later view that the cause for the partial exclusion of sodium and sucrose involves both enthalpic and entropic reasons.

As such, the idealized NP surface depicted in Figure 6 would be highly unstable. The positive and negative charges would neutralize each other and become non-polar. The real world NP systems like that shown in Figure 9 for AgCl is stable, because behind each N or P site, there is a P and N site respectively etc., etc. And it is the entire three-dimensional crystal that stays stable. Thus, what we draw as an N or P site is in fact a dipolar site with its respective negative and positive end facing the water molecules. Nonetheless, at least a layer of water molecules thirty thousand molecules thick has been made non-freezing by these banks of dipolar sites. This success provides indisputable evidence that what we call NP-NP systems but are in fact N(PNPN...)P(NPNP...)-N(PNPN...)P(NPNP...) systems really work.

The most outstanding difference between an isolated charged N or P site and their dipolar counterparts is the reach of their polarizing force. In the real world what we see as a NP surface is in fact dipolar or even multipolar. This recognition in turn leads one to believe that in the real world polarized-orientaed multilayers of water, the reach of each step of polarization orientation is short, even though the aggregate effect is long. Taking away the contribution from the longer acting isolated charges, the values of adsorption energy would end up being constant rather than steeply falling as implied in Figure 1 and shown in Figure 8. This idea of more constant water-to-water interation energy is also in harmony with the assumption of uniform water-to-water interaction energy of all water molecules in the theory of solute exclusion mentioned earlier (Ling 1993), which, in turn, is backed up by its success in explaining the size-dependent solute exclusion in frog muscle cells and model systems (Ling *et al* 1993.)

The reduced average kinetic energy of water molecules in polarized-oriented multilayers like those shown between polished AgCl plates and between polished glass surfaces.

It is known that the individual water molecule in a pool of pure liquid water is in possession of an average kinetic energy equal to kT, where k is the Botzmann constant and T the absolute temperature. At 25° C, this amounts to 3.90 x 10^{-14} ergs per molecule or 592 gram-calories per mole. This average kinetic energy arises from the constant bombardments each water molecule receives — from other water molecules. However, placed between suitable NP-NP systems of AgCl, glass or quartz plates, the water molecules are greatly restricted in their motion. Accordingly, the average kinetic energy must be reduced from that in normal liquid water, further enhancing the stability of the dynamically structured water.

How do you bridge the gap between conclusions derived from two-dimensional NP surfaces on bulk phase water to water in living cells, which contain only one-dimensional protein chains?

I have used the symbol NP-NP-NP system to describe how parallel arrays of fully-extended protein chains could function like a two-dimensional NP surfaces. But admit-

tedly that was just a vague stipulation — even though a vast amount of experimental data can be explained on the basis of that postulation. However, new progress made recently has provided more insight into the problem. I intend to publish soon another paper on the subject.

However, this much can be said here. First, Hori's work shows that while irregularity in the N and P site distribution on glass and quartz surface weakens long-range water polarized-orientation of water, it does so modestly. Second, the excess (negative) water-to-water interaction energy in living frog muscle (estimated at 126 cal mole^{-1}, Ling *et al* 1993) amounts to less than 2% of the excess (negative) adsorption energy of distant water produced by the idealized NP surface (17.76 − 9.72 = 8.04 kcal mole^{-1} or 8,040 cal mole^{-1}). Taken together, these two sets of facts provide generous margins for effective polarization-orientation of all the cell water by a relatively small amount of intracellular proteins that assume the fully-extended conformation of an NP-NP-NP system.

I thank Dr. Raymond Damadian and his Fonar, Inc. for their continued support, Margaret Ochsenfeld and Dr. Zhen-dong Chen for their dedicated and skillful help and valuable scientific contributions.

References

Abbé F. Fontana (1777) *Mem. Mat. Fis. Soc. Ital. 1:* 679
Anderson, J.S. (1914) *Z. physik. Chem. 88:* 212
Angell, C.A. (1982) "Supercooled Water" in "Water: A Comprehensive Treatise" (F. Franks, ed.) Vol. 7, Chapter 1, pp. 1–81
Benson, S.W. and Ellis, D.A (1948) *J. Amer. Chem. Soc. 70:* 3563
Benson, S.W., Ellis, D.A. and Zwanzig, R.W. (1950) *J. Amer. Chem. Soc. 72:* 2101
Bradley, R.S. (1936a) *J. Chem. Soc.* pp. 1467–1474
Bradley, R.S. (1936b) *J. Chem. Soc.* pp. 1799–1804
Brummer, S.B., Bradspies, J.I., Enrine, G., Leung, C. and Lingertat, H. (1972) *J. Phys. Chem. 76:* 457
Brunauer, S., Emmett, P.H. and Teller, E. (1938) *J. Amer. Chem. Soc. 60:* 369
Bull, H. (1944) *J. Amer. Chem. Soc. 66:* 1499
Cassie, A.B.D. (1945) *Trans. Farad. Soc. 41:* 450
Chambers, R. and Hale, H.P. (1932) *Proc. Roy. Soc. London Ser. B 110:* 336
Clegg, G.S., McClean, V.E.R., Szwarnowski, S. and Sheppard, R.J. (1984) *Phys. Med. Biol. 29:* 1409
Cohn, W. and Cohn, E.F. (1939) *Proc. Soc. Exp. Biol. Med. 41:* 445
Conway, B.E. (1952) "Electrochemical Data" Elsevier, New York
Coolidge, A.S. (1926) *J. Amer. Chem. Soc. 48:* 1796
Coolidge, A.S. (1927) *J. Amer. Chem. Soc. 49:* 712 (Figures 3 and 4)
Cope, F. W. (1969) *Biophys. J. 9:* 303
Damadian, R. (1971) *Science 171:* 1151
Dean, R. (1941) *Biol. Symp. 3:* 331
De Boer, J. H. and Zwikker, C. (1929) *Zeitschr. physik. Chem. B3:* 407
Debye, P. (1929) "Polar Molecules", Chemical Catalogue Co., New York
Deryaguin, B.V. (1933) *Z. Physik. 84:* 657
Deryaguin, B.V. (1987) *Langmuir (ACS Journal of Surfaces and Colloids) 3:* 601
Deryaguin, B.V. and Landau, L (1941) *Acta Physicochim. URSS 14:* 633
Dorsay, N.F. (1940) "Properties of Ordinary Water Substances" ACS Monograph 81, American Cancer Soc., New York
Drost-Hanson, W. (1971) In "Chemistry of the Cell Surface" Part B. (H.D. Brown, ed.) Academic Press, New York, p.1

Drost-Hansen, W. and Singleton, J. Lin (1991) "Our Aqueous Heritage: Evidence for Vicinal Water in Cells" in "Fundamentals of Medical Celll Biology" (E.E. Bittar, ed.) Vol. 3A, Chapter 5, JAJ Press, Inc.
Eastoe, J.E. and Leach, A.A. (1958) In "Recent Advances in Gelatin and Glue Research" (G. Stainsby, ed.) Pergamon Press, London
Ehrenpreis, S. (1967) *Ann. N.Y. Acad. Sci. (Discussion) 144:* 754
Eisenberg, D. and Kauzmann, W. (1969) "The Structure and Properties of Water" Oxford University Press, New York,
Fowler, R., and Guggenheim, E. (1960) "Statitical Thermodynamics", Cambridge Univ. Press, Cambridge, England
Fox, J.J. and Martin, A.E. (1940) *Proc. Roy. Soc., London 179:* 234
Gehler, L.S.T. (1825) *Phys. Wörterbuch* 1: 40, Leipzig, Germany
Giguère, P.A. and Harvey, K.B. (1956) *Canad. J. Chemistry 34:* 798
Glasstone, S. (1946) "Textbook of Physical Chemistry" Van Nostrand, New York
Glaus, S. and Calzaferri, G. (1999) *J. Phys. Chem. 103:* 5622
Gurney, R.W. (1949) "Introduction to Statistical Mechanics", McGraw-Hill, Inc., New York
Hallet, J. (1965) *Fed. Proc. Symp. 24:* S 34
Harkins, W.D. (1945) *Science 102:* 292
Hazlewood, C.F. , Nichols, B.L. and Chamberlain, P. F. (1969) *Nature 222:* 747
Heidorn, D.B., Rorschach, H.E., Hazlewood, C.F., Ling, G.N. and Nicklow, R.M. (1986) *Biophys. J. 49:* 92A
Henniker, J.C. (1949) *Review Modern Physics 21:* 322
Heppel, L.S. (1939) *Amer. J. Physiol. 127:* 385
Hill, T.L. (1946) *J. Phys. Chem. 14:* 263
Hoover, S.R. and Mellon, E.F. (1950) *J. Amer. Chem. Soc. 72:* 2562
Hori, T. (1956) *Low Temperature Science A15:* 34 (English translation) No. 62, US Army Snow, Ice and Permafrost Res. Establishment, Corps of Engineers, Wilmette, Ill.
Hutchings, B. L. (1969) *Bioch. Biophys. Acta 174:* 734
Israelachvili, J. (1985) "Intermolecular and Surface Forces", Academic Press, New York
Israelachvili, J., (1987) *Ace. Chem. Rev. 20:* 415
Israelachvili, J. and Adams, G.E. (1976) *Nature 262:* 774
Kaatze, U., Göttman, O., Rodbielski, R., Pottel, R. and Terveer, U. (1978) *J. Phys. Chem. 82:* 112
Kamnev, I. Ye. (1938) *Arkh. Anat. Gisiol. i Embry. 19:* 145
Kaplanski, S. Ya. and Boldyreva, N. (1934) *Fisiol. Zh. 17:* 96
Katchman, B. and McLaren, A.D. (1951) *J. Amer. Chem. Soc. 73:* 2124
Kayser, H. (1881) *Wied. Ann. der Physik 14:* 463
Langmuir, I. (1918) *J. Amer. Chem. Soc. 40:* 1362
Langmuir, I. (1921) *Trans. Farad. Soc. 17:* 9
Leeder, J.D. and Watt, I.C. (1974) *J. Coll. Interf. Sci. 40:* 339
Ling, G.N. (1952) In "Phosphorous Metabolism" (Volume II) (W.D. McElroy and B. Glass, eds) The Johns Hopkins Univ. Press, Baltimore pp. 748–795
Ling, G.N. (1962) "A Physical Theory of the Living State: the Association-Induction Hypothesis" Blaisdell, Waltham, MA
Ling, G.N. (1965) *Ann. N.Y. Acad. Sci. 125:* 401
Ling, G.N. (1969) *Intern. Review Cytology 26:* 1
Ling, G.N. (1970) *Intern. J. Neuroscience 1:* 129
Ling, G.N. (1972) In "Water and Aqueous Solutions: Structure, Thermodynamics and Transport Processes" (A. Horne, ed.) Wiley-Interscience, New York pp 663–699
Ling, G.N. (1972a) In "Water Structure at the Water-Polymer Interface" (H.H. Jellinek, ed), Plenum Press, New York pp. 4–13
Ling, G.N. (1973) *Biophys. J. 13:* 867
Ling, G.N. (1978) *Proc. Sixth Intern. Biphys. Symp.* (Kyoto) p. 389

Ling, G.N. (1980) In "Cooperative Phenomena in Biology" (ed., G. Karremann) Pergamon Press, New York, pp. 39–69
Ling, G.N. (1980–1981) "International Cell Biology" (ed., H.G. Schweiger) Springer Verlag, Berlin, New York pp. 904–914
Ling, G.N. (1983) *Physiol. Chem. Phys. & Med. NMR 15:* 155
Ling, G.N. (1984) "In Search of the Physical Basis of Life", Plenum, New York
Ling, G.N. (1985) In "Water and Ions in Biological Systems" (A. Pullman, V. Vaselescu and L. Packer, eds.) Plenum Press, New York pp. 79-94
Ling, G.N. (1987) *Physiol. Chem. Phys. & Med. NMR 19:* 159
Ling, G.N. (1992) "A Revolution in the Physiology of the Living Cell", Krieger, Malabar, Fl.
Ling, G.N. (1993) *Physiol. Chem. Phys. & Med. NMR 25:* 145
Ling, G.N. (1997) *Physiol. Chem. Phys. & Med. NMR 29:* 123
Ling, G.N. (2001) "Life at the Cell and Below-Cell Level; The Hidden History of a Fundamental Revolution in Biology" Pacific Press, New York
Ling, G.N. (2004a) *Physiol. Chem. Phys. & Med. NMR* (in press)
Ling, G.N. and Hu, W.H. (1987) *Physiol. Chem. Phys. & Med. NMR 19:* 251
Ling, G.N. and Hu, W.H. (1988) *Physiol. Chem. Phys. & Med. NMR 20:* 293
Ling, G.N. and Murphy, R.C. (1983) *Physiol. Chem. Phys. & Med. NMR 15:* 137
Ling, G.N. and Negendank, W. (1970) *Physiol. Chem. Phys. 2:* 15
Ling, G.N. and Ochsenfeld, M.M. (1987) *Physiol. Chem. Phys. 19:* 177
Ling, G.N. and Ochsenfeld, M.M. (1989) *Physiol. Chem. Phys. 21:* 19
Ling, G.N. and Walton, C.L. (1976) *Science 191:* 293
Ling, G.N. and Zhang, Z.L. (1983) *Physiol. Chem. Phys. & Med. NMR 15:* 391
Ling, G.N., Miller, C. and Ochsenfeld, M.M. (1973) *Ann. N.Y. Acad. Sci. 204:* 6
Ling, G.N., Ochsenfeld, M.M., Walton, C., Bersinger, T.J. (1980) *Physiol. Chem. Phys. 12:* 3
Ling, G.N., Niu, Z. and Ochsenfeld, M.M. (1993) *Physiol. Chem. Phys. & Med. NMR 25:* 177
Ling, G.N., Walton, C., and Ochsenfeld, M.M. (1981) *J. Cell Physiol. 106:* 385
Lippincott, E.R., Cessac, G.L., Stromberry, R.R. and Grant, W.H. (1971) *J. Coll. and Interfcial Sci. 36:* 443
Lloyd, D.J. (1933) *Biol. Rev., Cambridge Philos. Soc. 8:* 463
Lloyd, D. and Phillips, H. (1933) *Trans. Farad. Soc. 29:* 132
Lonsdale, K. (1958) *Proc. Roy. Soc. A 247:* 424
McBain, J.W. (1932) "The Sorption of Gases and Vapors by Solids", George Rutledge and Sons, Ltd., London
McClellan, A.L. (1963) "Dipole Moments", Freeman, San Francisco
McLaren, A.D. and Rowen, J.W. (1951) *J. Polymer Sci. 7:* 289
Mellon, E.F., Korn, A.H. and Hoover, S.R. (1948) *J. Amer.Chem. Soc. 70:* 3040
Mellon, E.F., Korn, A.H, and Hoover, S.R. (1949) *J. Amer. Chem. Soc. 71:* 2761
Miller, C. and Ling, G.N. (1970) *Physiol. Chem. Phys. 2:* 495
Moeller, T. (1952) "Inorganic Chemistry: An Advanced Textbook", John Wiley & Sons, Inc., New York p. 139, p. 828
Moelwyn-Hughes, E.A. (1964) "Physical Chemistry", 2nd Ed., McMillan, New York,
Narton, A.H., Danford, M.D, and Levy, H.A. (1967) *Discuss. Farad. Soc. 43:* 97
Nasonov, D.H. and Aizenberg, E.I. (1937) *Biol. Zh. 6:* 165
Pashley, R.M., McGuiggan, P, M., Hinham, B.W. and Evans, D.F. (1985) *Science 229:* 1088
Pauling, L. (1960) "The Nature of the Chemical Bond", Cornell Univ. Press, Ithaca, New York, p. 465
Peschel, G. and Belouschek (1979) In "Cell-Associated Water" (W. Drost-Hanson and J. Clegg, eds.) Academic Press, New York
Polányi, M. (1914) *Verh. Deut. Physik. Ges. 16:* 1012
Polge, C., Smith, A.U. and Parkes, A. S. (1949) *Nature 164:* 666
Pulker, H.K. (1984) "Coatings on Glass" in Thin Film Science and Technology 6, Elsevier, Science Publishing Co., New York, p. 9

Rall, W.F. (1987) *Cryobiology 24:* 387
Reyerson, L.H. and Peterson, L. (1955) *J. Phys. Chem. 59:* 1117
Rorschach, H.E. (1984) In "Water and Ions in Biological Systems" (V. Vasilescu, ed.) Pergamon, New York
Rossini, F.D., Wagman, D.D., Evans, W.H., Levine, S. and Jaffe, I. (1952) Chemical Thermodynamic Properties, National Bureau of Standards, Circular 500
Rothschuh, K.E. (1973) "History of Physiology" Kreiger Publ. Co., Malabar, FL
Rushbrooke, G.S. (1949) "Introduction to Statistical Mechanics" Oxford, at Clarenden Press
Sänger, R. and Steiger, O. (1928) *Helv. Phys. Acta 1:* 369
Saussure, T. de (1814) Gilbert's *Ann. der Physik 47:* 113
Steinbach, C. (1940) *J. Biol. Chem.. 133:* 695
Trantham, E.C., Rorschach, H.E., Clegg, J., Hazlewood, C.F., Nicklow, R.M. and Wabakayachi, N. (1984) *Biophys. J. 45:* 927
Urquhart, A.R. and William, A.M. (1924) *J. Text. Inst. 15:* T146
Wennerholm, U.B., Albertson-Wikland, K., Bergh, C., Hamberger, L., Niklasson, A., Nilsson, L, Thiringer, Wennergen, M.. Wikland, M., Borres, M.P. (1998) *Lancet 35:* (9109): 1085–90
Wu, H. and Yang, E.F. (1931) *Proc. Soc. Exper. Biol. Med. 29:* 248
Zacchariasen, W.H. (1932) *J. Amer. Chem. Soc. 54:* 3841
Zeise, H. (1928) *Z. physik Chem. 136:* 409, Figs. 6 and 7
Zocher, H. and Coper, K. (1928) *Zeits. f. physik. Chemie 132:* 295
Zsigmondy, R. (1911) *Zeits. anorg. Chem 71:* 356

Received May 20, 2000;
accepted December 10, 2003.

Physiol. Chem. Phys. & Med. NMR (2003) *35*: 131–143

Cepharanthine, an Anti-inflammatory Drug, Suppresses Mitochondrial Membrane Permeability Transition

Makoto Nagano[1,2], Tomoko Kanno[1*], Hirofumi Fujita[1,3], Shikibu Muranaka[1,3], Takuzo Fujiwara[1], Kozo Utsumi[1]

[1] *Institute of Medical Science, Kurashiki Medical Center, Kurashiki 710-8522, Japan*
[2]*Department of Surgery Omiya Medical Center, Jichi Medical School, Amanuma-cho, Saitama 330-0824, Japan* [3]*Doonan Institute of Medical Science, Ishikawa-cho, Hakodate 041-8502, Japan*
**Corresponding author*

Abstract: Cepharanthine (CEP), a biscocrourine alkaloid, has been widely used in Japan for the treatment of several disorders. Furthermore, accumulated evidence shows that CEP protects against some cell death systems but not others. Recently, it was found that mitochondria play an important role in a mechanism of apoptosis involving membrane permeability transition (MPT). Although CEP stabilizes the mitochondrial membrane structure and protects some functions of mitochondria from damage, the mechanism of action of CEP on MPT remains obscure. In this study, therefore, we examined the effect of CEP on Ca^{2+}- and Fe^{2+}/ADP-induced MPT of isolated mitochondria. CEP inhibited Ca^{2+}-induced swelling, depolarization, Cyt.c release, and the release of Ca^{2+} in a concentration dependent manner. CEP also inhibited Ca^{2+}-induced generation of reactive oxygen species and Fe/ADP-induced swelling and lipid peroxidation. Furthermore, CEP suppressed Ca^{2+}-induced thiol modification of adenine nucleotide transloase (ANT). These results suggested that CEP suppressed MPT by a decrease in affinity of cyclophilin D for ANT. From these results it was concluded that the suppression of MPT by CEP might be due to its inhibitory action on Ca^{2+} release and antioxidant activity and that CEP might suppress the mechanism of apoptotic cell death when directly interacted with mitochondria in cells.

Abbreviations: AA, arachidonic acid; CEP, Cepharanthine; CMPT, classic membrane permeability transition; CsA, cyclosporin A; Cyt.c, ferricytochrome c; diS-C3-(5), 3,3'-dipropyl-2,2'-thiodicarbocyanine iodide; L-012, 8-amino-5-chloro-7-phenulpyrido[3,4-*d*]pyridazine-1,4-(2*H*,3*H*)dioen; M_t, mitochondria; MPT, membrane permeability transition; $O2^-$, superoxide; PUFA, polyunsaturated fatty acid; RCR, respiratory control ratio; ROS, reactive oxygen species; TBA, thiobarbituric acid; TBARS, TBA reactive substances; TFP, trifluoperazine.

CEPHARANTHINE (CEP) is a biscoclaurine alkaloid isolated from *Stephania cepharantha Hayata*. The chemical structure of CEP is shown in Figure 1. CEP is known to act as a membrane stabilizer [1], an inhibitor of neutrophil superoxide generation [2, 3], and a drug to combat the anti-multidrug resistance action of cancer cells [4, 5]. Thus, CEP has been widely used in Japan for the treatment of several disorders. Recently, it was reported that the alkaloid induces caspase-dependent and Fas-independent apoptosis in Jurkat and K52 human leukemia cells [6, 7]. In other words, CEP exerts antitumour effects via its apoptosis-inducing activity [8]. On the contrary, it has also been reported that CEP inhibits TNF-α- and gp120-induced apoptosis in differentiated human neuroblastoma cells [9–11]. These results indicate that the mechanism of action of CEP against programmed cell death remains obscure.

Accumulated evidence indicates that mitochondria play an important key role in the mechanism of apoptosis in various cells. Mitochondria contain many proteins for controlling apoptosis and the release of these proteins from the mitochondria into the cytosol is mediated by the opening of the membrane permeability transition (MPT) pore [12]. MPT is characterized by mitochondrial swelling, loss of membrane potential and a non-specific release of ions, small molecules and some proteins via a cyclosporin A (CsA)-, Ca^{2+}- and trifuloperazine-sensitive mechanism [13–16]. In this context, we reported recently that CEP suppressed the mitochondrial dysfunctions induced by several conditions, such as anoxia and lipid peroxidation [16–18]. Thus, it is predicted that CEP affects the opening of the MPT pore of mitochondria when induced by various reagents. In this study, therefore, we examined the effects of CEP on the changes in various functions of isolated mitochondria, such as swelling, depolarization, Cyt.c release, lipid peroxidation. In this paper, we report that CEP suppresses the mitochondrial MPT, Cyt.c release, generation of reactive oxoygen species (ROS) and thiol modification of adenine nucleotide transloase (ANT) brought about by Ca^{2+}, and that CEP inhibits the mitodhondrial and lipid peroxidation by Fe^{2+}/ADP.

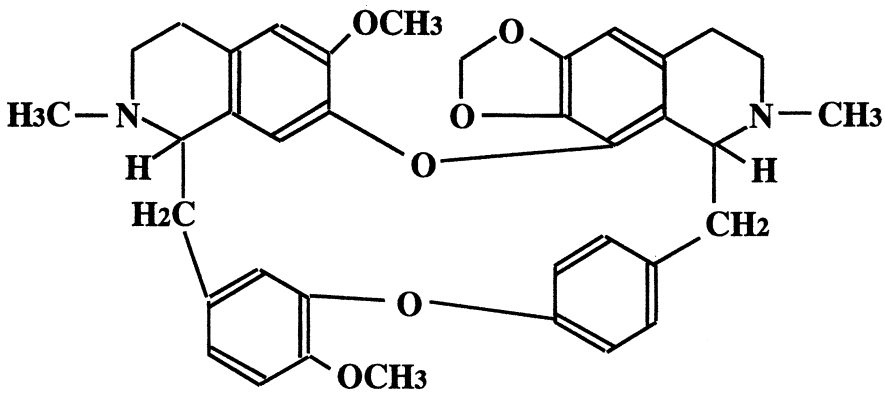

FIGURE 1. Chemical structure of CEP

Materials and Methods

Chemicals

Antipyrylazo III, Cyclosporin A (CsA), Cyt c, horseradish peroxide, and trifluoperazine (TFP) were obtained from Sigma Co. LTD (USA). Monoclonal anti-body against Cyt.c was purchased from PharMingen (USA). Rabbit antiserum to ANT was a gift from Dr. Hiroshi Terada (University of Tokushima, Tokushima, Japan). 4-aminophenylarsine oxide agarose (ThioBond Resin) was purchased from Invitrogen, Carlsbad, CA. USA. 3,3'-dipropyl-2,2'-thiodicarbocyanine iodide (diS-C3-(5)), a cyanine dye, was obtained from the Hayashibara Biochemical Laboratories (Okayama, Japan). 8-amino-5-chloro-7-phenulpyrido[3,4-*d*]pyridazine-1,4-(2*H*,3*H*) dioen (L-012) was donated by Dr. Imada (Osaka City Univ. Med. Sch, Osaka, Japan).

Isolation of mitochondria

Male Wistar rats weighing 200 g were used after overnight fasting. Mitochondria (Mt) were isolated from liver by the method of Hogeboom using sucrose density gradient centrifugation as described previously [17].

Generation of reactive oxygen species by xanthine/xanthine oxidase system

Superoxide was generated by the reaction of 50 μM hypoxanthine (HX) and 1 mU/ml xanthine oxidase in the medium of 10 mM Tris-HCl buffer (pH 7.4) containing 150 mM KCl at 25°C.

Assay for oxygen uptake of mitochondria

Mitochondrial oxygen uptake was monitored polarographically using a Clark type oxygen electrode fitted to a 2 ml water jacketed closed chamber at 25°C. Mitochondria (0.5 mg protein /ml) were incubated in the medium of 10 mM Tris-HCl (pH 7.4) containing 150 mM KCl with various concentrations of Fe^{2+}/ADP as described previously [19].

Assay for calcium transport in mitochondria

Ca^{2+} transport was assessed by monitoring the metallochromic indicator, antipyrylazo III, at 720–790 nm in a Shimadzu UV-3000 dual-wavelength spectrophotometer equipped with a magnetic stirrer and thermostatic control [20]. Mitochondria (0.5 mg protein /ml) were incubated in the medium of 10 mM Tris-HCl (pH 7.4) containing 150 mM KCl with 2.5 mM succinate, 1 mM phosphate buffer (pH 7.4). Mitochondrial Ca^{2+} uptake and release are accompanied proportionally by a decrease and increase in the absorbency, respectively. The amounts of mobilized Ca^{2+} were calibrated at the end of each experiment using authentic $CaCl_2$ solutions, in the presence of 2.5 μM 2,4-dinitrophenol.

Assay for mitochondrial swelling and membrane potential

Mitochondrial swelling and depolarization were assessed by spectrophotometric and fluorometric analyses, respectively. Mitochondria (0.1 mg protein /ml) were incubated in 10 mM Tris-HCl (pH 7.4) containing 150 mM KCl at 25°C. The change in absorbence at 540 nm was recorded using a Shimadzu UV-3000. The membrane potential of the mitochondria was measured in the incubation medium containing 0.2 μg/ml diS-C3-(5).

Fluorescence intensity at 670 nm was recorded in a fluorescence spectrophotometer (Hitachi 650-10LC) during excitation at 622 nm [18].

Western Blot analysis of Cyt.c

Cyt.c release from mitochondria was analyzed by Western blot assay using rat anti-Cyt.c antibody. Mitochondria (0.1 mg protein/ml) were incubated in 10 mM Tris-HCl (pH 7.4) containing 0.15 M KCl at 25°C, and then centrifuged. The supernatants were added to 1/2 the volume of a SDS-sample buffer (125 mM Tris-HCl, pH 6.8, 4% SDS, 10% β-mercaptoethanol, 20% glycerol, and 0.002% bromophenol blue) and boiled at 100°C for 5 min. The samples were then subjected to SDS-polyacrylamide gel electrophoresis. After a transfer of proteins in the gel to an Immobilon filter (Millipore Co.), the filter was incubated with a primary antibody of anti-Cyt.c and then with horseradish peroxide-linked secondary antibody and analyzed by using an ECL kit (Amercium Co) [21]. Protein concentrations were determined by the method of Bradford [22] using bovine serum albumin as a standard.

Assay for lipid peroxidation

Lipid peroxidation in mitochondria was assayed by the thiobarbituric acid (TBA) reaction and values were expressed as being the equivalent of TBA reactive substances (TBARS) [23].

Assay for the reactive oxygen species generation in mitochondria

For the analysis of ROS in mitochondria, a highly sensitive chemiluminescence (CHL) probe, L-012 was used since mitochondria contain a large amount of Mn-SOD [24]. The isolated mitochondria (0.2 mg protein/ml) were incubated in 10 mM Tris-HCl buffer (pH 7.4) containing 150 mM KCl, 2.5 mM succinate and 1 mM phosphate buffer (pH 7.4) in the presence of 100 μM L-120 at 25°C. After incubation of the mitochondria for 1 min, the reaction was started by the addition of 50 μM $CaCl_2$. During the incubation, chemiluminescence (CHL) intensity was recorded continuously for 10 ~ 20 min using an Intercellular Ion Analyzer (Jasco CAF-110) (CHL mord, Jasco PL-03).

Binding of ANT to a phenylarsine oxide-conjugated agarose

The reduced form of ANT was analyzed as described previously [25]. Briefly, mitochondria (2 mg protein) treated with 100 μM $CaCl_2$ in the presence or absence of various reagents were centrifuged at 12,000 × g at 4°C for 5 min. Proteins in the precipitate were solubilized in 100 μl of a 50 mM HEPES buffer (pH 7.4) containing 0.15 M Na_2SO_4, 1 mM EDTA, 3% Triton X-100, 1 mM PMSF, and 1 μM leupeptine. After centrifugation of the lysate at 15,000 × g and 4°C for 5 min, the supernatant fraction was incubated with ThioBond Resin, equilibrated with the 50 mM HEPES buffer (pH 7.4) containing 0.15 M Na_2SO_4, 1 mM EDTA, 0.25% Triton X-100, 1 mM PMSF, and 1 μM leupeptine. After incubation at 4°C for 15 min, the resin was washed three times with 0.5 ml of the buffer by centrifugation at 15,000 × g and 4°C for 1 min. Proteins bound to the resin were eluted by 50 μl of the buffer containing 10 mM dithiothreitol, and analyzed by SDS-PAGE and Western blotting using anti-ANT antiserum.

Results

CEP suppressed Ca^{2+}-induced swelling of mitochondria

Swelling of mitochondria is recognized as a marker of MPT. Ca^{2+} induces a typical MPT and the MPT was inhibited by CsA and TFP. Ca^{2+} induced a typical MPT and CsA and TFP inhibited the swelling. A similar inhibition in a concentration dependent manner was observed when CEP was present in the incubation medium (Figure 2).

CEP suppressed Ca^{2+}-induced depolarization coupled with swelling and Cyt. c release

It is well known that Ca^{2+}-induced swelling is accompanied by depolarization of the inner membrane of mitochondria and Cyt.c release in a CsA inhibitable mechanism (Figure 3A, B, C). CEP suppressed the swelling and the accompanying depolarization and Cyt.c release in a concentration dependent manner.

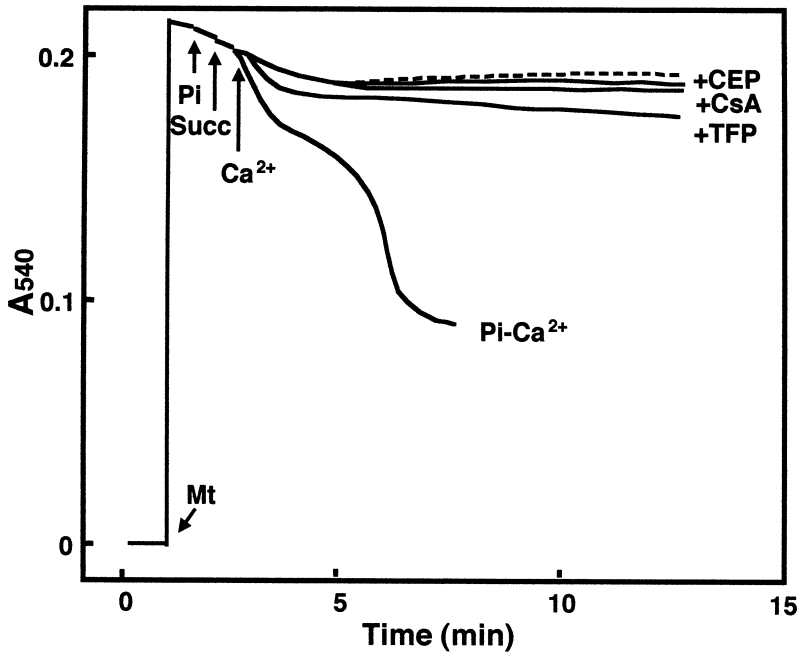

FIGURE 2. Suppression of Ca^{2+}-induced swelling of mitochondria by CsA, TFP and CEP. Mitochondria (0.1 mg protein/ml) were incubated in Tris-HCl buffer (pH 7.4) containing 150 mM KCl at 25°C in the presence or absence of various reagents. Mitochondrial swelling was monitored by absorption at 540 nm. Mitochondrial swelling was induced by 10 μM Ca^{2+} after addition of 2.5 mM succinate and 1 mM inorganic phosphate in the presence or absence of various reagents. Concentrations of CsA, TFP and CEP were 1 μM, 20 μM, and 20 μM respectively. Similar results were obtained in three separate experiments.

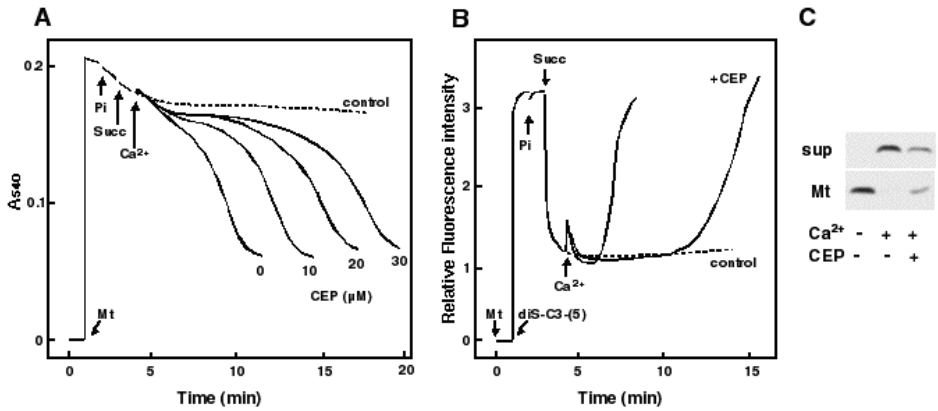

FIGURE 3. Suppression of Ca^{2+}-induced depolarization and Cyt.c release by CEP. Experimental conditions were the same as described in Figure 1. (A) Effect of various concentrations of CEP on the Ca^{2+}-induced swelling of mitochondria. (B) Effect of CEP on depolarization of inner membrane of mitochondria. Membrane potential was monitored by fluorescence of dis-C3-(5). Reagents used were 2.5 mM succinate, 1 mM phosphate, 0.2 μg/ml diS-C3-(5) and 10 μM of Ca^{2+}. (C) Effect of CEP on the release of Cyt.c from mitochondria by Ca^{2+}. Mitochondria were treated for 10 min with 15 μM Ca^{2+} in the presence or absence of 20 μM CEP and fractionated in mitochondria (Mt) and supernatant (Sup). Cyt.c was detected by Western blot using anti-Cyt.c antibody. Similar results were obtained in three separate trials.

CEP suppressed Ca^{2+} release from mitochondria induced by high concentration of Ca^{2+}

The swelling, depolarization, and Cyt.c release induced by Ca^{2+} in mitochondria were all dependent on the transport of Ca^{2+} across the inner mitochondrial membrane. Thus, the effect of CEP on Ca^{2+} transport in mitochondria was examined. If the amount of added Ca^{2+} to the medium in which the mitochondria were suspended was high, the Ca^{2+} was immediately taken up transiently into the mitochondria and then released concomitantly with depolarization and swelling (Figure 4). CEP suppressed the release of Ca^{2+} from the mitochondria in a concentration-dependent manner.

CEP suppressed the Ca^{2+}-induced generation of ROS in mitochondria

Recently it has been reported that Ca^{2+} increased the generation of H_2O_2 in mitochondria [26]. Thus, the effect of Ca^{2+} on the generation of L-012 chemiluminescence (CHL) in mitochondria was examined [24]. HX/XO system generated superoxide and produced $^{\cdot}OH$ through Fenton type Haber Weiss reaction thereby the CHL of L-012 was observed. This CHL was suppressed by CEP in a concentration dependent manner. In this case, XO activity was not inhibited by CEP (data not shown). CHL of L-012 in the mitochondrial suspension was increased by the simple addition of Ca^{2+} in the presence of respiratory substrate and Pi (Figure 5B). This CHL of L-012 was also suppressed by CEP in a concentration-dependent manner.

CEP suppressed Fe^{2+}/ADP-induced swelling coupled with Cyt. c release

Fe^{2+}/ADP also induced the swelling of mitochondria in a CsA-insensitive mechanism. TFP and CEP suppressed both the swelling and Cyt.c release induced by Fe^{2+}/ADP in a

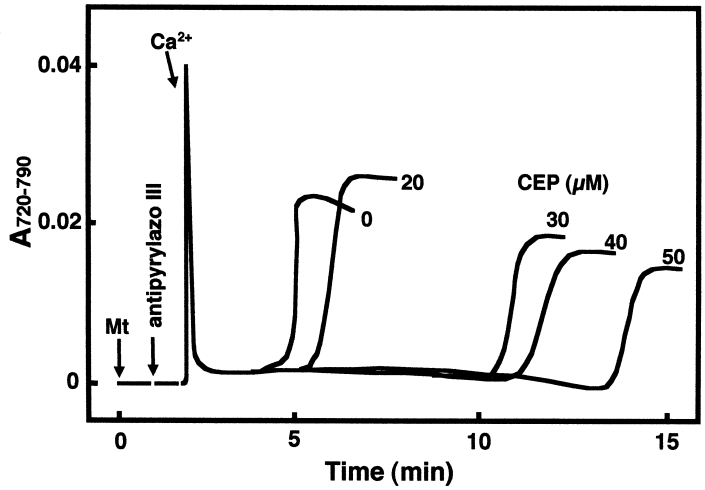

FIGURE 4. The effect of CEP on Ca^{2+}-transport in mitochondria. Mitochondria (0.5 mg protein/ml) were incubated in medium consisting of 10 mM Tris-HCl buffer (pH 7.4), 150 mM KCl, 1 mM phosphate, 2.5 mM succinate, and 50 μM antipyrylazo III. Ca^{2+}-transport in mitochondria was induced by addition of 50 μM in the presence or absence of various concentrations of CEP. Similar results were obtained in three separate trials.

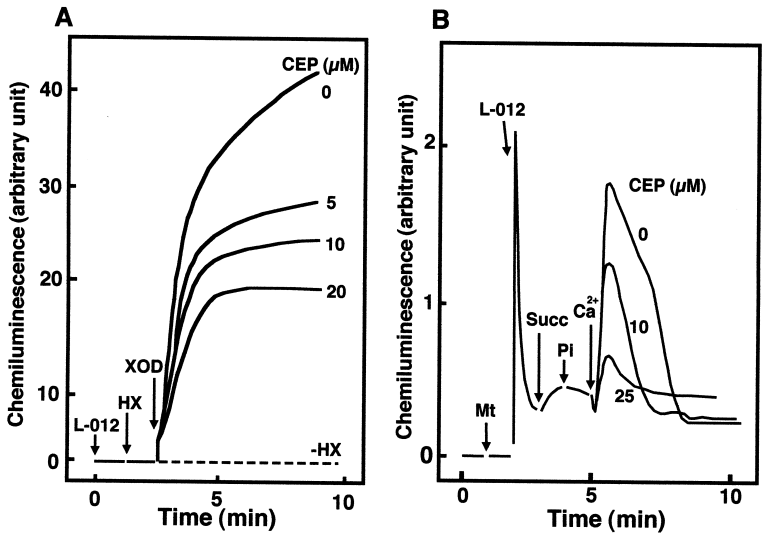

FIGURE 5. Effect of CEP on the ROS generation by HX/XO system- and Ca^{2+}-treated mitochondria. (A) Effect of CEP on the ROS generated by HX/XO system. ROS was generated by 1 mU/ml XO in the medium containing 50 μM hypoxanthine (HX), 100 μM L-012 and various concentrations of CEP at 25°C. (B) Effect of CEP on the ROS generated by mitochondria. Mitochondria (0.2 mg protein/ml) were incubated in the medium of 10 mM Tris-HCl (pH 7.4) containing 150 mM KCl, L-012, and various concentrations of CEP at 25°C and ROS generation was induced by Ca^{2+} after addition of succinate and Pi. Concentrations of added L-012, succinate, inorganic phosphate and Ca^{2+} were 100 μM, 2.5 mM, 1 mM and 25 μM, respectively. Chemiluminescence of L-012 was monitored by Intercellular Ion Analyzer (Jasco CAF-110) (Chemiluminescence mode using Jasco PL-03).

concentration dependent manner (Figure 6A, 6B). The pattern of inhibition of swelling was different from that of Ca^{2+}-induced swelling and the concentration of CEP required for half maximum inhibition was very low, e.g. 10 μM.

CEP inhibited the Fe^{2+}/ADP-induced lipid peroxidation of mitochondria

It has been reported previously that CEP suppresses the lipid peroxidation in mitochondria by means of its radical scavenging activity [27, 28]. To gain further insight into the mechanisms of suppression of Fe^{2+}/ADP-induced mitochondrial oxygen consumption and the generation of TBARS by CEP, the following experiments were carried out. A study of Fe^{2+}/ADP stimulated oxygen consumption by mitochondria in the absence of respiratory substrate showed that the time of oxygen uptake was retarded in the presence of CEP in a concentration dependent manner (Figure 7A). This inhibition was observed from a concentration of 5 μM and reached a maximum at 20 μM. The Fe^{2+}/ADP also induced the production of TBARS in mitochondria and this production was suppressed by CEP as well as by α-tocopherol and TFP but not by δ-tocopherol (Figure 7B). These results indicate that Fe^{2+}/ADP induces lipid peroxidation in mitochondria and that the production of TBARS was suppressed in an antioxidant-sensitive manner [29].

Suppression of the Ca^{2}-induced oxidation of ANT thiol in mitochondria by CEP

ANT is a component of MPT in the inner mitochondrial membrane and has an important role in the ADP/ATP exchange reaction. ANT has three important thiol groups in its amino acid sequence and the ADP/ATP exchange reaction was shown to be inhibited by cross linking these thiol groups between Cys^{160} and Cys^{257} thereby increasing the affinity

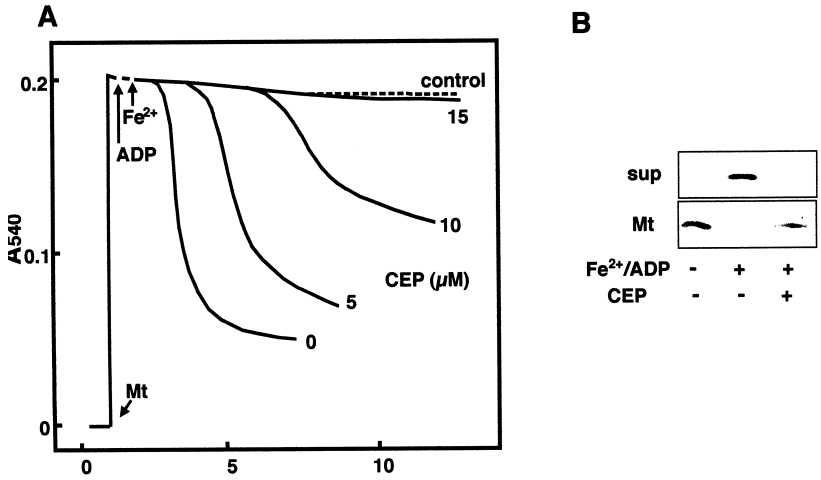

FIGURE 6. Suppression of Fe^{2+}/ADP-induced swelling and Cyt.c release by CEP. Experimental conditions were the same as described for Figure 2. (A) Effect of various concentrations of CEP on the swelling of mitochondria induced by Fe^{2+}/ADP. Mitochondrial swelling was induced by 10 μM Fe^{2+}/100 μM ADP in the presence various concentrations of CEP. (B) Effect of 20 μM CEP on the release of Cyt.c from mitochondria induced by 10 μM Fe^{2+}/100 μM ADP. Cyt.c release was assayed as described in Figure 2C. Similar results were obtained in three separate trials.

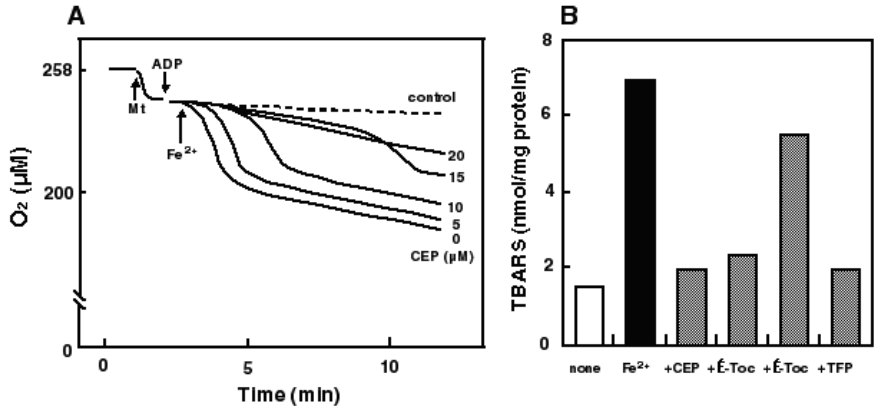

FIGURE 7. Effect of CEP on the oxygen uptake and formation of TBARS of mitochondria induced by Fe^{2+}/ADP. (A) Effect of CEP on the oxygen uptake of mitochondria induced by 10 μM Fe^{2+}/ 100 μM ADP. Mitochondria (0.5 mg protein/ml) were incubated in the medium of Tris-HCl buffer (pH 7.4) containing 150 mM KCl at 25°C in the presence or absence of 5 ~ 25 μM CEP. Oxygen uptake was induced by 10 μM Fe^{2+}/100 μM ADP. Similar results were obtained in three separate trials. (B) Effect of various antioxidants on the Fe^{2+}/ADP-induced lipid peroxidation of mitochondria. Lipid peroxidation was induced by 10 μM Fe^{2+}/100 μM ADP for 20 min at 25°C. Experimental conditions were the same as (A). The concentrations of added CEP, VE, δ–Tocopherol, TFP were 20 μM, 40 μM, 40 μM, and 20 μM, respectively.

of CypD to Pro^{62} near to Cys^{57} [30]. In a preliminary experiment, we thought that Ca^{2+}-Pi oxidized the thiol status of the ANT in mitochondria. Thus, the effect of CEP on the thiol status of ANT was examined with a phenylarsine oxide agarose, an affinity matrix that interacts selectively with vicinal dithiols in some proteins and critical cysteine residues in ANT [25]. Figure 8 shows that the binding of ANT to phenylarsine oxide agarose was inhibited by pretreating the mitochondria with Ca^{2+}-Pi for 5 ~ 10 min (Figure 8A). CEP suppressed the oxidation as observed with CsA and TFP (Figure 8B).

Discussion

In this study, we found that CEP, a non-steroid anti-inflammatory drug, inhibited the Ca^{2+}-induced MPT of isolated mitochondria. All of the Ca^{2+}-induced changes in mitochondria, such as the loss of membrane potential (Delta psi (m)), swelling, Cyt.c release, and the release of Ca^{2+} were suppressed by CEP. A specific inhibitor of MPT, CsA, also inhibited these mitochondrial fractions. CEP also inhibited CsA-insensitive swelling of mitochondria induced by Fe^{2+}/ADP. This inhibitory effect of CEP might be attributable to its antioxidant activity as in the case of TFP. Furthermore, CEP inhibited the Ca^{2+}-induced generation of ROS which modify some ANT thiol groups.

Mitochondria play a central role in both apoptosis and necrosis through a Cyt. c release which leads to the opening of the mitochondrial MPT pore [31]. Many apoptosis related substances are distributed in the intramembrane space between the outer and inner membranes and are released into the cytosol by either classic MPT or the non-classic MPT mechanism [32]. Classic MPT is characterized by the following five properties: swelling,

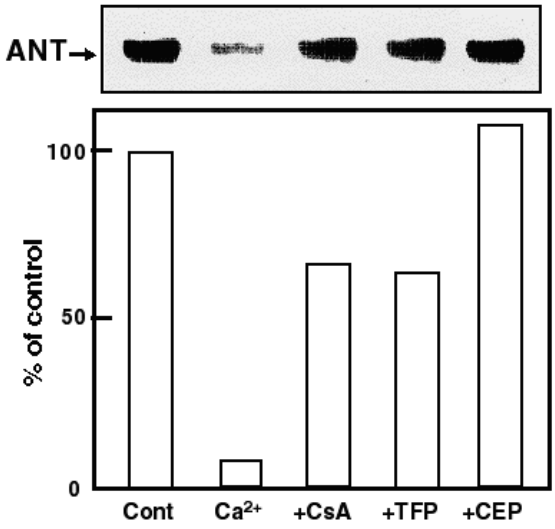

FIGURE 8. Suppression of Ca^{2+}–induced modification of ANT thiol groups by CEP. Mitochondria (2.0 mg/ml) was incubated at 25°C for 5 min in the medium of 10 mM Tris-HCl buffer (pH 7.4) containing 150 mM KCl, 2.5mM succinate, 1 mM phosphate buffer (pH 7.4), 100 μM Ca^{2+} in the presence or absence of 1 μM CsA and 50 μM CEP. Non oxidized ANT was analyzed using phenylarsine oxide agarose and Western blot analysis with anti-ANT antibody. Similar results were obtained in three separate trials.

depolarization, Ca^{2+} release, energy dependence, and CsA- and TFP-sensitive reactions [31, 33]. The MPT pore is formed by the ANT in the inner membrane and VDAC in the outer membrane [34]. The matrix protein, CypD, can interact with ANT, as well as apoptosis-regulatory proteins from the Bax/Bcl-2, Bax family proteins [30]. ANT has two opposite functions. One is a vital, specific antiporter, which accounts for the exchange of ATP and ADP and the other is the ability to form a non-specific pore [34]. Pore formation by ANT is induced by a variety of different agents (e.g., Ca^{2+}, atractyloside, thiol oxidation, the pro-apoptotic HIV-1 protein Vpr, etc.) [34]. Non-specific pore formation is a consequence of a MPT. In isolated mitochondria, pore formation by ANT leads to an increase in the permeability of the inner membrane to solutes up to 1500 Da, swelling of the mitochondrial matrix, and outer membrane permeability, presumably due to the physical rupture of the outer membrane [34]. The MPT is characterized by a strict dependence on matrix Ca^{2+} and sensitivity to CsA. However, it is becoming increasingly clear that other experimental conditions can elicit increases in mitochondrial permeability as non-classic MPT that are insensitive to CsA or Ca^{2+} distinct from the classic MPT [21, 35].

Recently, we classified the mitochondrial swelling into three types [21]. One is the CsA-sensitive swelling, called classic MPT(CMPT), and is induced by various substances, such as Ca^{2+}, fatty acid, 6-OHDA, T3, etc.[35, 36]. The second is the CsA-insensitve swelling, induced by lipid peroxidation caused by Fe^{2+}/ADP, Fe^{2+}/H_2O_2 and AAPH [35]. The third is the CsA-insensitive swelling associated with a coupled membrane depolarization reaction induced by ionophore [37]. CEP inhibited the first and the second types of swelling but not the third type.

As a mechanism of MPT pore opening by Ca^{2+}, a possible hypothesis was proposed by Kowaltowski, A.J. *et al* [26]. They suggested that Ca^{2+} increased the generation of H_2O_2 in mitochondria which may induce oxidation of the protein thiol group and lipid peroxidation. In a preliminary experiment, we observed that Ca^{2+} generated ROS in mitochondria in the presence of respiratory substrate and Pi and cross-linked the ANT thiol groups. In this context, McStay, G.P. *et al.* reported that the affinity of CypD to ANT is increased by the cross-linking of ANT thiol groups [30]. Thus the affinity of ANT was increased by cross-linking of the thiol group by Ca^{2+}-induced generation of ROS thereby bringing about opening of the MPT pore by CypD. In this study, we found that CEP suppressed both generation of ROS and modification of the ANT thiol groups in mitochondria after stimulation by Ca^{2+}. In this context, we found no effect of Ca^{2+} on the concentrations of protein-associated and low molecular weight thiols in mitochondria [38]. Furthermore, we confirmed that CEP suppressed the lipid peroxidation of the mitochondrial membrane induced by Fe^{2+}/ADP [4, 17, 28]. A similar inhibition was also observed in lipid peroxidation induced by Fe^{2+}/H_2O_2 (data not shown). Although the molecular mechanism of anti-MPT action of TFP is not well known, TFP is known as a specific inhibitor of MPT [38]. Preliminary experiments in this laboratory showed the inhibition of membrane lipid peroxidation by TFP. In addition to the antioxidant activity, CEP has membrane stabilization properties [16, 17].

From these results, it is considered that apoptotic cell death might be suppressed by CEP through the inhibition of MPT and lipid peroxidation when CEP interacts directly with mitochondria in the cells. In this context, it has obscured that CEP is rapidly incorporated into the inner leaflet of plasma membrane and affects the morphological structure of red blood cells. Thus it is possible that CEP transfers from cell membrane to mitochondria in the cells. CEP is incorporated dose-dependently into cells in the same concentration range [40]. Furthermore, CEP metabolizes to several intermediates in cells, which also might affect cell death mechanism. Further studies are needed to clarify the molecular mechanism of the action of CEP on MPT and the effects on apoptitic cell death.

This work was supported, in part, by grants from the Ministry of Education, Science and Literature, and the Japan Keirin Association. We would like to thank Dr. Alan A Horton for his help in the preparation of this paper.

References

1. Utsumi, K., Miyahara, M., Sugiyama, K., Sasaki, J. (1976) Effect of biscoclaurine alkaloid on the cell membrane related to membrane fluidity. *Acta Histochem Cytochemi 9:* 59–68.
2. Kobuchi, H., Li, M.J., Matsuno, T., Yasuda, T., Utsumi, K. (1992) Inhibition of neutrophil priming and tyrosyl phosphorylation by cepharanthine, a nonsteroidal antiinflammatory drug. *Cell Struct Funct 17:* 385–393.
3. Matsuno, T., Orita, K., Edashige, K., Kobuchi, H., Sato, E.F., Inoue, B., Inoue, M., Utsumi, K. (1990) Inhibition of active oxygen generation in guinea-pig neutrophils by biscoclaurine alkaloids. *Biochem Pharmacol 39:* 1255–1259.
4. Shiraishi, N., Shimada, T., Hagino, Y., Kohno, K., Kobayashi, M., Kuwano, M., Akiyama, S. (1988) Potentiation by a biscoclaurine alkaloid, cepharanthine, of the toxicity of conjugates of epidermal growth factor with Pseudomonas exotoxin in HeLa cells. *Cancer Res 48:* 1307–1311.

5. Shiraishi, N., Akiyama, S., Nakagawa, M., Kobayashi, M., Kuwano, M. (1987) Effect of bisbenzylisoquinoline (biscoclaurine) alkaloids on multidrug resistance in KB human cancer cells. *Cancer Res 47:* 2413–2416.
6. Wu, J., Suzuki, H., Akhand, A.A., Zhou, Y.W., Hossain, K., Nakashima, I. (2002) Modes of activation of mitogen-activated protein kinases and their roles in cepharanthine-induced apoptosis in human leukemia cells. *Cell Signal 14:* 509–515.
7. Wu, J., Suzuki, H., Zhou, Y.W., Liu, W., Yoshihara, M., Kato, M., Akhand, A.A., Hayakawa, A., Takeuchi, K., Hossain, K., Kurosawa, M., Nakashima, I. (2001) Cepharanthine activates caspases and induces apoptosis in Jurkat and K562 human leukemia cell lines. *J Cell Biochem, 82:* 200–214.
8. Harada, K., Bando, T., Yoshida, H., Sato, M. (2001) Characteristics of antitumour activity of cepharanthine against a human adenosquamous cell carcinoma cell line. *Oral Oncol 37:* 643–651.
9. Okamoto, M., Ono, M., Baba, M. (2001) Suppression of cytokine production and neural cell death by the anti-inflammatory alkaloid cepharanthine: a potential agent against HIV-1 encephalopathy. *Biochem Pharmacol 62:* 747–753.
10. Maruyama, H., Kikuchi, S., Kawaguchi, K., Hasunuma, R., Ono, M., Ohbu, M., Kumazawa, Y. (2000) Suppression of lethal toxicity of endotoxin by biscoclaurine alkaloid cepharanthine. *Shock. 13:* 160–165.
11. Oyaizu, H., Adachi, Y., Yasumizu, R., Ono, M., Ikebukuro, K., Fukuhara, S., Ikehara, S. (2001) Protection of T cells from radiation-induced apoptosis by Cepharanthin. *Int Immunopharmacol 1:* 2091–2099.
12. Zoratti, M., Szabo, I. (1995) The mitochondrial permeability transition. *Biochim Biophys Acta 1241:* 139–176.
13. Gunter, T.E., Pfeiffer, D.R. (1990) Mechanisms by which mitochondria transport calcium. *Am J Physiol 258:* C755–786.
14. Igbavboa, U., Zwizinski, C.W., Pfeiffer, D.R. (1989) Release of mitochondrial matrix proteins through a Ca^{2+}-requiring, cyclosporin-sensitive pathway. *Biochem Biophys Res Commun 161:* 619–625.
15. Broekemeier, K.M., Pfeiffer, D.R. (1989) Cyclosporin A-sensitive and insensitive mechanisms produce the permeability transition in mitochondria. *Biochem Biophys Res Commun 163:* 561–566.
16. Miyahara, M., Okimasu, E., Mikasa, H., Terada, S., Kodama, H., Utsumi, K. (1984) Improvement of the anoxia-induced mitochondrial dysfunction by membrane modulation. *Arch Biochem Biophys 233:* 139–150.
17. Aono, K., Shiraishi, N., Arita, T., Inouye, B., Nakazawa, T., Utsumi, K. (1981) Changes in mitochondrial function by lipid peroxidation and their inhibition by biscoclaurine alkaloid. *Physiol Chem Phys 13:* 137–144.
18. Furuno, T., Kanno, T., Arita, K., Asami, M., Utsumi, T., Doi, Y., Inoue, M., Utsumi, K. (2001) Roles of long chain fatty acids and carnitine in mitochondrial membrane permeability transition. *Biochem Pharmacol 62:* 1037–1046.
19. Utsumi, T., Okuma, M., Kanno, T., Takehara, Y., Yoshioka, T., Fujita, Y., Horton. A.A., Utsumi, K. (1995) Effect of the antiretroviral agent hypericin on rat liver mitochondria. *Biochem Pharmacol 50:* 655–662.
20. Scarpa, A., Brinley, F.J. Jr., Dubyak, G. (1978) Antipyrylazo III, A "middle range" Ca^{2+} metallochromic indicator. *Biochemistry 17:* 1378–1386.
21. Kanno, T., Fujita, H., Muranaka, S., Yano, H., Kajitani, N., Yoshioka, T., Inoue, M., Utsumi, K. (2003) Mitochondrial membrane permeability transition and cytochrome c release: correlation with cyclosporin A-sensitivity and Ca^{2+}-dependency. *Physiol Chem Phys & Med NMR 34:* 1–15.
22. Bradford, M.M. (1976) A rapid and sensitive method for the quantitation of microgram quantities of protein utilizing the principle of protein-dye binding. *Anal Biochem 72:* 248–254.

23. Ohkawa, H., Ohnishi, N., Yagi, K. (1979) Assay for lipid peroxides in animal tissues by thiobarbituric acid reaction. *Anal Biochem 95:* 351–358.
24. Imada, I., Sato, E.F., Miyamoto, M., Ichimori, Y., Minamiyama, Y., Konaka, R., Inoue, M. (1999) Analysis of reactive oxygen species generated by neutrophils using a chemiluminescence probe L-012. *Anal Biochem 271:* 53–58.
25. Nishikimi, A., Kira, Y., Kasahara, E., Sato, E.F., Kanno, T., Utsumi, K., Inoue, M. (2001) Tributyltin interacts with mitochondria and induces cytochrome c release. *Biochem J 356:* 621–626.
26. Kowaltowski, A.J., Castilho, R.F., Vercesi, A.E. (2001) Mitochondrial permeability transition and oxidative stress. *FEBS Lett 495:* 12–15.
27. Shiraishi, N., Arima, T., Aono, K., Inouye, B., Morimoto, Y., Utsumi, K. (1980) Inhibition by biscoclaurine alkaloid of lipid peroxidation in biological membranes. *Physiol Chem Phys 12:* 299–305.
28. Kogure, K., Goto, S., Abe, K., Ohiwa, C., Akasu, M., Terada, H. (1999) Potent antiperoxidation activity of the bisbenzylisoquinoline alkaloid cepharanthine: the amine moiety is responsible for its pH-dependent radical scavenge activity. *Biochim Biophys Acta 1426:* 133–142.
29. Hara, S., Endo, T., Kuriiwa, F., Kano, S., Iwata, N. (1992) Antioxidant effect of calmodulin antagonists in rat brain homogenate. *Res Commun Chem Pathol Pharmacol 76:* 367–370.
30. McStay, G.P., Clarke, S.J., Halestrap, A.P. (2002) Role of critical thiol groups on the matrix surface of the adenine nucleotide translocase in the mechanism of the mitochondrial permeability transition pore. *Biochem J 367:* 541–548.
31. Lemasters, J.J., Nieminen, A.L., Qian, T., Trost, L.C., Elmore, S.P., Nishimura, Y., Crowe, R.A., Cascio, W.E., Bradham, C.A., Brenner, D.A., Herman, B. (1998) The mitochondrial permeability transition in cell death: a common mechanism in necrosis, apoptosis and autophagy. *Biochim Biophys Acta 1366:* 177–196.
32. Sultan, A., Sokolove, P.M. (2001) Free fatty acid effects on mitochondrial permeability: an overview. *Arch Biochem Biophys. 386:* 52–61.
33. Tatton, W.G., Olanow, C.W. (1999) Apoptosis in neurodegenerative diseases: the role of mitochondria. *Biochim Biophys Acta 1410:* 195–213.
34. Vieira, H.L., Haouzi, D., El Hamel, C., Jacotot, E., Belzacq, A.S., Brenner, C., Kroemer, G. (2000) Permeabilization of the mitochondrial inner membrane during apoptosis: impact of the adenine nucleotide translocator. *Cell Death Differ 7:* 1146–1154.
35. Sultan, A., Sokolove, P.M. (2001) Palmitic acid opens a novel cyclosporin A-insensitive pore in the inner mitochondrial membrane. *Arch Biochem Biophys 386:* 37–51.
36. Kashiwagi, A., Kanno, T., Arita, K., Ishisaka, R., Utsumi, T., Utsumi, K. (2001) Suppression of T(3)- and fatty acid-induced membrane permeability transition by L-carnitine. *Comp Biochem Physiol B Biochem Mol Biol 130:* 411–418.
37. Inai, Y., Yabuki, M., Kanno, T., Akiyama, J., Yasuda, T., Utsumi, K. (1997) Valinomycin induces apoptosis of ascites hepatoma cells (AH-130) in relation to mitochondrial membrane potential. *Cell Struct Funct 22:* 555–563.
38. Kanno, K., Sato, F.E., Muranaka, S., Fujita, H., Fujiwara, T., Utsumi, T., Inoue, M., Utsumi, K. (2003 In press) Oxidative stress underlies the mechanism for Ca^{2+}-induced Permeability transition of mitochondria. *Free Rad Res*.
39. Kushnareva, Y.E., Sokolove, P.M. (2000) Prooxidants open both the mitochondrial permeability transition pore and a low-conductance channel in the inner mitochondrial membrane. *Arch Biochem Biophys 376:* 377–388.
40. Sato, T., Kanaho, Y., Fujii, T. (1980) Relation of characteristic action of biscoclaurine alkaroids on the erythrocyte membrane and their incorporation into the membrane. *Cell Struct Funct 5:* 155–163.

Received May 23, 2003;
accepted August 20, 2003.

Physiol. Chem. Phys. & Med. NMR (2003) *35*: 145–156

MR Imaging of Vertebral Metastases at 0.2 Tesla: Clinical Evaluation of T1-weighted Opposed-phase Gradient-echo Imaging

Seiichiro Ohno[1,*], Izumi Togami[2], Tetsuro Sei[3], Kentaro Ida[3], Masatoshi Tsunoda[3], Kiyonori Yamaoka[4], Susumu Kanazawa[3] and Yoshio Hiraki[3]

[1]*Central Division of Radiology, Okayama University Hospital, Okayama 700-8558, Japan,* [2]*Department of Radiology, Okayama Saiseikai General Hospital, Okayama 700-8511, Japan,* [3]*Department of Radiology, and* [4]*Medical Radioscience, Okayama University Medical School, Okayama 700-8558, Japan,* **Corresponding author*

Abstract: The purpose of this study was to evaluate clinically T1-weighted spin-echo imaging (T1-SE) and T1-weighted opposed-phase gradient-echo (T1-opposed GRE) in medical examinations for vertebral metastases using 0.2 Tesla MRI. Twenty-one patients (9 males and 12 females, 105 vertebrae) with non-neoplastic lesions were assigned to the normal group (Group N), whereas 27 patients (16 males and 11 females, 133 vertebrae) with malignant metastatic vertebral lesions were assigned to the metastatic group (Group M). Using quantitative analysis , the contrast to noise ratio (CNR) for bone marrow to muscle in the region of interest (ROI) defined by the operator were determined with both groups, whereas the CNR for lesion to bone marrow was determined with Group M. In the subjective analysis, 275 vertebrae of 27 patients in Group M were evaluated. There were significant differences in the Group M between CNR values, T1-SE and T1-opposed GRE. The evaluation by T1-SE image alone was rated as 85.0% for sensitivity, 99.3% for specificity, respectively. On the other hand, evaluation rate only by T1-opposed GRE was 98.5% for sensitivity, 82.4% for specificity, respectively. T1-opposed GRE image is an effective tool for 0.2 Tesla MRI to examine metastatic bone marrow tumors. These findings indicate the necessity of both T1-SE and T1-opposed GRE in diagnostic imaging of vertebral metastases using 0.2 Tesla MRI.

Abbreviations: CHESS—chemical shift selective saturation; CNR—contrast to noise ratio; CT—computed tomography; GRE—T1-weighted opposed-phase gradient-echo; MRI—magnetic resonance imaging; SD—standard deviation; SI—signal intensity; STIR—short TI inversion recovery; T1-opposed ROI—region of interest; T1-SE—T1-weighted spin-echo; TE—time of echo; TR—time of repetition; TSE—turbo spin echo.

IN CURRENT diagnostic imaging, MRI is indispensable for bone marrow in particular. Since the tissue contrast of bone marrow is high, very sensitive images can be obtained by MRI. The image quality is largely influenced by the magnetic strength of the instrument. Open type MRI has been widely used, especially for patients with claustrophobia and biopsy. The main instruments used in the clinical field are low-field and middle-field MRI, which have the following faults; poor image quality and long scan times. Especially for 0.2 Tesla MRI, the frequency difference between water and lipid is only 28 Hz and so, the chemical shift selective saturation method (CHESS method), a frequency specific method usually applied to 1.5 Tesla can not be used. Previously we suggested that the opposed-phase gradient-echo (GRE) chemical shift technique might be applicable to the spine to compensate for such fault [1,2]. Open type low-field MRI has been spreading in Europe, especially the Scandinavian area and about 1,200 MRIs of less than 0.35 Tesla are working in Japan (May 2001). Presently in Japan about 30% of the MRIs are such types. It is important to effectively utilize these instruments for improvement of clinical efficiency in Japan [3,4]. The purpose of this study was to evaluate the diagnostic value of T1-weighted opposed-phase gradient-echo sequences for the detection of vertebral metastases by using a 0.2 Tesla MRI unit.

Materials and Methods

Patients

MRI examinations of 195 thoracic vertebrae and 80 lumbar vertebrae were retrospectively evaluated for the following two patient groups: i.e., twenty-one patients (9 males and 12 females, 105 vertebrae) with non-neoplastic lesions were assigned to the normal group (Group N), whereas 27 patients (16 males and 11 females, 133 vertebrae) with metastatic vertebral lesions were assigned to the metastatic group (Group M). The mean age was 59 years (19–73 years, 59.0 ± 11.1) for Group N and 58 years (27–81 years, 58.0 ± 10.5) for Group M. Group N included the patients who visited our hospital with chief complaints of backache and lumbago, and were examined by X-ray, CT or MRI, where no abnormality or non-neoplastic disease such as spondylosis, herniated disk were disclosed. On the other hand, Group M included the patients in whom metastases to vertebral body were revealed by X-ray, CT or scintigraphy examination. Metastatic disease of Group M was confirmed in a patient (one vertebral body) by biopsy and 4 patients (29 vertebral bodies) by autopsy. For the remaining patients of this group, histological data were not obtainable to confirm the metastatic disease. The primary neoplasm was lung cancer for 9 patients, breast cancer for 4, esophageal cancer for 3, hepatocellular carcinoma for 3, prostatic cancer for 3, rectal cancer for 2 and one each of pancreatic cancer, uterine cervix cancer and gastric cancer. Neither group included patients with compression fractures. This study was conducted in accordance with the "Recommendations Guiding Medical Doctors in Biomedical Research Involving Human Subjects," contained in the Declaration of Helsinki.

MR imaging

A 0.2-Tesla resistive magnet (Magnetom Open, Siemens, Erlangen, Germany) with a small body coil was used for MR imaging. T1-weighted spin-echo imaging (T1-SE) and T1-opposed GRE of the thoracic or lumbar spines were conducted in the sagittal plane.

The MR protocol consisted of a T1-SE sequence and T1-opposed GRE acquisition. The conditions for the former were TR/TE 621 ms/26 ms, flip angle 90°, slice thickness 5 mm, matrix 256 × 192, field of view 32 cm, No. of excitation 2, anterior saturation pulse, band width 39 Hz/pixel, scan time 7 min and 36 sec for the former. The conditions for T1-opposed GRE acquisition were TR/TE 500 ms/17ms, flip angle 90°, slice thickness 5 mm, matrix 256 × 192, field of view 32 cm, No. of excitation 2, anterior saturation pulse, band width 56 Hz/pixel and scan time 4 min and 51 sec.

Quantitative analysis

The contrast to noise ratio (CNR) for bone marrow to muscle in the region of interest (ROI) defined by the operator were determined with both groups, whereas the CNR for lesion to bone marrow was determined with Group M. A total of 74 vertebrae in the center of the image, which were applicable to measure a ROI of 50 mm^2 or more, were used as the image subjects. For Group N, ROI was set to the largest possible, while for the Group M ROI was set to the outlines of the metastatic tumors. Signal intensity (SI) of ROI greater than 50 mm^2 was determined for the vertebral muscle at identical positions on different slices. Bone marrow to muscle CNR was defined as the absolute value of the difference between the mean SI of bone marrow (SI-bone) for the normal bone marrow of Group N or an affected one of Group M and the mean SI of muscle (SI-muscle) divided by the mean standard deviation of ROIs for air parts at the four corners (SDair). Whereas, lesion to bone marrow CNR was defined as the absolute value of the difference between the mean SI of affected bone marrow and the mean SI of normal bone marrow divided by SDair.

Subjective analysis

Evaluation was made with 275 vertebrae from 27 patients in Group M. Monitoring by T1-SE and T1-opposed GRE MRI were independently carried out by two radiologists who were blind to the clinical information of the patients. The recording of lesion sites were made in random order by the radiologists. The assessment criteria for metastasis were a low signal in T1-SE and a high signal in T1-opposed GRE. As to the evaluation criteria, the number of vertebrae was used as the recorded score even if one vertebra included more than one lesion. When an unclear-bordered abnormal signal like a node was found in a vertebra or abnormal signal was found in all vertebrae, the case was judged as a lesion. When there were discrepancies in the number and the position of lesions between the two readers, a decision was made in consensus. The final decision as to metastasis or not was also made in consensus based on the findings of the T1-SE images, the T1-opposed GRE images, the contrast enhanced images, X-ray, CT or scintigraphy examination, biopsy, autopsy or follow up images if available and the conclusion was regarded as the total clinical evaluation (the gold standard). The comparison criteria of the superiority of T1-opposed GRE image to the T1-SE one was judged according to the following; "excellent": The T1-opposed GRE images indicated the same numbers of lesion as in the gold standard (total clinical evaluation), compared with the T1-SE images, while the latter indicated different numbers of lesion; "equal": Numbers of lesion and sites shown in the above two kinds of the images and the gold standard were the same, "poor": The T1-opposed GRE images indicated different numbers of lesion or wrong sites, compared with the gold standard, while the T1-SE images indicated the same numbers of lesion as in the gold standard; and "both poor": false positive and false negative for both T1-opposed GRE and T1-SE.

Statistical analysis

The values of CNR for normal bone marrow to muscle of Group N and those for affected bone marrow to muscle of Group M obtained by T1-SE and T1-opposed GRE images, were expressed as mean ± SD. Statistical analysis was performed with the Welch's t-test and the non-paired Student's t-test. The reason for this is that it is desirable to use the Student's t-test if distribution of two groups is equal, and to use the Welch's t-test if it differs clearly. CNR values of the normal and the affected bone marrow of Group M by T1-SE and T1-opposed GRE, were expressed as mean ± SD. Statistical analysis was performed with the paired Student's t-test. For clinical evaluation, monitoring by T1-SE and T1-opposed GRE MRI were independently evaluated in random order by two radiologists. Statistical analysis was performed with the Wilcoxon's signed ranks test.

Results

Quantitative analysis

The values of CNR for normal bone marrow to muscle of Group N and those for affected bone marrow to muscle of Group M obtained by T1-SE and T1-opposed GRE images are presented in Figure 1. The CNR of the former group, 18.7 ± 4.7 (n = 105) on the T1-SE image, was significantly higher than that of the latter, 5.8 ± 3.4 (n = 74) ($p < 0.0001$, Welch's t-test), and also on T1-opposed GRE, the CNR of normal bone marrow to muscle of Group N (20.1 ± 4.5, n = 105) was significantly higher than that of affected bone marrow to muscle of Group M (5.7 ± 4.5, n = 74) ($p < 0.0001$, non-paired Student's t-test).

CNR values of the normal and the affected bone marrow of Group M by T1-SE and T1-opposed GRE are shown in Figure 2. There were significant differences between CNR values, 14.6 ± 7.2 (n = 74) for T1-SE and 20.2 ± 6.0 (n = 74) for T1-opposed GRE ($p < 0.001$, paired Student's t-test).

Subjective analysis

Clinical evaluation for each patient is shown in Table 1 and the results were totaled in Tables 2 and 3. The evaluation by T1-SE image alone was rated as 85.0% (113/133) for sensitivity, 99.3% (141/142) for specificity, 92.4% (254/275) for accuracy, and 99.1% (113/114) and 87.6% (141/161) for positive and negative predictive values, respectively. On the other hand, the evaluation rate only by T1-opposed GRE was 98.5% (131/133) for sensitivity, 82.4% (117/142) for specificity, 90.2% (248/275) for accuracy, and 84.0% (131/156) and 98.3%(117/119) for positive and negative predictive values, respectively. The evaluation by both T1-SE image and T1-opposed GRE was rated as 100% (133/133) for sensitivity, 100% (142/142) for specificity, 100% (275/275) for accuracy, and 100% (114/114) and 100% (161/161) for positive and negative predictive values, respectively. Thus, the results as to superiority between T1-opposed GRE and T1-SE imaging was as follows: 7 cases (25.9%) for "excellent", 13 (48.1%) for "equal", 4 (14.8%) for "poor" and 3 (11.1%) for "both poor". Wilcoxon's signed ranks test showed no significant differences among them ($p = 0.366$).

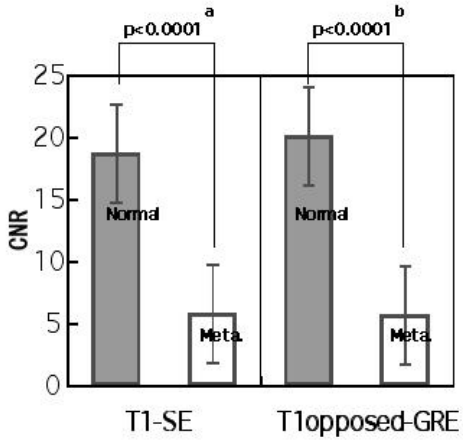

FIGURE 1. The values of CNR of normal bone marrow to muscle of the Normal group and those for affected bone marrow to muscle of the Metastatic group obtained by T1-SE and T1-GRE images. Results were expressed as mean ± SD. Statistical analysis was performed with the Welch's t-test[a] and the non-paired Student's t-test[b].

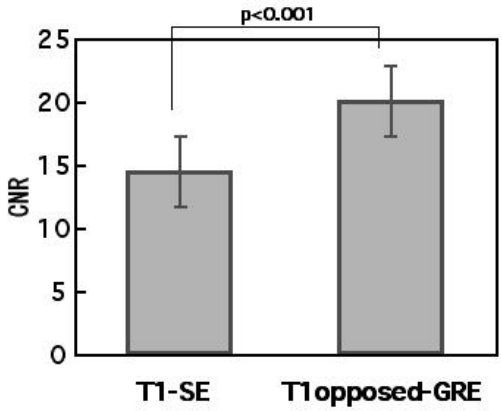

FIGURE 2. CNR values of the normal and the affected bone marrow of the Metastatic group by T1-SE and T1-opposed GRE images. Results were expressed as mean ± SD. Statistical analysis was performed with the paired Student's t-test.

TABLE 1. Clinical evaluation for each patient

Patient	Age/gender	Number of metastatic vertebrae on T1-SE image	Number of metastatic vertebrae on T1-opposed GRE image	Number of metastatic vertebrae on the Total clinical evaluation	Superiority of T1-opposed GRE image to T1-SE image
1	60/M	2	4	4	excellent
2	81/F	1	1	1	equal
3	51/F	1	1	1	equal
4	56/F	2	3	2	poor
5	61/M	1	1	1	equal
6	52/M	2	4	4	excellent
7	77/M	3	3	3	equal
8	63/M	2	2	2	equal
9	69/F	21	21	21	equal
10	67/M	4	7	4	poor
11	61/M	3	2	2	excellent
12	69/M	1	6	1	poor
13	69/M	2	2	2	equal
14	38/M	10	10	10	equal
15	50/F	2	11	11	excellent
16	65/F	4	13	6	both poor
17	44/F	2	3	3	excellent
18	47/F	3	3	3	equal
19	66/F	1	3	1	poor
20	27/F	3	4	4	excellent
21	39/M	1	1	1	equal
22	76/M	3	8	4	both poor
23	47/M	11	11	11	equal
24	61/M	6	6	6	equal
25	52/M	6	8	7	both poor
26	56/M	12	12	12	equal
27	72/M	5	6	6	excellent
Total	275	114	156	133	

TABLE 2. Clinical evaluation on the T1-SE images (275 vertebrae)

T1-SE	Signal	No signal	Total
Metastasis	113	20	133
Normal	1	141	142
Total	114	161	275

Sensitivity: 85.0% (113/133), Specificity: 99.3% (141/142), Accuracy: 92.4% (254/275), Positive predictive values: 99.1% (113/114), Negative predictive values: 87.6% (141/161).

TABLE 3. Clinical evaluation on the T1-opposed GRE images (275 vertebrae)

T1-SE	Signal	No signal	Total
Metastasis	131	2	133
Normal	25	117	142
Total	156	119	275

Sensitivity: 98.5% (131/133), Specificity: 82.4% (117/142), Accuracy: 90.2% (248/275), Positive predictive values: 84.0% (131/156), Negative predictive values: 98.3% (117/119).

TABLE 4. Clinical evaluation on both the T1-SE and T1-opposed GRE images (275 vertebrae)

T1-SE and T1-opposed GRE	Signal	No signal	Total
Metastasis	133	0	133
Normal	0	142	142
Total	133	142	275

Sensitivity: 100% (133/133), Specificity: 100% (142/142), Accuracy: 100% (275/275), Positive predictive values: 100% (133/133), Negative predictive values: 100% (142/142).

Figure 3 shows MR images of a 72-year-old woman who was presented with osteolytic metastases from lung cancer. On the T1-SE sagittal image, focal lesions are shown as low-intensity areas, whereas the normal bone marrow is shown as high-intensity area. On the T1-opposed GRE sagittal image, focal lesions are shown with high-signal intensity, whereas the normal bone marrow is shown with low-signal intensity. MR images of a 66-year-old woman who was presented with an osteosclerotic metastasis from breast cancer are seen in Figure 4. On the T1-SE sagittal image, a focal lesion is shown as a low-intensity area. On the T1-opposed GRE image, a low-intensity area is found in the high intensity area.

Discussion

It is well known that bone scintigraphy is used as the first tool to examine vertebral metastasis. However, a high uptake image on bone scintigraphy does not always indicate the presence of a vertebral metastasis and so, MR imaging becomes necessary as the second tool for final diagnosis. Detection of metastatic tumor focus by MRI is highly sensitive because it allows disclosing of metastatic focus as abnormal signals before the structural destruction of trabecula. Generally, metastatic tumor of bone is imaged with low-signal intensity on T1-SE and slightly heterogeneous signals on T2-weighted turbo spin echo (TSE). Fat tissue tends to have a higher intensity signal because of the influence of adjacent 180° pulse in TSE than SE and so, the former is not so useful in practice. Therefore, T1-SE and T1-opposed GRE were chosen in this study.

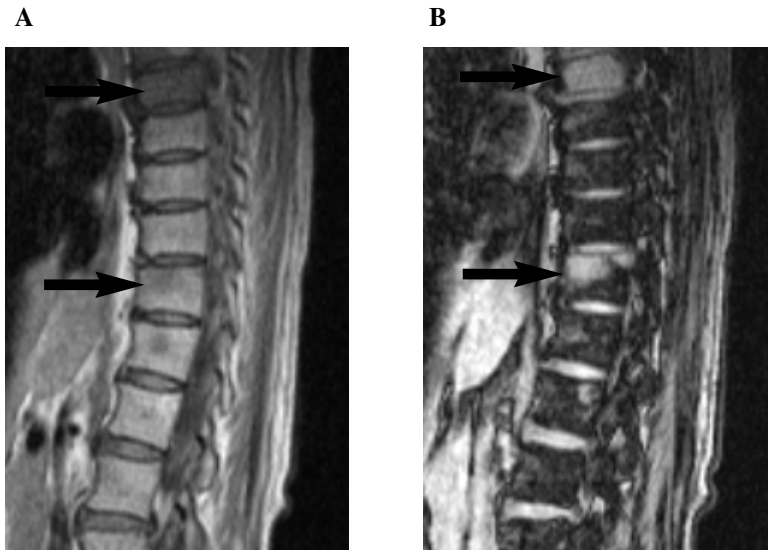

FIGURE 3. Seventy-two-year-old woman who was presented with osteolytic metastases from lung cancer, A) focal lesions are shown as low-intensity areas on the T1-SE sagittal image, whereas the normal bone marrow is shown as a high-intensity area. B) focal lesions are shown with high-signal intensity on the T1-opposed GRE sagittal image, whereas the normal bone marrow is shown with low-signal intensity.

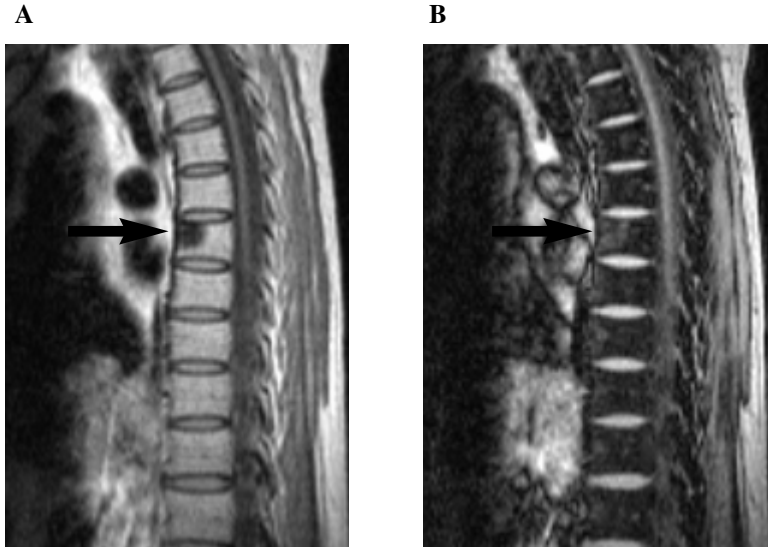

FIGURE 4. Sixty-six-year-old woman who was presented with an osteosclerotic metastasis from breast cancer, A) a focal lesion is shown as a low-intensity area on the T1-SE sagittal image. B) a low-intensity area was found in the high intensity area on the T1-opposed GRE image.

The compositions of normal red and yellow bone marrow have been reported as 40% water, 40% fat and 20% protein, and 15% water, 80% fat and 5% protein, respectively [5]. The bone marrow changes from red to yellow depending on age and positional differences in its changes are also age-dependent [6,7]. Especially in the spine, it was reported that about 50% of red bone marrow remains at age 70 [5]. The favorite localization of metastatic bone marrow tumor was reported to be coincident with the presence of red bone marrow in adults [8]. Also there is a report showing that when normal bone marrow is completely changed to red bone marrow, lipids are not included [9]. Therefore, the T1-SE image shows high intensity of signal in normal bone marrow because of the presence of lipids, whereas it shows low intensity in the metastatic tumor.

The protons of water and lipid make precession in the vertical plane to the magnetic direction with slightly different frequencies, ca. 220 Hz for 1.5 Tesla and ca. 28Hz for 0.2 Tesla. The protons of water rotate at higher speed, resulting in them preceding by 360° to that of lipid. Therefore, the phase of both protons changes time-dependently from in-phase to opposed-phase. This phenomenon appears in the GRE method not in the SE method using 180° pulse. In the in-phase image where the phase of protons from water and lipid is coincident, the sum of intrinsic intensities of water and lipid produces a signal intensity on the image. On the other hand, for opposed-phase in which the phase of protons from water is not coincident to that of lipid, the signal intensity is not different from that of a tissue consisting of water or lipid alone. However, the phases of protons from water and lipid drown each other, so that the signal intensity on the image is produced by the difference between the intrinsic signal intensities of water and lipid. In the opposed-phase image, a signal with a low intensity is more distinctive and detectable because the signals of proteins from water and lipid offset each other in a tissue containing water and lipid, similar to a voxel [1,10,11]. Therefore, the signal intensity of normal red bone marrow becomes lower in an opposed-phase image [10].

It has been reported that opposed-phase GRE technique is useful for examination of bone marrow with pathological abnormalities [11,12,13]. However, initial cases of bone marrow lesions studied using 0.6 Tesla MRI were described in these reports. Disler *et al.* [9] indicated that opposed-phase GRE was more effective to predict bone marrow lesions using 1.5 Tesla. Moreover, they pointed out that in a lesion in which fatty bone marrow is substituted with tumor cells, a lowering of signal intensity is not observed on the opposed GRE image, but lowering occurs in cases of edema, hemorrhage and inflammation because preexisting fat cells remain in the lesion. Seiderer *et al.* [10] reported systemic data indicating that the signal intensity is related to tissue parameters and image parameters of the opposed GRE technique and concluded that the opposed GRE image is a sensitive method to clarify pathogenic features of red bone marrow. In the report of Zampa *et al.* [14] , it was described that opposed GRE is useful to discriminate malignant and benign vertebral lesions using 0.5 Tesla. However, there is no report describing that metastatic vertebral tumor was examined using low-field MRI with 0.2 Tesla. So, we attempted to evaluate the opposed-phase GRE method for examination of metastatic vertebral tumor.

To suppress the effects of lipid, various methods such as the CHESS method, short TI inversion recovery method (STIR method), opposed-phase GRE method are ordinarily applied at present [14]. The CHESS method is used as a frequency-selective fat saturation method, which is useful for 1.5 Tesla in which the frequency difference between water and fat is 220 Hz [15]. For 0.2 Tesla in which the difference is 28 Hz, the method is not

applicable to a low-field apparatus [15]. On the other hand, the STIR method aims to repress the fat effects using an inversion recovery method. Eustace *et al.* [17] reported that regarding 1.5 Tesla, the STIR method is more sensitive than bone scintigraphy to assess the bone of the whole body with metastasis to bone, but further study is needed for its clinical significance. In addition, there are some reports describing that the STIR method is more sensitive for examination of bone marrow lesions [18,19]. Our previous study indicated that the efficacy of the STIR method was better than that of opposed-phase GRE method, especially for tissues where lipid content is high [1]. However, scan time using the apparatus was as long as 9 min for STIR and 6 min for the turbo-STIR method. The STIR method thus takes a longer time for imaging and the number of images is restricted. Slicing for the STIR method must be conducted with an interval more than 30% of the slice thickness, whereas slicing for T1-SE, T2-TSE and opposed GRE imaging can be done without an interval. Therefore, clinical availability of the STIR method is lower because imaging at an identical position is not possible with the method. The opposed-phase GRE method is a method of phase-selective fat saturation. In this method, fat effects are repressed by making good use of phase differences between water and lipid and the effects are more repressed with an increase of lipid content [15]. This is usable in low-field apparatus and for the apparatus, including GRE sequence, imaging can be done in a comparatively short time without dependence on magnetic field intensity [1,15]. The T1-weighted system of opposed GRE was used in this study since signal intensity at flip angle 90° for T1-weighted is stronger [1] and the system is more profitable for comparative study because it has been most frequently used for the evaluation of metastatic bone marrow tumor.

Regarding quantitative analysis, there were significant differences in the respective measurements of CNR for the normal bone marrow and muscle of Group N, and the affected bone marrow and muscle of Group M, between the T1-SE and T1-opposed GRE image. This means that both T1-SE and T1-opposed GRE were able to disclose significant differences between Group N and Group M. However, the differences in the respective measurements of CNR for the normal bone marrow and the affected bone marrow obtained by T1-SE and T1-opposed GRE were significant ($p < 0.001$), indicating that for metastatic bone marrow tumor, CNR obtained by T1-opposed GRE was superior to that obtained by T1-SE. Vertebra in the center region of an image that had a measurable ROI greater than 50 mm^2 was chosen for imaging to prevent variation of signal intensity due to a small ROI and a lowering of sensitivity in the peripheral regions. In subjective analysis, it was shown that the positive predictive value for single use of T1-SE was 99.1%, higher than the 84.0% for that of T1-opposed GRE, whereas the negative predictive values for the former were 87.6%, lower than the 98.3% for the latter. These results indicated that false positives were less in the single use of T1-SE, while false negatives were less in that of T1-opposed GRE. The superiority of the T1-opposed GRE image to that of T1-SE was not significant ($p = 0.366$). The false negatives for the single use of T1-SE seemed to be due to the difficulties in discriminating the lesion region and the remaining red bone marrow, and to disclose the lesion in the peripheral region of the image because of lower sensitivity. Whereas the false positives were thought to be due to the difficulties in disclosing the lesion in patients with previous experience of radiological therapy or osteosclerotic metastasis, and in the elderly with degeneration in the side of the endplate. In the cases with previous radiological therapy, the treated site mostly changed to fatty tissue and in

those of osteosclerotic metastasis, signal loss is apt to occur because of susceptibility due to calcium. The differences in susceptibility between trabecular tissue and soft tissue might cause magnetic hindrance, resulting in strong inhomogeneities due to dephasing of transverse magnetization in the static magnetic field [20]. These changes are different from those of osteolytic metastasis. Zampa *et al.* [14] described that the opposed-phase GRE technique is less useful in cases of lymphoma and myeloma, which are disorders that can contain neoplastic elements mixed with fat, and in the cases of osteosclerotic metastasis because the increased mineralized bone results in signal loss. Thus, T1-opposed GRE is able to compensate for the faults of the T1-SE image. So, it is thought that the sensitivity of examination for metastatic bone marrow tumor by the conventional T1-SE technique using 0.2 Tesla MRI would be raised by the addition of T1-opposed GRE. In diagnostic imaging using 0.2 Tesla MRI, we insist on the necessity of both.

There are some case reports of compression fracture [14,21]. However, the cases of compression fracture were excluded from the subjects of this study because present low-filed MRI is not applicable to them and further study is necessary.

The limiting factor of this study was the number of patients, i.e., Group M consisted of only 27 patients and the cases of primary neoplasm did not satisfy the ordinal distribution. However, the number of cases were larger than the previous report by Uchida *et al.* [16] and the present results well reflected the respective characteristics of T1-SE and T1-opposed GRE. Although the number of subject cases in this study was limited, the present findings were thought reliable after consideration of previous studies [16]. Contrast enhanced images were used only as a reference. In conclusion, the T1-opposed GRE image is an effective tool for 0.2 Tesla MRI to examine bone-marrow metastases of solid tumors. Results suggest the necessity of both T1-SE and T1-opposed GRE in diagnostic imaging of vertebral metastases using 0.2 Tesla MRI.

References

1. Ohno, S., Togami, I., Sasai, N., Kitayama, T., Ohkawa, Y,. Kobashi, T., Arioka, T., Kimura, F., Morioka, Y. (2000) Study of opposed-phase image in examination of metastatic bone marrow tumor using low-field MRI scanner. *Jpn. J. Radiol. Technol.* 56(9): 1163–1169. (In Japanese)
2. Togami, I., Ohno, S., Sasai, N., Yuzurio, A., Sei, T., Tsunoda, M., Akaki, S., Joja, I., Hiraki, Y. (2001) Opposed-phase bone marrow imaging with low-field MRI basic studies and initial clinical experience. *Jpn. J. Tomo.* 28(1): 9–16.
3. Merl, T., Scholz, M., Gerhardt, P., Langer, M., Laubenberger, J., Weiss, H.D., Gehl, H.B., Wolf, K.J., Ohnesorge, I. (1999) Results of a prospective multicenter study for evaluation of the diagnostic quality of an open whole-body low-field MRI unit. A comparison with high-field MRI measured by the applicable gold standard. *Eur. J. Radiol. 30:* 43–53.
4. Ertl-Wagner, B.B., Reith, W., Sartor, K. (2001) Low field-low cost: can low-field magnetic resonance systems replace high-field magnetic resonance systems in the diagnostic assessment of multiple sclerosis patients? *Eur. Radiol. 11(8):* 1490–1494.
5. Vogler, III, J.B., Murphy, W.A. (1988) Bone marrow imaging. *Radiology 168:* 679–693.
6. Dooms, G.C., Fisher, M.R., Hricak, H., Richardson, M., Crooks, L.E., Genant, H.K. (1985) Bone marrow imaging: magnetic resonance studies related to age and sex. *Radiology 155:* 429–432.
7. Ricci, C., Cova, M., Kang, Y.S., Yang, A., Rahmonui, A., Scott, Jr, W.W., Zerhouni, E.A. (1990) Normal age-related patterns of cellular and fatty bone marrow distribution in the axial skeleton: MR imaging study. *Radiology 177:* 83–88.

8. Russel, W.J., Yoshinaga, H., Antoku, S., Mizuno, M. (1966) Active bone marrow distribution in the adult. *Br. J. Radiol. 39:* 735–739.
9. Disler, D.G., McCauley, T.R., Ratner, L.M., Kesack, C.D., Cooper, J.A. (1997) In-phase and out-of-phase MR imaging of bone marrow. *AJR 169:* 1439–1447.
10. Seiderer, M., Staebler, A., Wagner, H. (1999) MRI of bone marrow: opposed-phase gradient-echo sequences with long repetition time. *Eur. Radiol. 9:* 652–661.
11. Neumann, K., Hosten, N., Venz, S. (1995) Screening for skeletal metastases of the spine and pelvis: gradient-echo opposed-phase MRI compared with bone scintigraphy. *Eur. Radiol. 5:* 276–284.
12. Wismer, G.L., Rosen, B.R., Buxton, R., Stark, D.D., Brady, T.J. (1985) Chemical shift imaging of bone marrow: preliminary experience. *AJR 145:* 1031–1037.
13. Rosen, B.R., Fleming, D.M., Kushner, D.C., Zaner, K.S., Buxton, R.B., Bennet, W.P., Wismer, G.L., Brady, T.J. (1988) Hematologic bone marrow disorders: quantitative chemical shift MR imaging. *Radiology 169:* 799–804.
14. Zampa, V., Cosottini, M., Michelassi, M.C., Ortori, S., Bruschini, L., Bartolozzi, C. (2002) Value of opposed-phase gradient-echo technique in distinguishing between benign and malignant vertebral lesions. *Eur. Radiol. 12:* 1811–1818.
15. Delfaut, E.M., Beltran, J., Johnson, G., Rousseau, J., Marchandise, X., Cotton, A. (1999) Fat suppression in MR imaging: techniques and pitfalls. *Radiographics 19:* 373–382.
16. Uchida, N., Sugimura, K., Kajitani, A., Yoshizako, T., Ishida, T. (1993) MR imaging of vertebral metastases: evaluation of fat saturation imaging. *Eur. J. Radiol. 17:* 91–94.
17. Eustace, S., Tello, R., DeCarvalho, V., Carey, J., Wroblicka, J.T., Melhem, E.R., Yucel, E.K. (1997) A comparison of whole-body turbo STIR MR imaging and planar 99mTc-methylene diphosphonate scintigraphy in the examination of patients with suspected skeletal metastases. *AJR 169:* 1655–1661.
18. Mirowitz, S.A., Apicella, P., Reinus, W.R., Hammerman, A.M. (1994) MR imaging of bone marrow lesions: relative conspicuousness T1-weighted, fat-suppressed T2-weighted, and STIR images. *AJR 162:* 215–221.
19. Pui, M.H., Chang, S.K. (1996) Comparison of inversion recovery fast spin-echo(FSE) with T2-weighted fat-saturated FSE and T1-weighted MR imaging in bone marrow lesion detection. *Skeletal Radiol. 25:* 149–152.
20. Majumdar, S. Thomasson, D. Shimakawa, A. Genant, HK. (1991) Quantitation of the susceptibility difference between trabecular bone and bone marrow: experimental study. *Magn. Reson. Med. 22:* 111–127.
21. Baur, A., Stabler, A., Bruning, R., Bartl, R., Krodel, A., Reiser, M.F., Deimling, M. (1998) Diffusion weighted MR imaging of bone marrow: differentiation of benign versus pathologic compression fractures. *Radiology 207:* 349–356.

Received July 17, 2003;
accepted February 13, 2004.

Physiol. Chem. Phys. & Med. NMR (2003) *35*: 157–167

Photo-Induced Arousal Response by Hornets

Vitaly Pertsis*, Ana Sverdlov, Maria Kozhevnikov and Jacob S. Ishay**

Department of Physiology and Pharmacology, Sackler Faculty of Medicine,
Tel-Aviv University, Ramat-Aviv 69978, Israel.
** Part of a PhD thesis to be submitted by V.P. to the Tel-Aviv University Senate.*
***To whom correspondence should be addressed.*

Abstract: When an Oriental hornet *Vespa orientalis* is subjected to ether anesthesia and then exposed to ultraviolet A light (UVAL) (at a wavelength of 366 nm), it commences showing signs of awakening by starting to move its limbs. While in the process of waking the voltage on its body surface surges sharply from 17–180 mV (median = 71.0) to a level of 93–570 mV (median = 327.5). This elevated level is maintained for several minutes but subsequently drops sharply to starting level. The increase in voltage is throughout accompanied by fluttering of the wings and movements of the legs, as well as attempts to extricate itself from the bindings to the electrodes. These movements by the awakening hornet persist for several minutes even after the irradiation source is turned off but shortly after the switch-off the hornet lapses into sleep again. The described scenario is generally similar in worker, queen and drone hornets, and may even occur in decapitated specimens. The same type of awakening can be repeated in the same fashion after a while, but then the increase in voltage will be smaller than the first time. Continuous UV irradiation of an anesthetized hornet results in a generalized and protracted awakening which, however, is significantly shorter than in a hornet left anesthetized in the dark.

AS KNOWN the Oriental hornet *Vespa orientalis* (Hymenoptera, Vespinae) is a stinging insect. Hence anyone interested in investigating such insects in the laboratory has to anesthetize them before treating them (transporting them from their natural habitat in the field etc.). In the past, we have tested out various anesthetic agents and ways of administering them, ultimately realizing that the best and simplest method of anesthetizing hornets was by injecting about 10 ml of diethyl ether into a hole dug in the ground directly into the interior of the nest. This procedure leads to full anesthesia of the total nest population within 5–10 minutes, following which the narcotized hornets are amenable to transport to the laboratory and performance of all the necessary scientific procedures (Ishay, 1975). In nature, the nest of hornets is usually located within the ground (Spradbery,1973; Matsuura and Yamane, 1990), and even if hornets of the studied (*Vespa orientalis*) or other species build their nest above ground, they then enwrap it in envelopes, so that whichever the

case, the nest interior is subjected to relative darkness even during the daytime hours. In previous studies we rated that anesthetized hornets inside the nest, which had been accidentally exposed to insolation or fluorescent light awake from the anesthesia before their nest mates that remained in the shade or darkness (Ishay *et al.*, 1994).

We need to point out that in a hornet colony growing up in the nature environment or reared in the laboratory within an artificial breeding box (ABB), the hornets returning from the illuminated field into the dark nest, move over the brood comb cells, in the course of various nest activities, with their back facing down, whereas the hornets that had succumbed to anesthesia, all drop off the combs to lie on the floor of the nest, usually motionless, with their back facing up. The latter condition prevails for about an hour or two until the hornets spontaneously wake up from the anesthesia. We need to remind here that repeated exposures to anesthesia gradually curtail the duration of the process but even so, in the dark, the awakening time is still longer than under illumination (Kirshboim and Ishay, 1998). Regarding the narcotization process, its various stages have been amply described in an earlier publication (Ishay *et al.*, 1994). One caveat needs to be mentioned, namely, that in the course of the anesthesia precautions must be taken to ensure that the liquid ether itself does not touch the hornets, for it is lethal to them. The hornets are subjected only to the ether fumes, which put them to sleep for a certain period of time. Apparently the exposure to ether vapors *per se* is not harmful to the hornets, for previously we have exposed hornets to repeating (5–6) anesthesia session during the same day with no observed change in their behavior nor in their orientating faculties in the field (Kirshboim and Ishay, 2001).

The present investigation was initiated to ascertain whether anesthetized hornets awakening under illumination undergo any measurable electric changes and whether such electric changes must occur in the head region or rather occur in other parts of the body exposed to light, which then 'transmit' the information to the head. Additionally we also deemed it worthwhile to quantify the process of awakening from ether anesthesia in hornets and determine whether there were differences in this regard between worker hornets, queens and drones. Our paper provides some answers to the questions.

Materials and Methods

Colonies of the Oriental hornet were anesthetized *in situ* in the field as previously described (Ishay, 1975), and brood combs were then transported to the laboratory were the ecloding images were housed in ABBs according to age from eclosion, and were fed on a diet previously described till their exposure to anesthesia. Usually hornets of the same colony were kept in the same ABB to avoid possible friction between members of different colonies. The volume of the ABB was fixed, amounting to about 10,000 cm^3. As for the anesthetic, this was diethyl ether soaked into a cotton pad to the amount of 5 ml, and introduced into an ABB containing a group of hornets. Once anesthetized, the hornets are picked at random serially, and removed one by one to be affixed at two bodily points to electrodes (in so-called alligator fashion), and then placed in an incubator at a fixed 30°C and a relative humidity (RH) exceeding 90%. The electrode-connected hornets are illuminated for 20 minutes by a UV light beam of 366 nm wavelength (henceforth UVAL) and the strength of 44 Lux. The remaining minutiae of the measurement procedure are as

previously described (Pertsis *et al.*, 2001). The behavior of the UVAL exposed hornet can be monitored thought the translucent 'window' of the incubator. In recap, the protocol of the measurement is as follows: a) you anesthetize 10 adult workers of 5 or more days of age, albeit uniform of age inside the ABB; b) starting one minute later, you remove the first hornet (be it worker, drone or young queen, depending as the makeup of the group) and hook it up to 'alligators' connected to a voltmeter; c) the hooked-up hornet is placed in an incubator, irradiated with UV light, observed for its behavior and then measured for voltage for 20 minutes; d) next, the UVAL is switched off and measurement continues in the dark for several minutes; e) ultimately the measured hornet is returned to the ABB, after ascertaining that the voltage had reverted to or close to starting level. This procedure is run in successive fashion on one hornet after the other. However, in observations on a decapitated hornet, one first anesthetizes, then snips off the head with delicate scissors and seals the region with paraffin to prevent loss of hemolymph.

Results

In all, 20 hornets were used in the present study, of which 8 were decapitated specimens, and the total comprised of 6 drones, 7 queens and 7 workers. The results of our measurements are given in Table 1, in which x_1 refers to the moment of switching on the UVAL on an anesthetized hornet (0–90 seconds after the anesthesia) hooked up to electrodes, while y_1 is the starting voltage measured at this point (in time). The light is kept on for 20 minutes, during which time, the hornet's behavior is monitored through the window in the incubator. The awakening of each such hornet was gradual and sequential, to wit: first the antennae move, then the mouthparts, the legs and finally the other body parts. When all these movements became coordinated, about a minute after start of the irradiation, the hornet could be seen attempting to free itself, beating its wings, and at this point we ascertained the values of x_2 and y_2. When the voltage (y_2) reached a peak, this peak persisted throughout the wing fluttering and this marked point x_3 and y_3. At the end of this peak period we marked point x_4, y_4. After a while, i.e., after 1 min-26 min of maximal wakefulness, the hornet lapsed back into sleep, whereupon there was a sharp drop in the voltage down to starting level (x_5, y_5). In like fashion, albeit with minor individual differences, behaved all the measured hornets, be they workers, queens or drones, and so also the decapitated hornets. The entire process was repeatable, but on the second and subsequent repeats the recorded voltage was lower. In the event that a live, intact hornet managed to free itself of the electrode bonds ('alligators'), it flew out of the incubators window (if and when it was opened) to some secluded and shaded corner in the laboratory and after a while fell asleep again.

Figure 1 provides in graphic fashion all the voltage measurements undertaken on the 20 studied hornets, so that the various time points (x_s) are coordinated. Now we can observe a stereotypic rise in the voltage, taking place between point x_1 and x_2 and ranging between 32–430 mV. Subsequently, between the time points x_2–x_4, the voltage remains at a relatively high level, but between x_4 and x_5, there is, in most cases, reversion of the voltage to starting level. The means of all the time points are shown graphically in Figure 2,where the finding represent all the data simultaneously. Figure 3 pertains to all the intact hornets (12) while Figure 4 provides the results for the 8 decapitated hornets. When comparing

TABLE 1. Original Data on the Awake Hornets

Experiment number	Sex or Caste	Connection	X_1	Y_1	X_2	Y_2	X_3	Y_3	X_4	Y_4	X_5	Y_5
A	worker	headless	42	50	45	305	45	305	47	270	48	80
B	worker	whole body	53	180	58	412	60	415	65	390	65	125
C	queen	whole body	65	70	73	350	73	350	82	280	105	140
E	worker	headless	30	140	33	375	33	375	34	322	35	200
F	worker	whole body	95	40	110	269	110	269	120	225	123	130
G	worker	headless	12	160	17	414	25	425	25	425	27	150
I	queen	headless	30	120	37	360	37	360	40	305	45	100
J	worker	whole body	45	90	55	280	55	280	58	275	64	20
K	drone	headless	40	175	49	550	49	550	50	548	52	40
L	queen	whole body	20	60	29	230	29	230	37	180	39	5
M	queen	whole body	0	90	33	354	57	365	59	325	61	237
N	queen	whole body	40	25	46	260	46	260	49	230	49	230
O	worker	whole body	30	70	60	410	60	410	62	390	62	390
P	queen	whole body	25	140	38	570	38	570	47	500	54	437
Q	drone	headless	0	80	18	373	18	373	30	320	30	320
R	drone	headless	5	17	14	270	14	270	16	232	18	20
aa	drone	whole body	25	60	37	143	41	149	41	149	50	23
Ee	queen	headless	30	40	42	90	43	93	43	93	45	80
Ii	drone	whole body	30	47	35	79	41	108	42	80	48	36
rr	drone	whole body	10	72	22	156	29	188	35	156	35	156

Data recorded on 20 specimens used during the experiment. Experiment number: data on hornet experimented, sex or caste: the gender of the specimen, connection: the connecting electrodes were attached in headless between the thorax and the tip of the gaster and in those with the body intact, the electrode connection was between the head and the tip of the gaster; X_1 pertains to the time of UVA light start, while Y_1 is the starting voltage measurement at this time. For more details see Results in text.

PRESENTATION OF ALL THE GRAPHS OBTAINED IN THE COURSE OF THE STUDY. Each graph depicts the sequence of events pertaining to the awakening of a single hornet. In all, 20 hornets were observed and measured, of which 8 were headless and 12 were intact, while 6 were drones, 7 were queens and 7 were workers. Of the intact hornets 3 were drones, 5 were queens and 4 were workers, while of the headless 3 were drones, 2 were queens and 3 were workers.

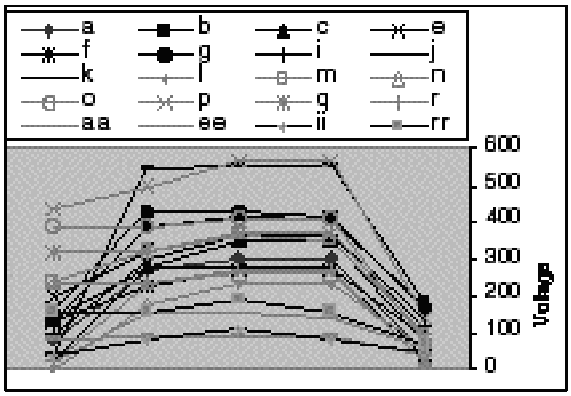

FIGURE 1. Typical narcotized hornet response to UVA illumination, to wit: each illuminated hornet invariably displayed rise in the voltage. First point marks the awakening process, second point — the rise in voltage, third point — the maximal voltage attained, fourth point — terminates of maximal voltage, and fifth point — drop in voltage down to starting level, whereupon the hornet falls asleep again.

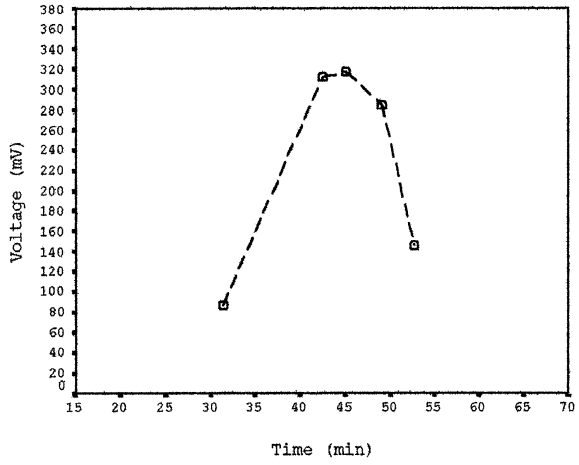

FIGURE 2. Graph based on all the means of measurements shown in Figure 1 for all the hornets measured (i.e. intact and headless ones).

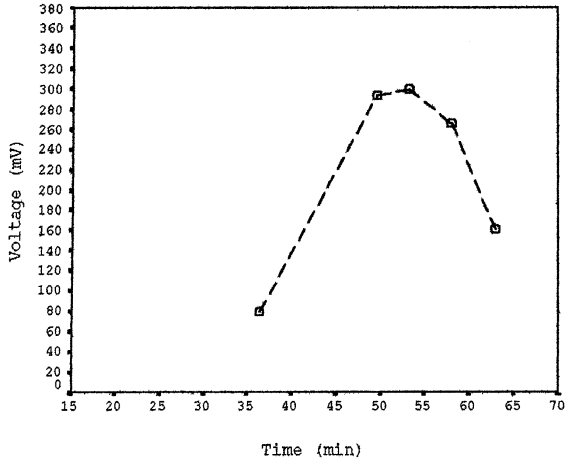

FIGURE 3. Results as in Figure 2, but here with summation of the means for intact (whole body) hornets.

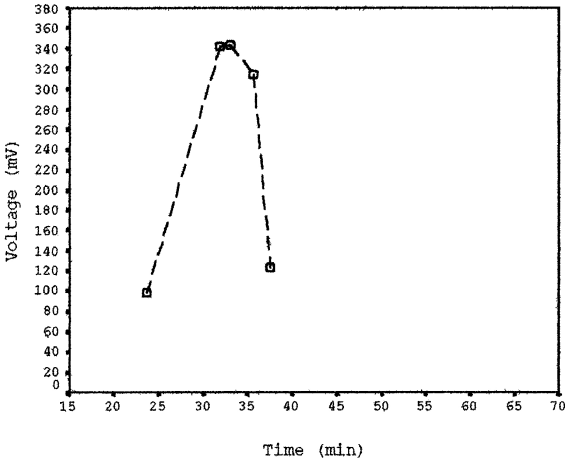

FIGURE 4. As in Figure 2, but with sum of means pertaining to headless hornets.

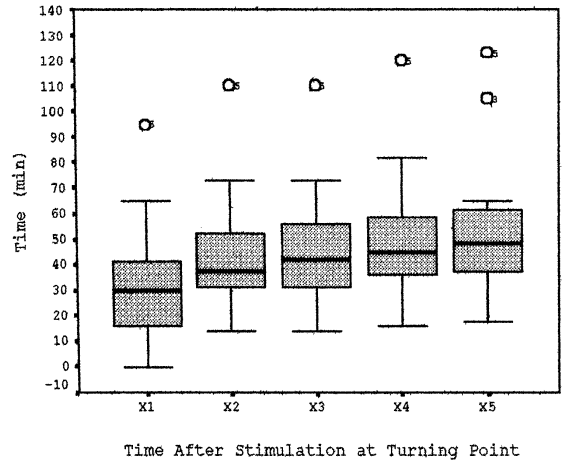

FIGURE 5. Box plot of time, with graphic presentation of the measured time points x_1–x_5. Bottom rectangle represents the bottom decile, and top rectangle-the uppermost decile, while middle line-the median, and circle-the extremal point.

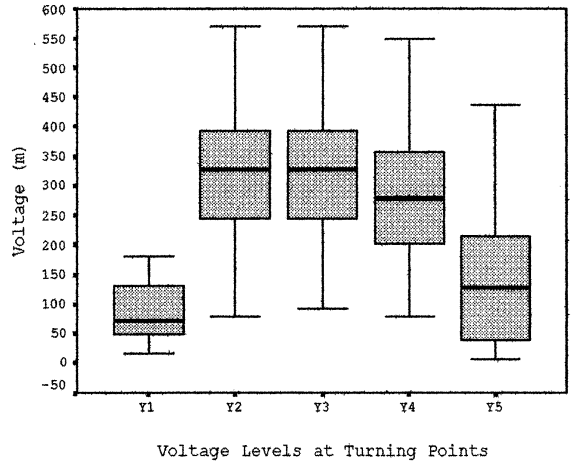

FIGURE 6. Box plot graphic presentation of the voltage features y_1–y_5. Explanations here are the same as for Figure 5.

Figure 3 and Figure 4, we note the following differences. In the intact hornets: 1) the maximal voltage level attained is lower, amounting to an average 299.5 mV; 2) the duration of the awakening is on average 26.4 minutes; and 3) the duration of the maximal voltage is longer (between x_2 to x_4), lasting about 8.4 minutes. In headless hornets: 1) the maximal voltage level is higher, amounting to 343.9 mV on the average; 2) the duration of the awakening process is shorter (between x_1–x_5) amounting to 13.9 minutes, with $p < 0.05$; and 3) the plateau of maximum voltage (x_2–x_4) is briefer — a mere 3.8 minutes.

Turning now to Box Plots, Figure 5 provides the relevant time points (x_5) and we can see that the awakening times, which coincide with the times of initial exposure to UVAL — the x_1 values — range between 0–65 minutes, barring one extreme instance of awakening occurring at 95 minutes. As for time point x_2, marking the onset of the voltage plateau, we note that it extends over 14–73 minutes, and so also the time span at x_3, but at x_4 the span becomes 16–82 minutes and at x_5, it ranges between 18–65 minutes. Throughout these measurements, there was one exceptional hornet, namely, hornet F (intact worker), and there was one more hornet (hornet C-intact queen) which stood out at point x_5. For each box we provide the median (middle line), the top quartile (upper line) and the bottom quartile (lower line). A similar presentation in graphic form is provided also in Figure 6, although there the reference to the voltage (y).

Discussion

The present investigation addressed the phenomenon of hornets awakening from ether anesthesia after their illumination by UVA beam. Nowadays people usually are not subjected to ether anesthesia, but even previously, when both humans and other mammals were narcotized with ether for surgical purposes, none of them awakened from the anesthesia following exposure to a light beam. In insects, however, this does happen, as already reported by us in previous publications (Ishay *et al.*, 1994; Goldstein *et al.*, 1996; Kirshboim and Ishay, 1998). Yet, in our earlier investigations we did not ascertain the factors responsible for the awakening but merely speculated that it had to do with the fact the Oriental hornet possesses throughout its cuticle and particularly in the region of its gaster, extra retinal photoreceptors which are sensitive to light and pick up the light energy, thereby effecting the observed awakening upon exposure to UV light (Goldstein and Ishay, 1996). In the present study we probed deeper and found that the awakening after illumination is a generalized response displayed by any narcotized hornet involved (Figure 1). Thus, all our narcotized hornets awakened within a minute of the UVAL, regardless of whether they were intact or decapitated albeit the headless hornets did not engage in flying upon awakening as did their intact cohorts. In each instance of awakening from ether anesthesia there was a typical rise in the cuticular voltage up to a given plateau, with a subsequent drop to almost starting level (Figure 2). The maximal voltage level attained by the awakening hornets is generally higher than that measured in live and active hornets (Pertsis *et al.*, in preparation). We should mention that such anesthetized hornets as have not been subjected to UVAL (i.e., rather in the dark) will awaken spontaneously regardless, but after a longer period of time than the illuminated ones. Furthermore, if the illumination period extends beyond the 20 minutes chosen by us in the present study, the

awakening hornets will not subsequently fall asleep again. The present study also evinced that in term of typical awakening behavior, there were four differences between the group of intact hornets (Figure 3) and the group of headless ones (Figure 4). Thus the headless hornets: 1) attained a higher maximal voltage; 2) displayed a sharper rise and sharper subsequent drop in the voltage; 3) the end-point voltage was closer to the starting level; and 4) the duration of the awakening process was shorter. As to why such differences exist, we should perhaps remind that in an earlier investigation on decapitated hornets we found that if we prevented the loss of hemolymph from the main thoracic artery in the wake of the decapitation, the headless hornet could survive for 48 hours (and perhaps more). Moreover, for a brief period after the decapitation the headless hornet is very alert and highly active, apparently reacting more rapidly than its intact cohort but for a shorter period of time. Conceivably, also, such hyperactivity by the decapitated hornet may affect its level of narcotization, rendering it more superficial then in the intact hornet (Kirshboim and Ishay, 1998). We therefore conjecture that had the exposure to ether anesthesia taken place 12 or more hours after the decapitation, the obtained results might have been different.

Let us now dwell briefly on the basic question as to why hornets subjected to ether anesthesia awaken under the influence of illumination. As we know, ether causes fluidization of biological membranes (Jørgensen *et al.*, 1991; Oliver *et al.*, 1991). If that be so, then the changes in the organization of the molecules in various membranes could conceivably lead to an inactivation, which is counteracted by a beam of light. Now in so far as a hornet will enter a 'sleep' state even in the absence of its head, it stands to reason that any change in the membranes is echoed also in the peripheral nerves and this explains the narcotization also in a headless hornet. Ether, of course, anesthetizes also vertebrates, but the underlying mechanism is still insufficiently clarified (Franks and Lieb, 1991; Krenjevic, 1991; Tinklenberg, 1991). What is clear, in so far as hornets, is that the ether is absorbed by the cuticle, because it is soluble in fats and probably also dissolves in the neuronal envelopes and in the brain of hornets. Ether is a compound of very low electrophilicity i.e., it is a poor electron donor compared to other solvents (Gutmann *et al.*, 1977; Gutmann *et al.*, 1983).

To date, we have never encountered Oriental hornets that were not susceptible to ether, although upon repeating narcotization, we found that they fell asleep for briefer periods (Kirshboim and Ishay, 1998). In addition, we got the impression that irradiating the cuticular yellow stripes with a light beam was more effective in awaking the hornets than irradiating the cuticular brown stripes, albeit this impression has thus far not been confirmed statistically (Krinstianpoller *et al.*, 1995).

Mutants have been reported in fly genus *Drosophila*, which showed altered sensitivity to diethyl ether anesthesia (Gamo *et al.*, 1998), and the investigators conjectured that the sodium channel and calreticulin might be the targets for ether anesthesia. Also encountered in genus *Drosophila* was an anesthetic resistant spontaneous mutant of *Drosophila melanogaster* (Gamo *et al.*, 1985).

Wasserkort and Koller (1997) surveyed the toxic effects of various volatile organic compounds and reached the conclusion that there were marked differences between various solvents and volatile mixtures like vapors of acetone, benzene, methanol, toluene, xylene, diethyl ether, leaded and unleaded gasoline and diesel fuel. The duration of the sleep induced by volatile organic compounds is in good agreement with the octanol water

coefficient. CO_2 production, in parallel to body activity can serve as a sensitive screening procedure in inhalation toxicology. Walcourt and Nash (2000) investigated the genetic effects on an anesthetic-sensitive pathway in the brain of *Drosophila*, especially in so far as an afore-described escape reflex was concerned (Wyman *et al.*, 1984; Trimarchi and Schneiderman, 1995).

Interestingly all the mentioned publications on *Drosophila* claim that the head of the fruit fly figures importantly in the induction of the anesthesia whereas in the case of the Oriental hornet we found that headless hornets will also fall asleep under the influence of ether. The latter finding implies that a head, or rather brain, is not essential for the process, and although there were some differences between intact and headless hornets in this regard (cf. Figure 3 with Figure 4), the overall picture was similar both in the stages of falling asleep as well as in the stages of awakening from the anesthesia-induced sleep.

References

Franks, N.P. and Lieb, W.R. (1991) Selective effects of volatile general anesthetics on identified neurons. In: Molecular and Cellular Machanism of Alcohol and Anesthetics (Rubin, E., Miller, K.W. and Roth, S.H., eds), *Ann N.Y. Acad. Sci. 625:* 54–70.

Gamo, S., Nakashima-Tanaka, E., Megumi, T. and Ueda, I. (1985) Anesthetic-resistant spontaneous mutant of *Drosophila melanogaster*: intensified response to ^{60}Cobalt radiation damage. *Life Sciences 36:* 789–794.

Gamo, S., Dodo, K., Matakatsu, H. and Tanaka, Y. (1998) Molecular genetical analysis of *Drosophila* ether sensitive mutants. *Tox. Let. 100–101:* 329–337.

Goldstein, O., Litinetsky, L. and Ishay, J.S. (1996) Extraretinal photoreception in hornets. *Physiol. Chem. Phys. & Med. NMR 28:* 129-136.

Goldstein, O. and Ishay, J.S. (1996) Morphology of a putative new peripheral photoreceptor in social wasps. *Physiol. Chem. Phys. & Med. NMR 28:* 255–266.

Gutmann, F., Keyzer, H., Lyons, L.E. and Somoano, R.B. (1983) *Organic Semiconductors*, Part B, R.E. Krieger Publ. Com., Malabar, Florida.

Gutmann, V. (1977) Ion pairing and outer sphere effect. *Chimia 31:* 1–7.

Ishay, J. (1975) Hyperglycemia produced by *Vespa orientalis* venom sac extract. *Toxicon 13:* 221–226.

Ishay, J.S., Pertsis, V. and Levtov, E. (1994) Duration of hornet sleep induced by ether anesthesia is curtailed by exposure to sun or UV-irradiation. *Experientia 50:* 737–741.

Jørgensen, K., Ipsen, J.H., Mouritsen, O.G., Bennett, D. and Zuckermann, M.J. (1991) Anesthetics affect membrane heterogeneity. In: Molecular and Cellular Mechanismus of Alcohol and Anesthetics. Part 1. (Rubin, E., Miller, K.W. and Roth, S.H. eds.). *Ann. N.Y. Acad. Sci. 625:* 747–750.

Kirshboim, S. and Ishay, J.S. (1998) Ether anesthesia of hornets: The development of tolerance and the influence exerted by various body parts on the duration of anesthesia. *Physiol. Chem. Phys. & Med. NMR 30:* 113–127.

Kirshboim, S. and Ishay, J.S. (2001) Learning and navigation of hornets: role of the various light perceiving organs. *Physiol. Chem. Phys. & Med. NMR 33:* 175–186.

Krenjevic, K. (1991) Cellular mechanisms of anesthesia. In: Molecular and Cellular Mechanism of Alcohol and Anesthetics. Part 1. (Rubin, E., Miller, K.W. and Roth, S.H., eds.), *Ann. N.Y. Acad. Sci. 625:* 1–16.

Kristianpoller, N., Goldstein, O., Litinetsky, L. and Ishay, J.S. (1995) Light curtails sleep in anesthetized hornets: Extraretinal light perception. *Physiol. Chem. Phys. Med. NMR 27:* 193–201.

Matsuura, M. and Yamane, S. (1990) *Biology of the Vespine Wasps.* Springer-Verlag, Berlin.

Oliver, A.E., Deamer, D.W. and Akeson, M. (1991) Sensitivity to anesthesia by pregnanolone appears late in evolution. In: Molecular and Cellular Mechanisms of Alcohol and Anesthetics. Part 1. (Rubin, E., Miller, K.W. and Roth, S.H., eds.), *Ann. N.Y. Acad. Sci. 625:* 561–565.

Pertsis, V., Sverdlov, A., Litinetsky, L., Rosenzweig, E. and Ishay, J.S. (2001) Navigation and thermo-photovoltaic activity by hornets at different light conditions: the influence of UVB blockers. *Physiol. Chem. Phys. & Med. NMR 33:* 187–202.

Spradbery, J.P. (1973) *Wasps.* Sidgwick and Jackson, London.

Tinklenberg, J.A., Segal, I.S., Tiazhi, G. and Maze, M. (1991) Analysis of anesthetic action on the potassium channels of the shaker mutant of *Drosophila*. In: Molecular and Cellular Mechanisms of Alcohol and Anesthetics. Part I. (Rubin, E., Miller, K.W. and Roth, S.H., eds). *Ann. N.Y. Acad. Sci. 625:* 532–539.

Trimarchi, J.R. and Schneiderman, A.M. (1995) Different neural pathways coordinate *Drosophila* flight initiations evoked by visual and olfactory stimuli. *J. Exp. Biol. 198:* 1099–1104.

Wasserkort, R. and Koller, T. (1997) Screening toxic effects of volatile organic compounds using *Drosophila melanogaster. J. Appl. Toxicol. 17:* 119–125.

Walcourt, A. and Nash, H.A. (2000) Genetic effects on an anesthetic-sensitive pathway in the brain of *Drosophila*. *J. Neurobiol. 42:* 69–78.

Wyman, R.J., Thomas, J.B., Salkoff, L. and King, D. (1984) The *Drosophila* giant fiber system. In: *Neural Mechanisms of Startle Behavior.* Eaton, R., (ed.). New York: Plenum. pp. 133–161.

Received June 3, 2003;
accepted September 12, 2003.

Physiological Chemistry and Physics and Medical NMR
INDEX
Volume 35, 2003